

AN EXPERIMENTAL INVESTIGATION INTO THE BEHAVIOUR OF A 5 TON ELECTRIC OVERHEAD TRAVELLING CRANE AND ITS SUPPORTING STRUCTURE

Johan Hendrik de Lange



Thesis presented in partial fulfilment of the requirements for the
degree of Master of Civil Engineering at the University of Stellenbosch

Study Leader: Prof. P.E. Dunaiski

March 2007

I, the undersigned, hereby declare that the work contained in this thesis was my own original work and that I have not previously in its entirety or in part submitted it at any university for a degree.

Signature:

Date:



Synopsis:

In structural engineering practice the actions imposed by overhead travelling cranes onto the supporting structure are defined as static forces amplified by dynamic coefficients and applied as pseudo-static forces without taking the interaction between crane and supporting structure into account.

To investigate the validity of this approach, the forces generated at the wheels of an experimental crane are measured, as the crane traverses on the supporting structure. The interaction at the wheels of the crane is also visually recorded. These wheel load results will also be used by other researchers, to calibrate a numerical model of the experimental system.

A full-scale 5 ton electric overhead travelling crane (EOTC) running on top of rails and a supporting structure, was designed and erected for research purposes. The crane has a span of 8.3 m and wheel spacing of 4 m, which can be modified. The supporting structure consists of three simply supported mono-symmetric plate girders on each side, with a total length of 13.8 m. This is supported by columns with a height of about 3.5 m. This paper describes the calibration of this system for measurement purposes.

A data acquisition system was implemented to capture forces, strains, deflections and accelerations at various points on the crane and the supporting structure as well as to measure the velocity of the crane. The forces at the crane wheels are measured through strain gauges on the end carriage load measuring system.

The calibrated facility is used to investigate the behaviour of the crane and the supporting structure under regular and exceptional wheel loads, which are classified as follows:

- **Regular wheel loads** occur during normal payload hoisting and lowering, longitudinal crane travel with payload and lateral crab travel with payload.
- **Exceptional wheel loads** occur during eccentric payload hoisting (payload outside normal operational area), impact forces on end-stops, maximum hoisting of the payload, failure of a longitudinal drive mechanism of the crane, misalignment of the supporting structure and skewing of the crane.

The maximum values of these experimentally determined wheel loads and the dynamic response of the system is used to help describe the behaviour of the electric overhead travelling crane and its supporting structure.

Samevatting:

In die praktyk van struktuur ingenieurswese word die aangewende laste van oorhoofse kraan op die ondersteuningsstruktuur gedefinieer as statiese laste wat vergroot word deur dinamiese koeffisiente en aangewend as pseudo-statische laste sonder om die interaksie tussen die oorhoofse kraan en die ondersteunings struktuur in ag te neem.

Om die korrektheid van hierdie benadering te ondersoek, is die wielkragte van 'n eksperimentele kraan gemeet, terwyl die kraan bo-op die ondersteunings struktuur beweeg. Die interaksie by die wiele van die kraan is ook waargeneem deur 'n videokamera. Die resultate is ook benodig deur PhD student Trevor Haas, vir die kalibrasie van 'n numeriese model van die eksperimentele sisteem.

Vir doeleindes van hierdie navorsingsprojek is 'n volskaalse 5 ton elektries aangedrewe oorhoofse kraan wat op spore loop en bo-op 'n ondersteunings struktuur gevestig is, ontwerp en opgerig. Die oorhoofse kraan het 'n span van 8.3 m en 'n wiel spasiëring van 4 m, wat veranderbaar is. Die ondersteuningsstruktuur bestaan uit drie eenvoudig opgelegde mono-simmetriese plaatbalke aan beide kante, met 'n totale lengte van 13.8 m. Die plaatbalke is bo-op kolomme met 'n hoogte van ongeveer 3.5 m. Hierdie navorsingsprojek beskryf die kalibrasie van die sisteem vir metings doeleindes.

'n Data insamelings sisteem is geïmplementeer om kragte, vervormings, defleksies en versnellings te meet op verskeie plekke op die oorhoofse kraan en ondersteunings struktuur, asook om die spoed van die kraan te bepaal. Die kragte by die wiele van die oorhoofse kraan word bepaal deur rekstrokies op die sekondêre kraanbalk lasmeet stelsel.

Die gekalibreerde fasiliteit word in die ondersoek na die gedrag van die oorhoofse kraan en die ondersteuningsstruktuur gedurende gereelde en besonderse wiellaste, wat as volg geklassifiseer word, gebruik:

- **Gereelde wiellaste** kom voor tydens normale ophysing en plasing van die belastingsvoorwerp, beweging van die oorhoofse kraan in die langsrigting met die belastingsvoorwerp en beweging van krap in die laterale rigting met belastingsvoorwerp.
- **Besonderse wiellaste** kom voor tydens eksentriese ophysing van die belastingsvoorwerp (belastingsvoorwerp buite normal gebruik area), impak laste op end-stoppe, maksimum ophysing van belastingsvoorwerp, faling van 'n langsrigting aandrywings meganisme van kraan, skeefspanning van ondersteuningsstruktuur en skeef trek van oorhoofse kraan.

Die maksimum waarde van hierdie eksperimenteel bepaalde wiellaste en die dinamiese reaksies van die sisteem word gebruik om die gedrag van die elektries aangedrewe oorhoofse kraan en die ondersteunings struktuur te help beskryf.

Acknowledgement

The following people played an important part in my life during these past 2 years of academic research. Without your support and guidance, this thesis would not have been possible.

My wife:

Thank you Louisa, for standing by my side when I did not believe I could finish this project.

Prof. P.E. Dunaiski:

Thank you for believing in my abilities and for always keeping me on the right (academic) track.

Johan Muller and Billy Boshoff:

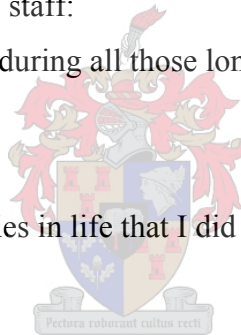
Thank you for always having the time to help solve any problem.

EOTC research assistants and workshop staff:

Thank you for your friendship and help during all those long hours in the lab.

My parents:

Thank you for giving me the opportunities in life that I did not think possible.



“Therefore humble yourselves under the mighty hand of God, that he may exalt you in due time, casting all your care upon Him, for He cares for you.” 1 Peter 5:6-7

Table of contents

List of Tables	ix
List of Figures	x
List of Photos	xiii
1. Introduction	
1.1 Research overview.....	1
1.2 Aspects of research methodology.....	2
1.3 Thesis overview.....	3
2. Literature review	
2.1 Crane load models in SABS 0160-1989.....	5
2.2 EN 1991-3: Actions induced by cranes on structures.....	6
2.3 Proposed SANS 10160 Section 10.....	6
2.3.1 Vertical loads from overhead travelling cranes.....	6
2.3.2 Horizontal loads from overhead travelling cranes.....	7
2.4 Mechanical failure.....	10
2.5 Serviceability limits.....	10
2.6 Construction tolerances for supporting structure.....	11
2.7 Documented overhead crane research models.....	12
2.8 Experimental techniques.....	13
2.9 Reference load models for investigation.....	13
3. EOTC supporting structure	
3.1 Definition of supporting members.....	14
3.2 Calibration of force measuring system.....	16
3.3 Payload to be used in experimental investigation.....	18
4. Overhead crane and instrumentation	
4.1 Design drawings of overhead crane.....	19
4.2 Crane orientation and sign convention of wheel forces.....	21
4.3 Characteristics of crane.....	22
4.3.1 Longitudinal crane motion.....	22
4.3.2 Lateral crab motion.....	23

4.3.3	Hoisting behaviour of crab.....	24
4.4	Crab and payload position.....	24
4.5	Strain gauges on overhead crane.....	25
4.6	Encoders and accelerometers on overhead crane.....	26
5.	Numerical modelling of overhead crane	
5.1	Discrete element beam model.....	27
5.2	Finite element shell model.....	27
5.2.1	Vertical load on crane bridge.....	29
5.2.2	Lateral horizontal loads on end carriage.....	30
6.	Calibration of end carriage load measuring system and supporting structure	
6.1	Configuration of crane during calibration process.....	32
6.2	Strain data transformation.....	32
6.3	Calibration for measuring vertical wheel loads.....	34
6.4	Calibration for measuring lateral horizontal wheel loads.....	35
6.4.1	Pulling the wheels together on a side.....	36
6.4.2	Pulling the wheels together on both sides.....	37
6.4.3	Pushing the wheels apart.....	38
6.4.4	Pulling and pushing the wheels.....	38
6.4.5	Summary of lateral horizontal calibrations.....	39
6.5	Calibration for longitudinal horizontal wheel forces.....	40
6.6	Calibration results of crane compared with results from numerical model.....	41
6.7	Applying of direct loads on supporting structure.....	42
6.7.1	Behaviour of supporting structure under vertical loads.....	43
6.7.2	Behaviour of supporting structure under lateral horizontal loads.....	46
7.	Regular loads on overhead crane and supporting structure	
7.1	Forces due to own weight of crane.....	47
7.2	Forces and loads due to hoisting and lowering of payload.....	48
7.3	Forces and loads during longitudinal travel of crane with payload.....	50
7.3.1	Crab at centre of crane bridge.....	50
7.3.2	Crab at most eccentric position on crane bridge.....	51
7.4	Loads during lateral travel of crab with payload.....	52

8.	Exceptional loads on overhead crane and supporting structure	
8.1	Loads due to hoisting payload to maximum height.....	55
8.2	Forces due to longitudinal buffer impact.....	56
8.3	Forces induced by electrical driving motors.....	58
8.4	Loads due to eccentric payload hoisting from the ground.....	59
8.5	Loads due to deactivated electrical motor.....	60
8.6	Loads due to misalignment of supporting structure.....	64
	8.6.1 Quasi-static loads due to misalignment.....	64
	8.6.2 Kinematic loads due to misalignment.....	65
9.	Summary of wheel loads and crane characteristics	67
10.	Conclusions relating to behaviour of system	
10.1	Description of behaviour of system.....	71
10.2	Description of skewing behaviour.....	72
10.3	Description of misalignment behaviour.....	72
10.4	Possible future research.....	72
	References	73
	Appendix A – Own weight of crane and crab	75
	Appendix B – Data acquisition system	
B1	Hardware and software.....	77
B2	Wheatstone full-bridge connections.....	77
B3	Implementation of data acquisition system.....	79
	Appendix C – Theoretical model of end carriage load measuring system	
C1	Characteristics of end carriage load measuring system.....	81
C2	Behaviour due to applied load vectors.....	84
C3	Summary of theoretical stresses.....	90
	Appendix D – Design drawings of 5 ton lead/concrete payload	92
	Appendix E – Wheel load calculations according to load models	93
	Appendix F – Video data of experiments on DVD	99

List of Tables

Table 2.1: Summary of crane load models in SAISCH ^[2]	5
Table 6.1: Summary of calibration coefficients.....	39
6.2: Summary of vertical wheel load calibrations.....	41
6.3: Summary of stress results due to lateral horizontal wheel loads.....	41
6.4: Summary of lateral horizontal wheel load calibrations.....	41
6.5: Summary of stress results due to longitudinal horizontal wheel loads.....	41
6.6: Reaction forces measured in crane supporting columns.....	45
Table 8.1: Summary of longitudinal impact forces.....	57
8.2: Influence of deactivating an electrical motor on acceleration behaviour of crane.....	62
Table 9.1: Summary of critical experimental wheel loads.....	67
9.2: Comparison of results from the experimental investigation with crane load models from SABS 0160 and newly proposed SANS 10160.....	68
9.3: Comparison of general crane characteristics with similar information from literature.....	69
Table B1: Calibration coefficients implemented during experimental investigation.....	80
Table C1: Values implemented in homogeneous equation for torsion.....	88
C2: Differential equations for a torsional load on a cantilever beam.....	89
C3: Summary of theoretical stress response at strain gauge positions.....	90

List of Figures

Figure 2.1: Load arrangements for maximum vertical action on the runway beams.....	7
2.2: Force interaction due to acceleration or deceleration of the crane	7
2.3: Wheel loads due to acceleration and deceleration of the crab.....	8
2.4: Skewing behaviour when guidance means are the wheel flanges.....	8
2.5: Skewing behaviour when there is a separate guidance means.....	9
2.6: Wheel load configuration during misalignment.....	9
2.7: Force configuration during buffer impact.....	10
2.8: Limits on lateral deviation of supporting structure.....	11
Figure 3.1: 3-D view of supporting structure.....	15
3.2: Load measuring instrumentation implemented in supporting structure.....	17
Figure 4.1: Design drawing of overhead crane (girder and rail not as built).....	19
4.2: Detail drawing of end carriages.....	20
4.3: Plan view of overhead crane.....	21
4.4: Orientation of crane relative to supporting structure.....	21
4.5: Definition of specified points on the crane bridge.....	24
4.6: Orientation of strain gauges on end carriage load measuring system.....	25
4.7: Position of encoders and accelerometers.....	26
Figure 5.1: Beam element model of crane.....	27
5.2: Plate element model of crane.....	28
5.3: Numerical model of crane bridge to end carriage connection.....	28
5.4: Vertical deflection and bending stress behaviour of the crane bridge.....	29
5.5: Compressive stress in top flange of end carriages.....	29
5.6: Tensile stress in bottom flange of end carriages.....	30
5.7: Typical stress behaviour due to lateral horizontal wheel loads.....	31
Figure 6.1: General normal stress response at strain gauges on flanges of end carriages, due to wheel loads.....	33
6.2: Load cells and support point positions for vertical force calibrations.....	34
6.3: Bending stress behaviour at strain gauges.....	35

6.4: Linear elastic bending stress behaviour of end carriage load measuring system.....	35
6.5: Load cells and support positions for lateral horizontal force calibrations.....	36
6.6: Linear elastic normal stress behaviour due to pulling southern wheels together.....	37
6.7: Linear elastic normal stress behaviour due to pulling northern wheels together.....	37
6.8: Linear elastic normal stress behaviour due to pulling on both sides.....	38
6.9: Linear elastic normal stress behaviour due to pushing northern wheels apart.....	38
6.10: Linear elastic normal stress behaviour due to pulling and pushing the wheels.....	39
6.11: Load cells and supporting positions for longitudinal horizontal force calibrations....	40
6.12: Calibrated vertical wheel loads directly onto supporting structure.....	42
6.13: Position of individually applied vertical wheel loads.....	44
6.14: Vertical deflection behaviour of supporting structure.....	44
Figure 7.1: Position of crane at start of longitudinal travel experiments.....	47
7.2: Vertical reaction forces in columns when no payload is handled.....	48
7.3: Lateral horizontal wheel loads when no payload is handled.....	48
7.4: Dynamic response due to payload hoisting from the ground.....	49
7.5: Maximum lateral horizontal wheel loads due to normal payload hoisting.....	49
7.6: Dynamic response due to payload lowering onto the ground.....	50
7.7: Lateral horizontal loads at uneven rail splice.....	51
7.8: Vertical forces during longitudinal crane travel with eccentric payload.....	51
7.9: Vertical loads at wheels, due to lateral traversing of crab with payload.....	53
7.10: Lateral horizontal wheel loads due to crab's motion with payload hanging low.....	53
7.11: Maximum lateral horizontal wheel loads due to crab's acceleration.....	54
Figure 8.1: Linear relation between acceleration and dynamic response of crane.....	56
8.2: Longitudinal force at end-buffers and vertical force at payload.....	57
8.3: Longitudinal force per rail.....	58
8.4: Orientation of eccentric hoisting of payload.....	59
8.5: Skewing force mechanism when an electrical motor is deactivated.....	60
8.6: Lateral horizontal loads due to deactivated electrical motor.....	61
8.7: Longitudinal end carriage deviation resulting in skewing.....	62
8.8: Critical lateral horizontal wheel loads.....	63
8.9: Skewing behaviour due to static crane, restraint longitudinally at a wheel.....	63
8.10: Maximum lateral horizontal wheel loads without payload(without payload hoisted).65	
8.11: Configuration of system at start of misalignment investigation.....	65

8.12: Maximum wheel loads measured during inward misalignment.....	66
Figure 9.1 : Position of crane for largest forces and wheel loads on system.....	68
Figure 10.1: Diagram indicating aspects influencing dynamic behaviour.....	71
Figure B1: Photo and diagram indicating Wheatstone bridge for measuring bending strain.....	78
B2: Photo and diagram indicating Wheatstone bridge for measuring normal strain.....	78
Figure C1: Theoretical investigation of end carriage load measuring system.....	81
C2: Sectional properties of end carriages.....	81
C3: Saint–Venant torsional shear stress behaviour.....	83
C4: Shear stresses induced by warping torsion.....	83
C5: Warping normal stresses in the flanges.....	83
C6: Bending around the z-axis due to shear forces in the flanges.....	84
C7: Elevation of cantilever beam with vertical load vector.....	85
C8: Typical bending stress and shear stress response in web of cantilever beam.....	85
C9: Plan view of cantilever beam with lateral horizontal load vector at neutral axis.....	86
C10: Typical bending stress and shear stress response in the flanges of cantilever beam...	86
C11: Elevational view of cantilever beam with applied load vector at neutral axis.....	87
C12: Lateral elevation of cantilever beam with eccentric load vectors at wheel.....	87
C13: Dimensions of cantilever beam.....	88
C14: Torsional behaviour along length of cantilever beam.....	91
Figure D1: Design drawings of reinforced concrete for 5 ton payload.....	92

List of Photo's

Photo 3.1: Zwick Z250 and computer system.....	16
3.2: Load cell calibrated under axial load.....	16
3.3: 5 ton payload with load cell.....	18
Photo 4.1: Electrical driving motor at crane wheel.....	22
4.2: Emergency cut-out mechanism for longitudinal crane travel.....	23
4.3: Electrical motor on crab for lateral motion	23
4.4: Hoist drive mechanism on crab.....	24
Photo 6.1: Crane orientation on floor during calibration process.....	32
6.2: Load cell bolted to floor to simulate payload hoisting.....	34
6.3: Crane wheel load applied with cable tie connection.....	36
6.4: LVDT's measuring deflections of girders.....	43
Photo 8.1: Elastomeric buffer compression during impact.....	56
Photo A1: End carriage supported, to cancel out stress effects due to crane's own weight.....	75
Photo B1: Spider equipment with 32 channel-input data capacity.....	77
Photo F1: A digital video camera mounted close to the wheel contact surface.....	99

Chapter 1 – Introduction

In structural engineering practice the actions imposed by overhead travelling cranes onto the supporting structure are defined as static forces amplified by dynamic coefficients and applied as pseudo-static forces without taking the interaction between crane and supporting structure into account.

To investigate the validity of this approach, the forces generated at the wheels of an experimental crane are measured, as the crane traverses on the supporting structure. The interaction at the wheels of the crane is also visually recorded. These wheel load results will also be used by other researchers, to calibrate a numerical model of the experimental system.

1.1 Research overview

This research project is part of Project 1 – EOTC Support Structure Investigation. The purpose of Project 1 is to determine the reasons why in-service problems are experienced with electric overhead travelling crane support structures. To investigate the issue of in-service problems, the behaviour of the crane and its supporting structure under different loading conditions has to be defined. An extensive research program is executed at the Institute of Structural Engineering (ISE) at the University of Stellenbosch; where a systematic approach of looking at the problem on a statistical, numerical modelling, experimental verification and best-practice level, is undertaken.

This research work focuses on the experimental domain, by investigating the behaviour of the crane and supporting structure under specific loading situations. This will help to evaluate the proposal of implementing the load models from **Eurocode 1 Part 3 (EN 1991 – 3)**: Actions induced by cranes and machinery on structures, into Section 10: Actions induced by cranes and machinery on buildings and industrial structures of the newly developed South African loading code **SANS 10160**. The expected outcome of this code modification is future crane systems, which are better designed to resist the applied actions without suffering in-service problems.

1.2 Aspects of research methodology

An end carriage load measuring system consisting of strain gauges used to measure deformation of the end carriages, due to wheel loads, is implemented to determine the wheel loads during implementation of the crane. A numerical model of the crane is also developed for better understanding of the behaviour of the end carriage load measuring system, because the experimental results are limited to specific data capturing points, while the numerical results give a global view of the behaviour of the end carriages under loading.

The crane is isolated from the supporting structure and calibrated wheel loads are applied onto the end carriage load measuring system. A linear functional stress value per unit of applied wheel load is obtained. The process of determining the functional value for the different types of wheel loads, is referred to as calibration of the end carriage load measuring system. The results from the numerical model will also function as a sounding board against which these functional values are compared.

The behaviour of the supporting structure under measured static wheel load at mid-span of each girder is investigated. This simplistic loading situation is used for evaluating the force distribution characteristics of the supporting structure, which would otherwise not be possible during normal crane implementation. The influence of a splice in the crane rail on the load behaviour of the supporting structure is also investigated. A PhD candidate used this information to calibrate his finite element numerical model of the supporting structure.

The overhead crane and supporting structure were then exposed to load arrangements according to the load models as specified in literature, by means of a payload, in order to induce regular and exceptional loads at the wheels of the crane. The characteristics of these wheel loads are then used to describe the behaviour of the system.

1.3 Thesis overview

An overview of this thesis based on the chapters, is given.

Chapter 2

This chapter consists of a literature review relating to relevant crane loading codes and associated load models. The general approach followed in previous documented research on overhead travelling cranes was investigated, to determine the relevant parameters and approach to be followed.

Chapters 3 & 4

In chapter 3 the basic characteristics and force measuring capabilities of the supporting structure is defined. The characteristics and the force measuring capability of the payload and overhead crane are defined in chapter 4.

Chapters 5 & 6

In chapter 5 a numerical model of the crane is defined and tested under controlled loading. The numerical model will give insight into the experimental results, because the numerical model defines the global behaviour of the crane, while the experimental results are limited to specific data capturing points.

In chapter 6 the calibration of the end carriage load measuring system is explained and a linear stress function is determined for the different wheel loads that the crane can experience. The results from the numerical model are then compared with the experimental calibration of the end carriage load measuring system. The load carrying behaviour of the supporting structure is also determined under controlled loading.

Chapters 7 & 8

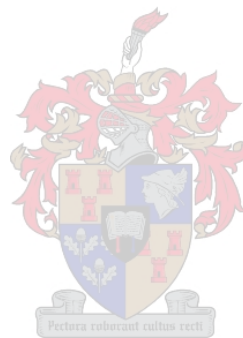
In these chapters the experimental investigation into the behaviour of the overhead crane under regular and exceptional wheel loads are described.

Chapters 9 & 10

In chapter 9 the experimental wheel loads are summarized and compared with those obtained from literature. The characteristics of the crane, which were determined experimentally, are also compared with results from similar research projects. In chapter 10 conclusions based on the load behaviour of the system are made. Misalignment and skewing behaviour based on experimental results are described. Remarks pertaining to possible future research are also made.

Appendixes

The technical information, theoretical calculations and graphically represented results relating to the crane and strain gauges are given. Design drawings of the payload are included and digital video data relating to certain experimental tests and design drawings of the supporting structure are included on an attached DVD.



Chapter 2 – Literature review

Crane loading codes under investigation and aspects from documented research, to define the behaviour of overhead cranes, are described in this chapter.

2.1 Crane load models in SABS 0160-1989^[1]

The crane load models, as described in chapter 5.7 in the South Africa loading code, to determine the wheel loads that may occur on an overhead crane system, are simplistic in nature. The main characteristics of these load models will be described briefly.

The utilization and application of a crane determines its classification. The least used and lightest loaded cranes are defined as class 1, while the heaviest loaded and continuously used cranes are defined as class 4. A direct relation between the class of crane and load factors are assumed; with the static gravitational loads multiplied by these load factors. Dynamic load factors are applied to vertical loading, due to hoisting of the payload only. The other factors are load coefficients, translating the gravitational loads into horizontal loads, as indicated in Table 2.1 below from the South African Institute of Steel Construction Handbook (SAISCH).

Type of loading	Direction of loading	Class of crane			
		1	2	3	4
Vertical loading per wheel, including impact $X_1 \cdot W$ (max. static wheel load)	↓	$X_1 = 1.1$	1.2	1.25	1.3
Horizontal transverse forces per wheel a) Crab acceleration and braking $X_2 \cdot (\text{Crab's weight} + \text{Load lifted}) / (\text{Number of wheels})$		$X_2 = 0.05$	0.10	0.15	0.20
b) Misalignment of wheels or gantry $X_3 \cdot (\text{Bridge's weight} + C + L) / N$		$X_3 = 0.05$	0.12	0.15	0.20
c) Skewing $X_4 \cdot (B + C + L) / N$		$X_4 = 0.075$	0.18	0.225	0.30
Horizontal longitudinal force (acceleration and deceleration)	↔	Force = $0.1 (\sum W \text{ of line per rail})$			
Force on end stops the lesser of:		Force = $1.0 (B + C)$ or alternatively full speed impact calculated from buffer and end stop characteristics			

Table 2.1: Summary of crane load models in SAISCH^[2]

2.2 EN 1991-3: Actions induced by cranes on structures

Eurocode is a compilation of construction standards of which EN 1991-3 is a part. Some of the basic definitions regarding overhead travelling cranes, as defined in EN 1991-3, will be described, as follows.

Dynamic factor: The ratio of the dynamic response to the static response.

Crab: Part of an overhead travelling crane that incorporates a hoist and is able to travel on the crane bridge.

Crane bridge: Part of an overhead travelling crane that spans between the crane runway beams and supports the crab or hoist block.

Guidance means: System used to keep a crane aligned on a runway, through horizontal reactions between the crane and runway beams. A guidance means can consist of flanges on the crane wheels or a separate system of guide rollers operating on the side of the crane rails or the side of the runway beams.

Self-weight of the crane: Self-weight of all fixed and movable elements including the mechanical and electrical equipment of a crane structure, however without the lifting attachment and a portion of the suspended hoist ropes or chains moved by the crane structure.

Hoist load: It includes the masses of the payload, the lifting attachment and a portion of the suspended hoist ropes or chains moved by the crane structure.

Natural frequency: The frequency of normal mode of vibration.

Free vibration: The vibration of a system that occurs in the absence of forced vibration.

Damping: The dissipation of energy with time or distance.

A load model for misalignment of the crane wheels or gantry rails is not included in EN 1991-3.

The load models in the proposed SANS 10160 Section 10 in the next sub-section are directly related to the load models in EN 1991-3. Refer to Appendix E for wheel load calculations for this experimental crane, based on EN 1991-3.

2.3 Proposed SANS 10160 Section 10

The load models in this proposed code will be described briefly.

2.3.1 Vertical loads from overhead travelling cranes

The relevant vertical wheel loads from a crane on a runway beam, should be determined by considering the load arrangements illustrated below.

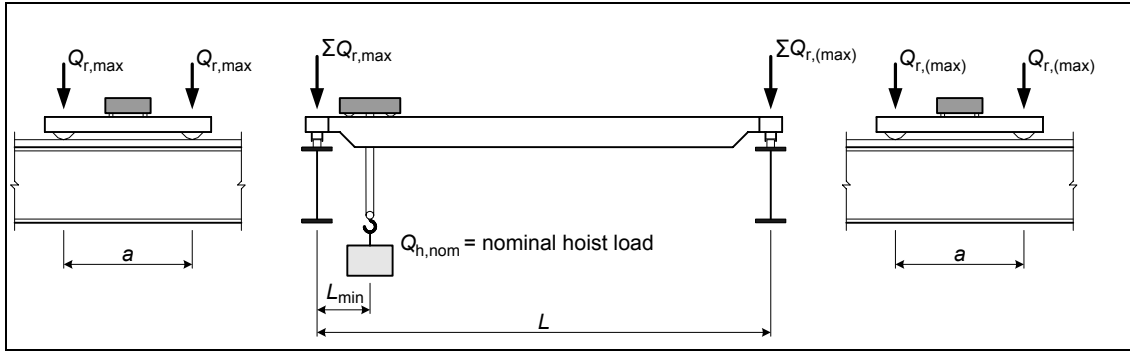


Figure 2.1: Load arrangements for maximum vertical action on the runway beams

where :

$Q_{r,max}$ is the maximum load per wheel of the loaded crane

$Q_{r,(max)}$ is the accompanying load per wheel of the loaded crane

$\Sigma Q_{r,max}$ is the sum of the maximum loads $Q_{r,max}$ per runway of the loaded crane

$\Sigma Q_{r,(max)}$ is the sum of the accompanying maximum loads $Q_{r,(max)}$ per runway of the loaded crane

$Q_{hl,nom}$ is the nominal hoist load, (or it is characteristic hoist load $Q_{hl,k}$)

Proposed SANS 10160 Section 10 refers to vertical dynamic factor $\phi_1 = 1.1$, while EN 1991-3 refers to it as the upper and lower values of a vibrational pulse varying between 0.9 and 1.1.

2.3.2 Horizontal loads from overhead travelling cranes

The horizontal loads at the wheels of an overhead crane, are due to the following situations.

2.3.2.1 Acceleration and deceleration of the crane

These forces are highest when the crane accelerates or decelerates along the crane beam, with the hoist load positioned as indicated in figure 2.2 below, close to the crane beam.

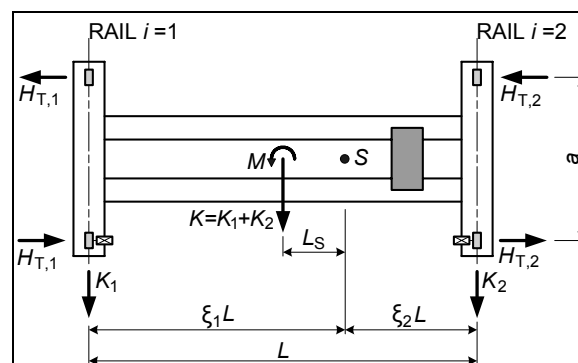


Figure 2.2: Force interaction due to acceleration or deceleration of the crane

a is the spacing of the guide rollers or the flanged wheels

L is the span of the crane bridge

\mathbf{K} is the drive force on the driven wheels, when wheel spin is prevented. This value should be given by the crane supplier, or can be calculated. \mathbf{S} is the center of gravity of the system (crane and payload). \mathbf{M} is the force moment as a result of the total drive force, relative to the center of gravity of the system. $\mathbf{H}_{T,1}$ and $\mathbf{H}_{T,2}$ are the **horizontal transverse forces** at the wheels, which act as a couple, as a result of the force moment. $H_{T,1}$ and $H_{T,2}$ are influenced by the wheel spacing and the dynamic behaviour of the crane during acceleration and deceleration.

These forces do not include the effects of oblique hoisting due to misalignment of load and crab because in general oblique hoisting is forbidden. Any effects of unavoidable small values of oblique hoisting are included in the inertial forces.

2.3.2.2 Acceleration and deceleration of the crab

Provided that the payload is free to swing, the horizontal load $\mathbf{H}_{T,3}$ in the figure below, represents the **horizontal transverse wheel forces** related to the movement of the crab. The wheel forces can also be in the opposite direction.

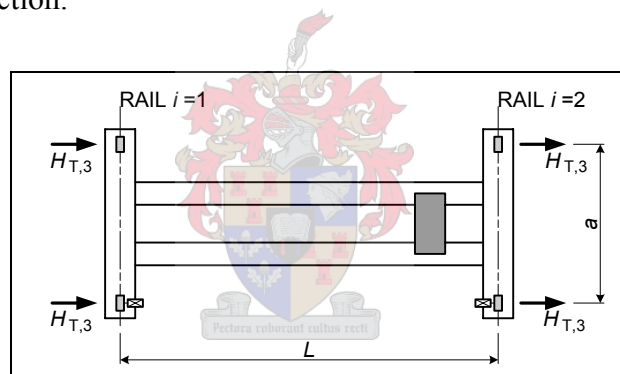


Figure 2.3: Wheel loads due to acceleration and deceleration of the crab

2.3.2.3 Skewing of the crane

The behaviour of the crane system during skewing for different guidance means, is defined in the figures 2.4 and 2.5 below. The skewing angle α , referred to should be equal to or less than 0.015 radians. $\mathbf{H}_{s,i,i,T}$ are **horizontal transverse forces** during skewing. \mathbf{S} is the guidance force in reaction to these forces.

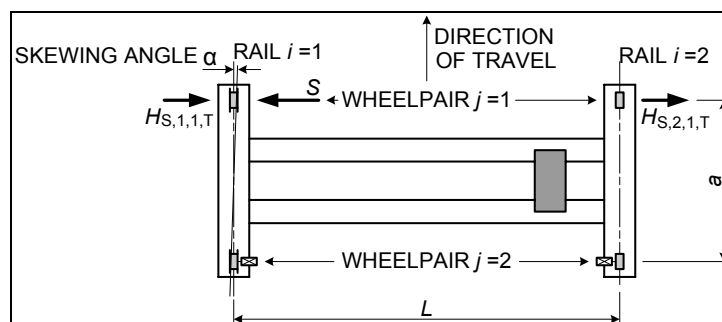


Figure 2.4: Skewing behaviour when guidance means are the wheel flanges

$H_{s,i,i,L}$ are horizontal longitudinal forces during skewing. S is the guidance force, in reaction to the force $H_{s,i,i,T}$.

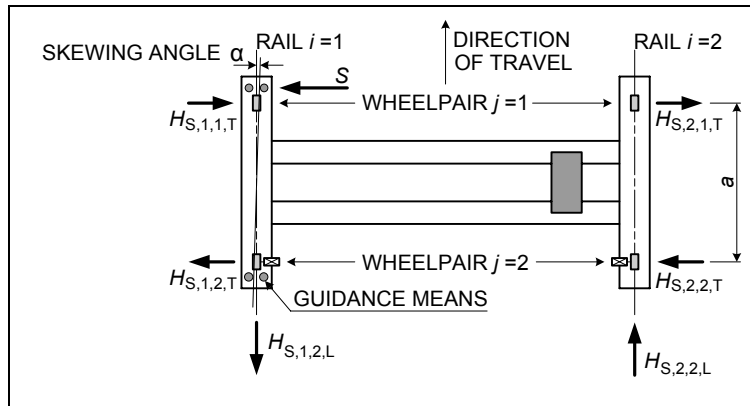


Figure 2.5: Skewing behaviour when there is a separate guidance means

The space between the guidance means and the rail as well as reasonable dimensional variation and wear of the appliance wheels and the rails should be taken into account, for determining the skewing angle.

2.3.2.4 Misalignment of crane wheels or gantry rails

A relation between the classification of the crane and the forces due to the misalignment of the crane wheels or gantry rails, are assumed. The number of wheels and the gravitational loads are directly implemented to determine the horizontal forces due to misalignment ($H_{M,i}$). The direction of these forces can also be reversed.

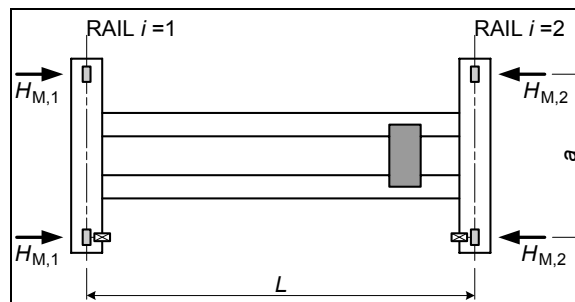


Figure 2.6: Wheel load configuration during misalignment

2.3.2.5 Impact into crane end stops

Where buffers are used, the forces on the crane supporting structure arising from collision with the end stops shall be calculated from the kinetic energy of all relevant parts of the crane moving at 0.7 to 1.0 times nominal speed.

F_{xi} is determined by analyzing the buffers as spring elements.

δ is the longitudinal deflection of the spring element.

Figure 2.7 below indicates the longitudinal impact forces and the relation of these forces to the deformation of the buffers.

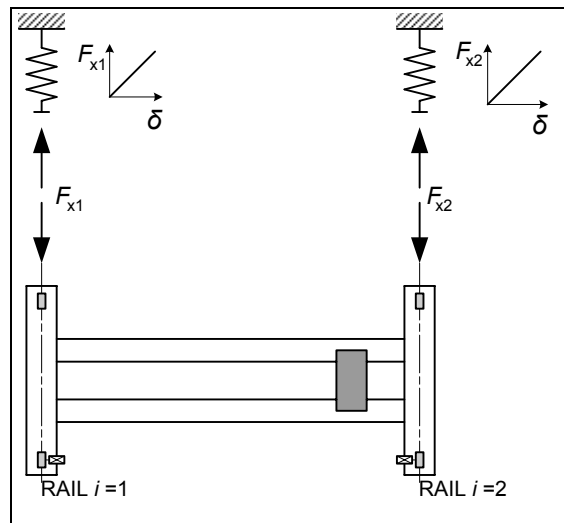
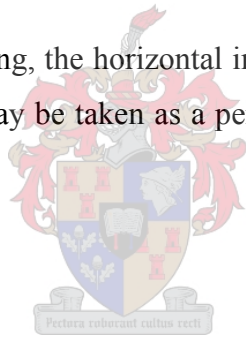


Figure 2.7: Force configuration during buffer impact

2.3.2.6 Impact into crab end stops

Provided that the payload is free to swing, the horizontal impact load representing the buffer forces related to the movement of the crab, may be taken as a percentage of the gravitational loads of the crab and hoist load.



2.4 Mechanical failure

Mechanical failure of a drive motor was experimentally investigated and is also described by Gorenc^[3]. The crane side where the mechanical failure occurs may be assumed to be jammed to a complete standstill in the worst case. The opposite end carriage of the crane is however still driven and will continue to travel forward until wheel slip occurs.

2.5 Serviceability limits

Deflections of the supporting structure in the vertical and lateral horizontal direction, are limited to span/600 for cranes of class 1 and span/1000 for cranes of class 4, according to proposed SANS 10160 Section 10. Crane Aid^[4] specifies a serviceability limit for vertical deflections of the overhead crane as (crane bridge span)/750.

2.6 Construction tolerances for supporting structure

According to South African Structural Steelwork Specifications for Construction, 1st Edition^[5], the following are parameters that must be adhered to, when erecting the supporting structure of an electric overhead travelling crane.

2.6.1 Crane gantry columns plumb

The horizontal deviation of the columns from the ground, can be 0.1% of the column's length, with a maximum deviation of 25 mm.

2.6.2 Crane gantries gauge of rail

The allowable lateral horizontal deviation between the supporting girders is dependent on the rail-to-rail distance between them. Figure 2.8 below indicates the limiting lateral horizontal parameters.

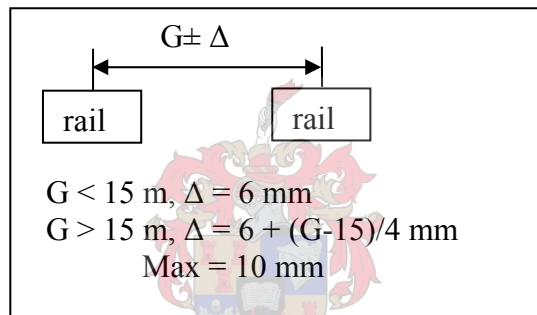


Figure 2.8: Limits on lateral deviation of supporting structure

2.6.3 Crane gantries rail track level

The maximum difference in level between the rails on the crane gantries, is 10 mm.

2.6.4 Joints in gantry crane rails

For class 1 and 2 cranes the maximum level difference at a rail joint is 2 mm.

For class 3 and 4 cranes the maximum level difference at a rail joint is 1 mm.

2.6.5 Crane rail deviation in plan

The maximum deviation of the crane rail in plan from a straight line, is 5 mm on either sides of the straight line.

2.6.6 Crane rail offset with girder web

The crane rail can be offset laterally on the crane girder, a maximum of half the thickness of the girder's web. For welded plate girders the distance from the face of the web to the end of the flanges may not deviate more than 2.5 mm on either sides. Local web distortion on the depth of the web, or along the length of the web, may not be more than 3 mm. The flanges to the web connection can have a maximum deviation of 3 mm from plumb.

2.7 Documented overhead crane research models

In defining the important parameters of the overhead travelling crane system, the general approach followed in previous documented research on overhead travelling cranes was investigated.

Frank Taylor^[6] compared the motions of a real crane and attached load with the simulated motions of a virtual crane and attached load. The characteristics of his model were as follows: Maximum velocity of crane was 0.534m/s. Maximum acceleration of crane was 0.37m/s². Angular deflection of payload's cable, from acceleration was 6.8°.

A.Z.Al-Garni^[7] developed a dynamic model of an overhead crane. In his model, the load is assumed to be concentrated at a point and hanging at the end of a mass-less cable.

The properties of his model are defined as smaller than a maximum limit.

Crane movement (speed, acc) \leq (2 m/s, 0.3 m/s²), crab movement (speed, acc) \leq (1 m/s, 0.3 m/s²) and vertical hoisting (speed, acc) \leq (0.5 m/s, 0.5 m/s²).

J.W. Auernig & H. Troger^[8] developed a mechanical model and equations of motion for overhead travelling cranes, which had the following simplified characteristics. The elastic deformation of the crane will be neglected and it will be assumed that all elements are of infinite stiffness. The change in rope length, due to swinging of the load, has been neglected.

Lee, Ho-Hoon^[9] developed a new approach for the anti-swing control of overhead cranes. This system proposes to help guide the crane in the longitudinal direction, so as to decrease the pendulum action of the payload.

R. Karmakar & A. Mukherjee^[10] made the following assumptions, to solve the mathematical crane model, which they developed. Critical dynamic loading occurs when the crab is at mid-span of the crane bridge. This model neglects shear deformation of the system. The end carriages supporting the elastic crane bridge, behave as simply supported beams, which are considered to be rigid for simplicity. The rope stiffness is considered to be inversely proportional to its length. When the hoist mechanism starts winding, the rope gets stretched and the girder deflects downwards. The load begins to be hoisted off the ground as soon as rope tension becomes greater than the load.

The results from these documented research reports will be compared with the experimentally determined characteristics of the overhead crane in chapter 9.

2.8 Experimental techniques

Strain gauges are to be used in this experimental investigation of the behaviour of an electric overhead travelling crane system. To understand the principles involved in implementing strain gauges correctly, the books by Karl Hoffmann^[11] and Louis Eder^[12] are very useful. The basic principles involved in experimentally measuring different types of strains, by implementing different types of Wheatstone bridge connections, are described.

2.9 Reference load models for investigation

This literature review indicates that the current South African loading code SABS 0160-1989 is more simplistic than EN 1991-3. The methodology for using coefficients for determining forces due to misalignment and lateral acceleration of the crab did not change, from SABS 0160-1989 to the proposed SANS 10160 Section 10. The load models of the proposed SANS 10160 Section 10, are defined and will be used as a reference during the experimental investigation. Chapter 9 will focus on comparing the results from literature on the behaviour of electric overhead travelling cranes, with the experimentally determined results in this thesis.

Chapter 3 – EOTC supporting structure

In this chapter the properties of the supporting structure will be described. The governing force sign convention in 3 dimensions, the force measuring capabilities implemented in the supporting structure and in the payload, will be described.

3.1 Definition of supporting members

The main members of the supporting structure, which are defined below, can be seen in figure 3.1 on the next page.

The **crane supporting columns** are UC 152x152x25 sections, with a strong axis orientation in the lateral direction. They are designed with the functionality of inserting or removing a load cell above the pin connected ball-joint base.

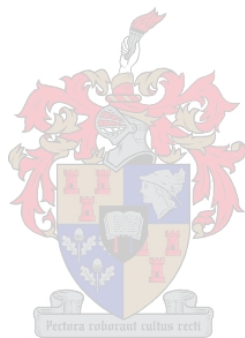
Simply supported, welded mono-symmetric **plate girders** are fixed on top of these columns. The top flange is wider than the bottom flange, to increase its moment of inertia against lateral horizontal forces. **Lateral horizontal restraining rods** connect the top flange of the girder to the reinforced concrete walls of the laboratory.

The **building columns** are connected in the lateral direction to the top flange of the girders and the capping plate of the crane supporting columns. These building columns are designed so that their lateral restraint at the top of the column, stiffness of base connection and the lay-out of the supporting structure can be modified to a portal frame, for future experimental research.

The longitudinal **bracing system** consists of symmetric angle sections fixed together to form a cross, which are fixed onto a frame made up of UC- sections, to increase the longitudinal stiffness of the supporting structure. Their design load is dependent on the applicable buffer impact forces.

A 7mm thick continuous **Gantrax pad** is positioned between the bottom flange of the rail and the top flange of the girder. It helps to distribute the vertical force onto the crane girder and increases the vertical elasticity of the system.

The **rail clips** are used to fasten the rails to the top flange of the crane girder. The lateral alignment of the rails can be adjusted with the rail clips. The rubber on the rail clips increase the elasticity of the system in the lateral direction. They are spaced at 0.4 m centres on both sides of the rail, which is very close, if compared with the acceptable norm. The **crane rail** is a 35 kg/m rail. For a 5 ton overhead crane, this rail size is larger than the norm.



3.2 Calibration of force measuring system

Load cells and lateral supporting rods with strain gauges on, were implemented in the supporting structure, to determine the behaviour thereof under loading. To achieve accurate experimental results, these load cells needed to be calibrated independent of the supporting structure. A Zwick Z250 universal material testing machine was used. Photo 3.1 shows the Zwick and the computer system on which the calibration was performed.



Photo 3.1: Zwick Z250 and computer system

The load cells were calibrated under axial compressive loads, as indicated in Photo 3.2 below.



Photo 3.2: Load cell calibrated under axial load

During this experimental investigation, forces are applied onto the supporting structure at different positions, in different directions. A fixed sign convention was defined for all the force measuring equipment implemented in the supporting structure, as indicated in figure 3.3 below. Columns, rods and end stops are areas where force-measuring equipment were implemented. They are graphically represented as the C-(column), R-(rod) and E-(end stop) in the same figure. The second alphabetical symbols are sequential for the data capturing equipment, as defined in the ISE-laboratory.

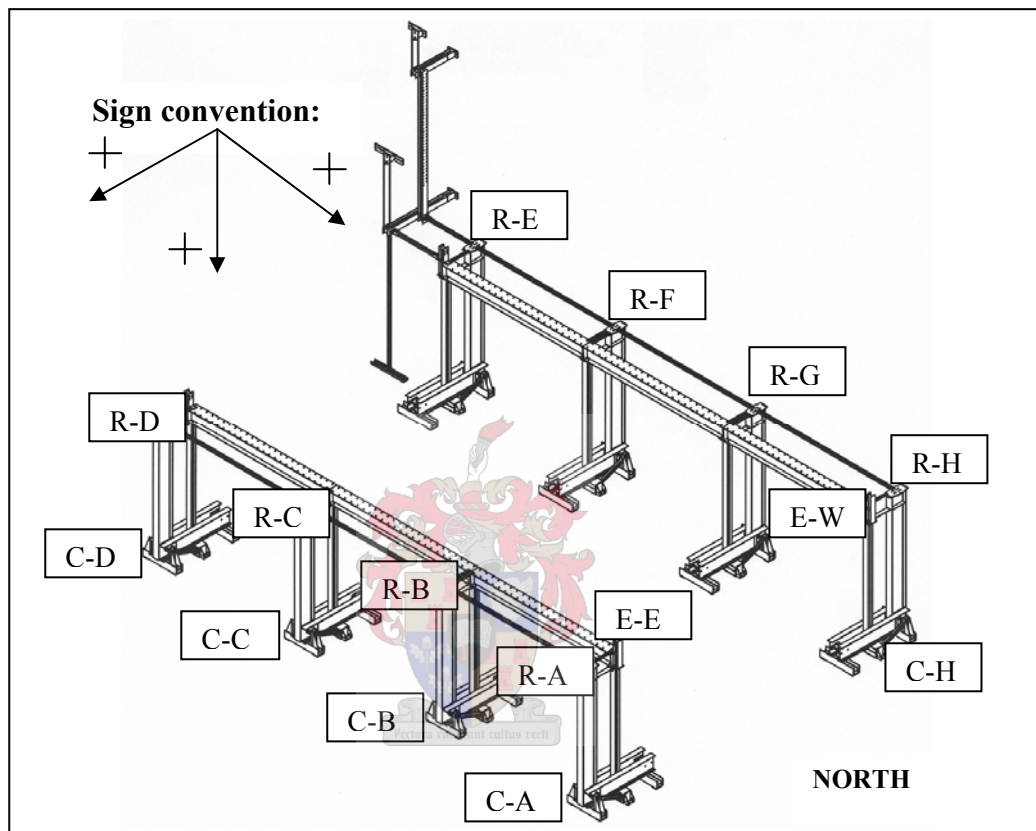


Figure 3.2: Load measuring instrumentation implemented in supporting structure

The load cells underneath the crane supporting columns measure the vertical forces that are applied by the crane, due to its own weight and also the influence of the payload on the behaviour of the crane and supporting structure. Only load cells C-A, C-B, C-C and C-D were calibrated and used during this experimental investigation.

The M24 lateral restraining rods have strain gauges mounted on them, which allowed the measuring of the axial strain in the rods. Only rods R-A, R-B, R-C and R-D were calibrated in the Zwick. The average calibration coefficient was then implemented on R-E, R-F, R-G and R-H.

The load cells mounted onto the end stops, allowed the measuring of the buffer-end stop forces during longitudinal crane impact. E-E refers to end stop East and E-W refers to end stop West.

3.3 Payload to be used in experimental investigation

A 5 ton payload was designed and built with a calibrated load cell at the top between the payload and the hook of the crab, for the measurement of the forces in the cable due to the crane hoisting the payload. The payload consists of 28 lead blocks, each weighing 1 kN, bolted onto a single concrete block weighing 22 kN. The center of gravity of the payload was calculated to be 0.41 m below the top surface of the payload.



Photo 3.3: 5 ton payload with load cell

In this chapter the characteristic properties of the crane supporting structure were defined. The sign convention in 3 dimensions, the force measuring characteristics of the supporting structure and that of the payload were defined.

Chapter 4 – Overhead crane and instrumentation

The characteristics of the overhead crane and the data capturing instrumentation on the overhead crane, are defined in this chapter. The orientation of the crane relative to the supporting structure and governing sign convention, will also be defined.

4.1 Design drawings of overhead crane

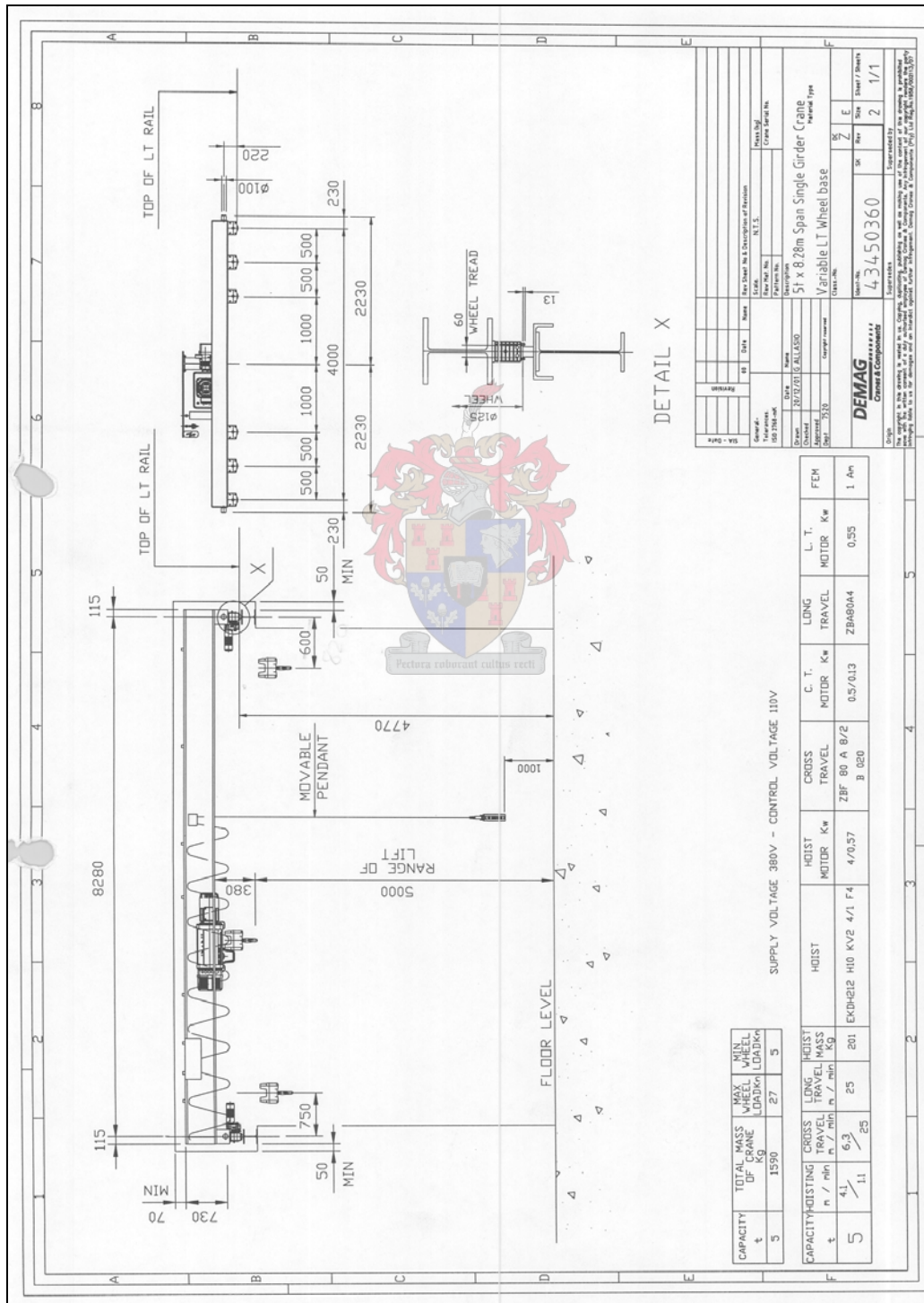


Figure 4.1: Design drawing of overhead crane (girder and rail not as built)

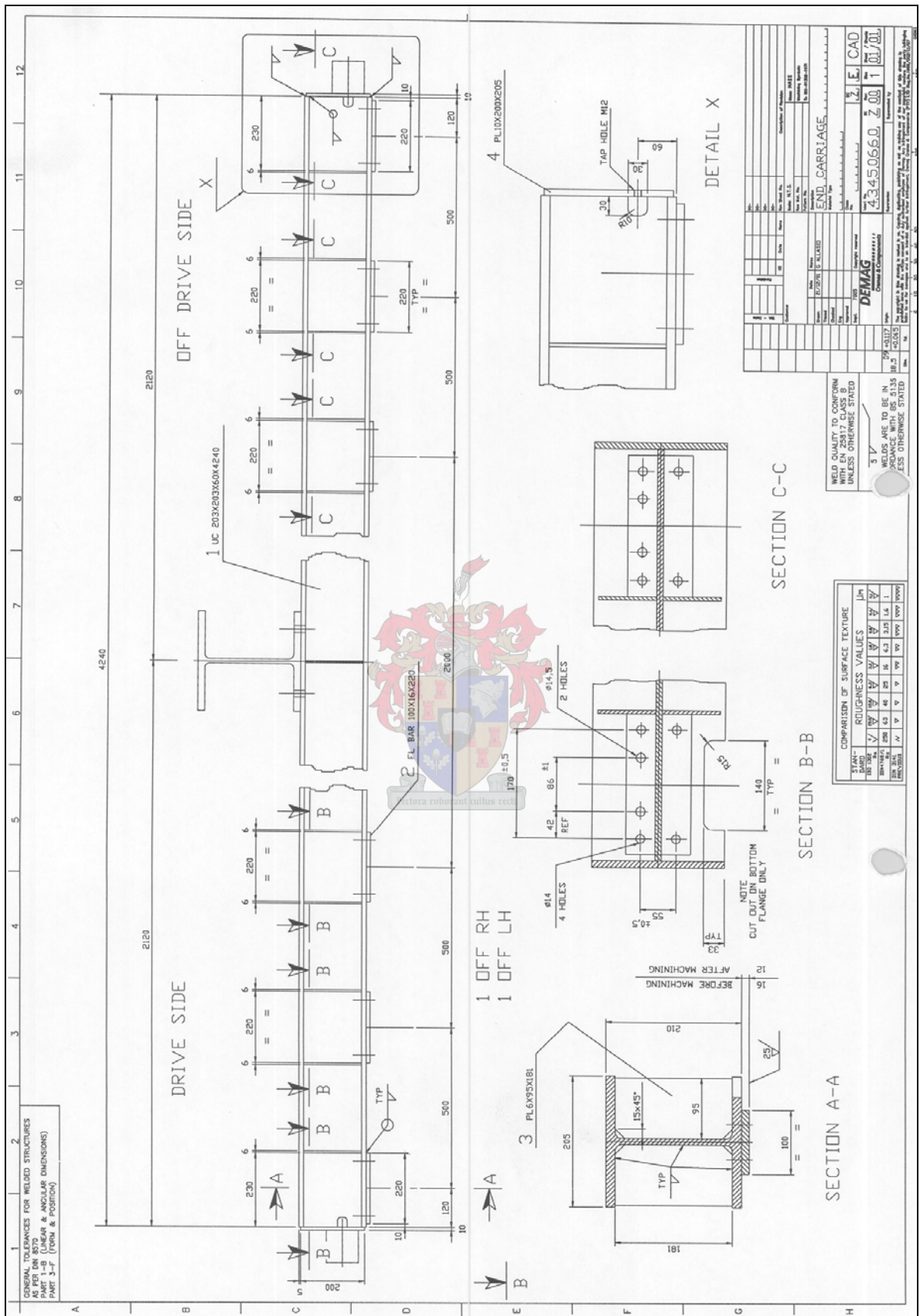


Figure 4.2: Detail drawing of end carriages

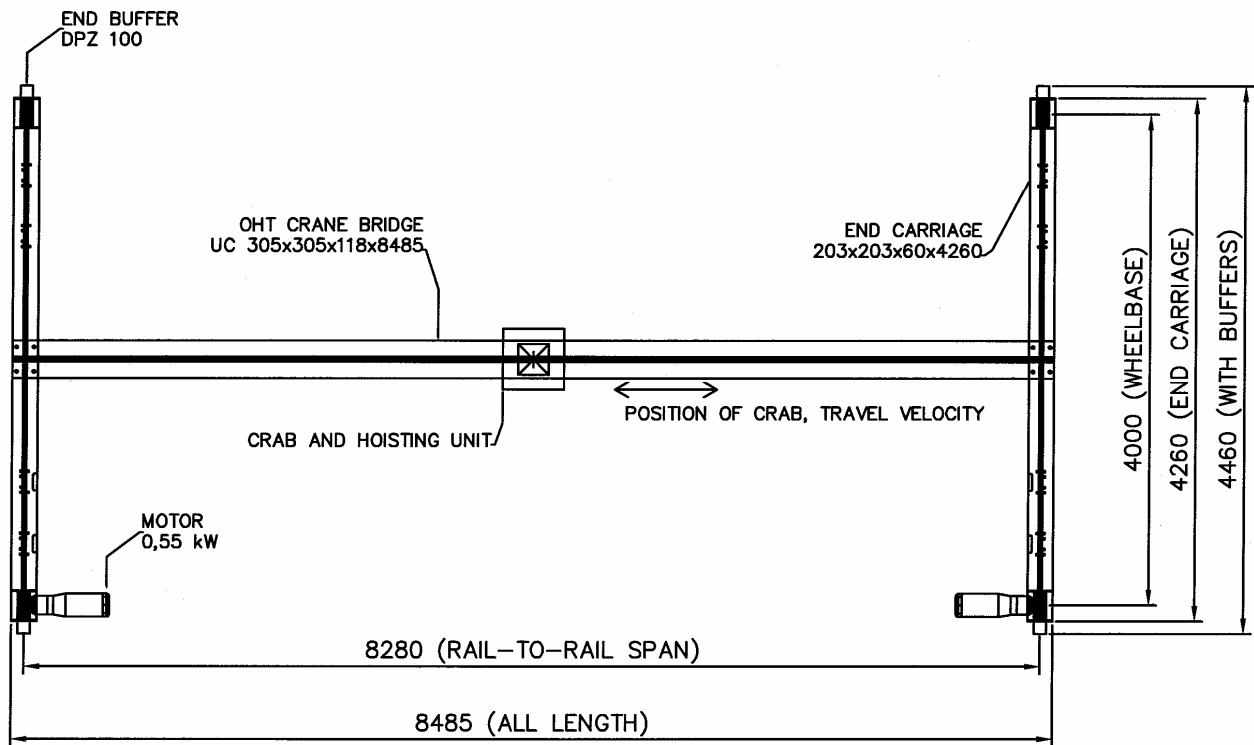


Figure 4.3: Plan view of overhead crane

4.2 Crane orientation and sign convention of wheel forces

The orientation of the crane and its wheels relative to the supporting structure and the force sign convention used in this experimental investigation, are indicated in figure 4.4 below.

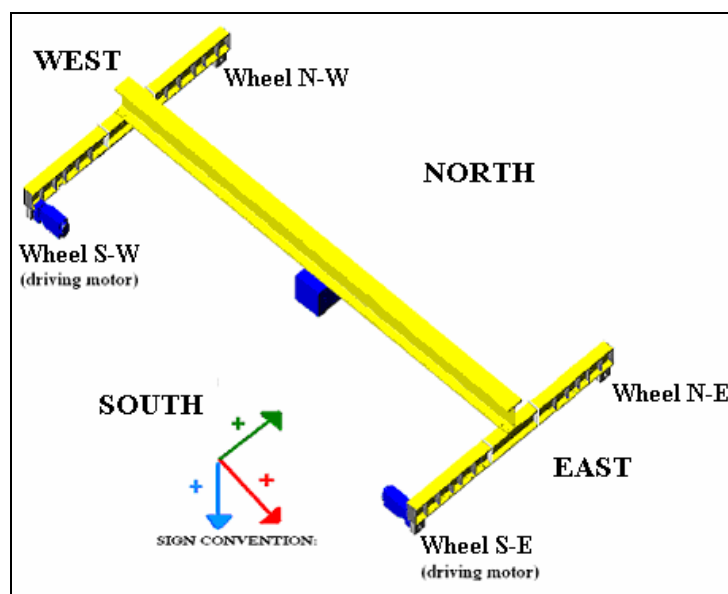


Figure 4.4: Orientation of crane relative to supporting structure

4.3 Characteristics of crane

Information about the crane's characteristics is indicated in figure 4.1 above. The physical behaviour of the crane, which is a result of electrical and mechanical systems, was verified experimentally, through numerous tests.

All the electrical systems, which control the mechanical systems, were housed in a steel box, which was bolted onto the crane bridge. This box weighs 0.9 kN.

4.3.1 Longitudinal crane motion:

Acceleration: 0.2m/s^2 in approx. 2.7 seconds

Max Speed: 0.55m/s

Deceleration: 0.22m/s^2 in approx. 2.5 seconds, due to braking mechanism

These characteristic properties are influenced by the capacity of the electrical motors.

This does not include the possible acceleration or deceleration due to the payloads pendulum action, or the deceleration encountered, when the crane cannot traverse an uneven rail joint.



Photo 4.1: Electrical driving motor at crane wheel

The electrical motors at the crane wheels, as shown in figure 4.3 above, have the following specifications:

Power : 0.55 kW , 1410 rpm

Brakes : 5.6 Nm

Weight: 19.5 kg

A switch in the electrical system allows deactivation of the electrical motor at wheel S-E.

This allows experimental investigation of an exceptional loading scenario, known as 'failure of driving mechanism', which induces skewing behaviour of the crane.

The mechanical safety mechanism for longitudinal crane travel, indicated in photo 4.2 below, was deactivated to allow for longitudinal impact tests on end stops.



Photo 4.2: Emergency cut-out mechanism for longitudinal crane travel

4.3.2 Lateral crab motion:

Slow speed:

Acceleration: 0.056m/s^2 in approx. 0.3 seconds

Speed: 0.11m/s

Deceleration: 0.056m/s^2 in approx. 0.3 seconds

Fast speed:

Initial speed :

Acceleration: 0.4m/s^2 in 0.2 seconds.

Slow speed for 2.1 seconds @ 0.11m/s .

Secondary fast speed:

Acceleration: 0.5m/s^2 in 0.5 seconds.

Fast speed : 0.45m/s .

Deceleration: 0.35m/s^2 in approx. 1.3 second.

The electrical motor for lateral travel of the crab, has the following specifications:

Slow/fast speed:

Power : $0.13/0.5\text{ kW}$, $640/1410\text{ rpm}$

Brakes: 3.3 Nm

The mechanical safety mechanism that de-activates the lateral crab movement, can be seen in photo 4.3 below.



Photo 4.3: Electrical motor on crab for lateral motion

4.3.3 Hoisting behaviour of crab:

Slow speed: 0.02 m/s for 4.7 seconds.

Fast speed: 0.075 m/s

Maximum normal acceleration occurs when payload is suddenly lowered: 1.0 m/s²

The electrical hoist mechanism at the crab has the following specifications:

Power : Slow speed - 0.97 kW, 680 rpm

Fast speed - 4 kW, 2805 rpm

Brakes : IP 20

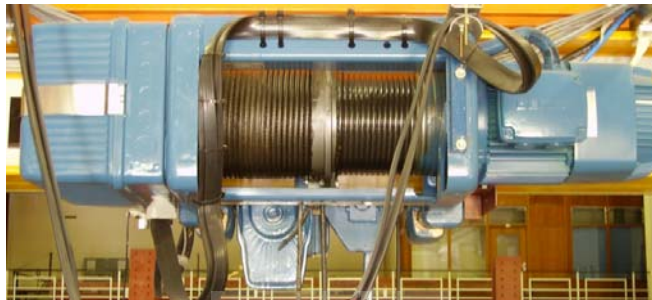


Photo 4.4: Hoist drive mechanism on crab

4.4 Crab/Payload position

The points indicated in figure 4.5 below on the crane bridge are used as reference points in this experimental investigation. The mid-span position of the crab on the crane bridge was determined and is referred to as point **A**. The most eccentric positions of the crab, due to the electric cut-out switches, are referred to as points **B1** and **C1**.

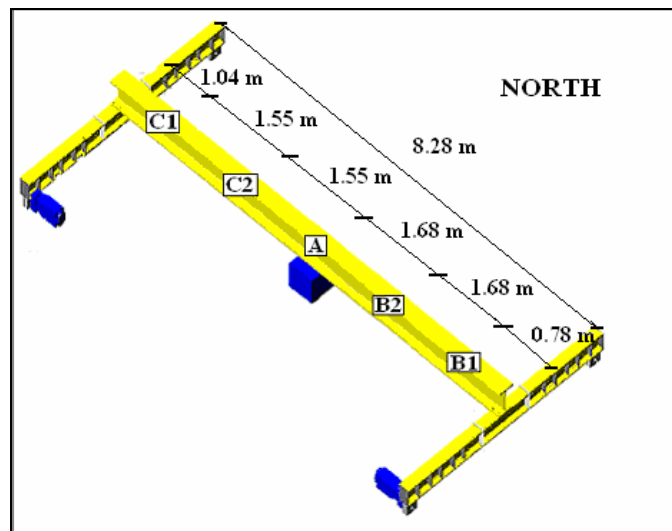


Figure 4.5: Definition of reference points on the crane bridge

B1 is the critical crab position, due to the unsymmetrical position of the mechanical cut-out switch on the crab as can be seen on photo 4.3.

4.5 Strain gauges on overhead crane

There are 48 strain gauges on the end carriages of the crane, which give 24 strain results, which will be used to transform the end carriages into a load measuring system. These strain gauges are numbered SG_1 to SG_27 and their positions are indicated in the cross sectional views of the end carriages, in the figure 4.6 below. The strain gauges are connected to Wheatstone bridges. Refer to Appendix B2 for details relating to the different Wheatstone bridges.

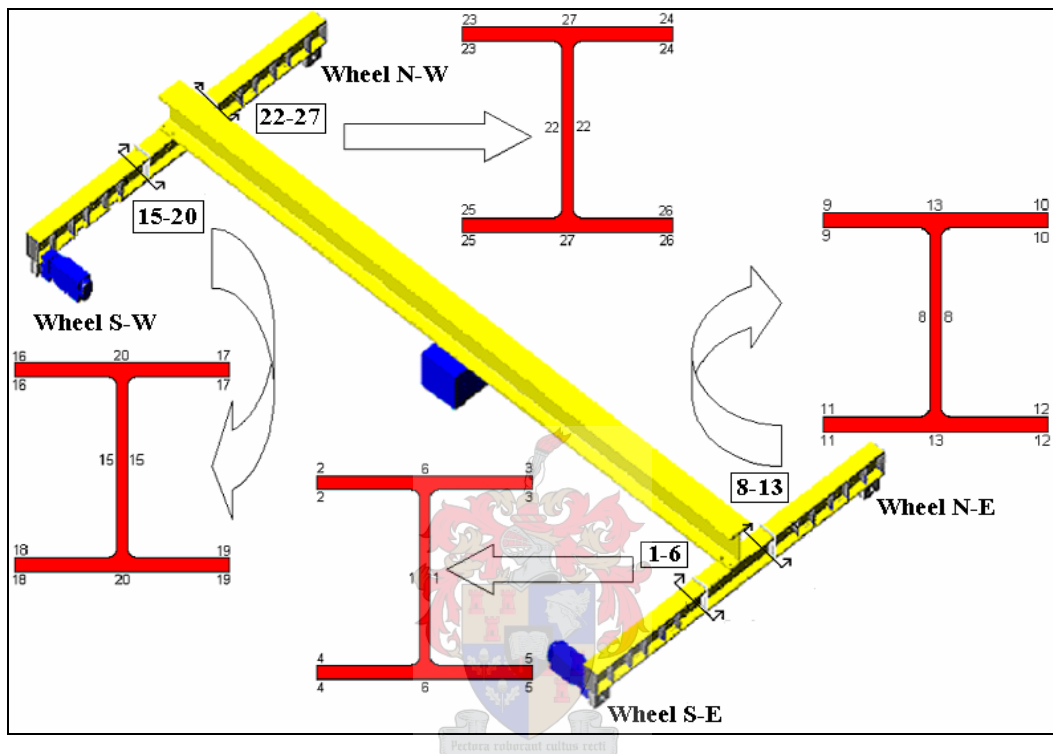


Figure 4.6: Orientation of strain gauges on end carriage load measuring system

The identical numbers on the edges of the flanges, refer to two strain gauges giving an average normal longitudinal strain at those locations. The strain gauges at the centre of the top and bottom flanges give only strong axis bending strains at the outside fibres of the cross section.

The strain gauges at the centre of the web are close to the neutral axis of the end carriages. The theoretical longitudinal strain at the neutral axis due to bending of the end carriages is zero. This resulted in the experimental longitudinal strain at those points being very low.

In retrospect, a more economical strain gauge layout at the edges of the flanges could have been to apply a single strain gauge, on the centre line of the flanges, on the outside.

4.6 Encoders and accelerometers on overhead crane

The position of encoders that were fixed onto the axle of the crane's wheels and accelerometers, which were fixed directly onto the crane and crab are indicated in the figure 4.7 below.

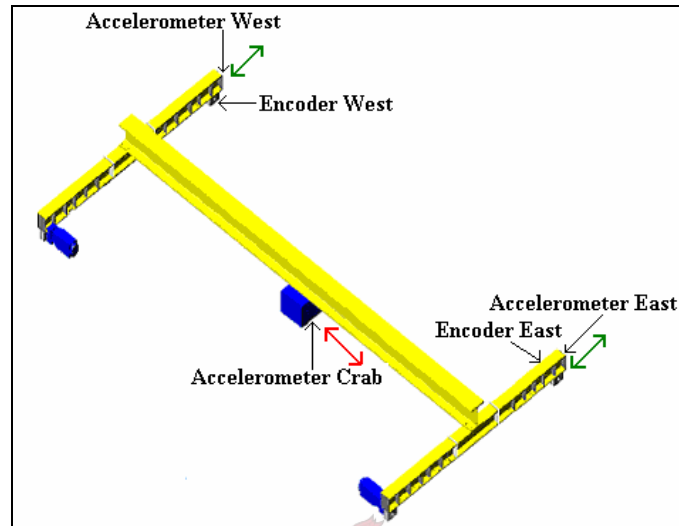


Figure 4.7: Position of encoders and accelerometers

Encoders measure rotational displacements per unit of time. One rotation of the crane's wheel axle in a second, results in a measurement of 100 units. This is multiplied with the circumference of the cranes wheels. This gives the relative crane displacement per measurement interval. These values are then added consecutively and multiplied with the measuring period, to give the relative displacement over time of the crane, as it traverses longitudinally. This data was also used to determine the cranes maximum longitudinal traversing speed.

Accelerometers were used to determine the acceleration that the crane and crab experience. This has a direct influence on the crane's wheel force behaviour. Gravity (9.81m/s^2) was used as a calibration parameter for the accelerometers.

The orientation of the crane relative to the supporting structure and governing force sign convention of the wheel forces of the crane onto the supporting structure, were defined in this chapter.

The characteristics of the overhead crane, its mechanical components and the data capturing instrumentation on the overhead crane, were also defined.

Chapter 5 – Numerical modelling of crane

A numerical model of the overhead crane was developed to determine the crane's behaviour under loading. This numerical model will give insight into the stress behaviour of the crane, which experimentally determined stress results would not give. These numerical results will be compared with the experimentally calibrated crane's behaviour in the next chapter.

5.1 Discrete element beam model

A numerical crane model consisting of beam elements was developed.

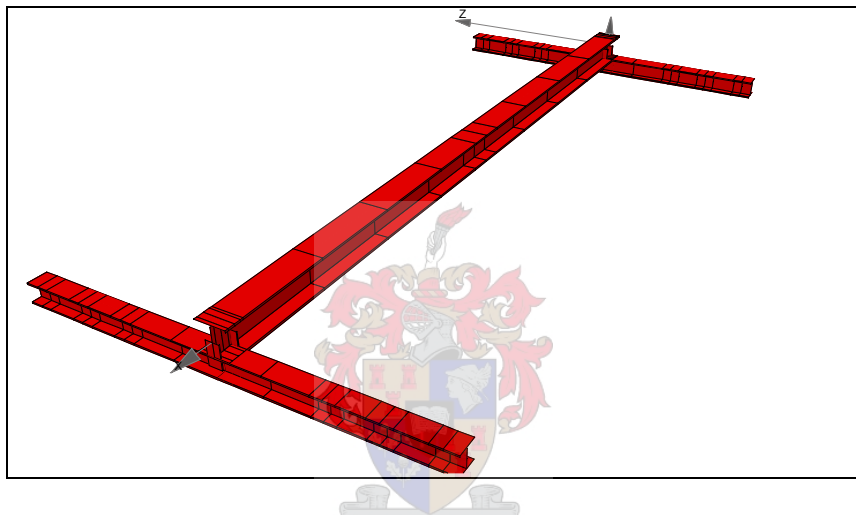


Figure 5.1: Beam element model of crane

This model consists of approximately 60 nodes. When vertical loading is applied onto the crane bridge, it deflects downwards. This results in a rotational deformation at the crane bridge to end carriage connection. This rotation results in torsional deformation of the end carriages. The beam element model was unable to model these torsional deformations in the end carriages. This resulted in further investigation into a more appropriate numerical analysis technique.

5.2 Finite element shell model

The crane is modelled by shell elements, which are defined by the shell centre lines, with the corresponding shell thickness assigned to each member. Figure 5.2 below shows the finite element model including the boundary conditions for the different loading situations.

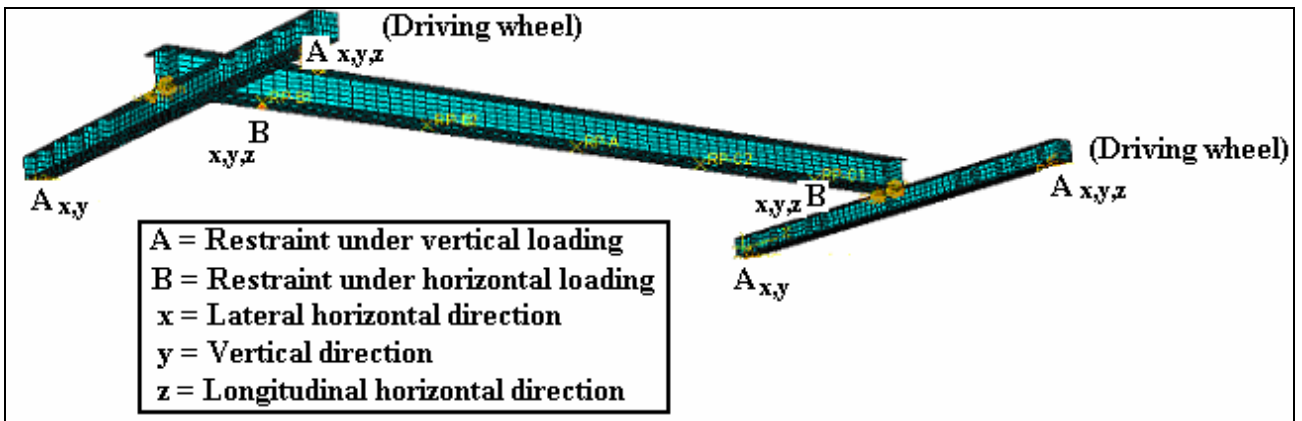


Figure 5.2: Shell element model of crane

The model consists of 4192 elements and 4341 nodes. The shell element mesh of the numerical model is defined so that nodes of the numerical model correspond to points on the experimental crane that are important for modelling it accurately, for example the positions of the strain gauges. The crane bridge has a top seated bolted connection onto the end carriages. The nodes at the bolt positions of the bottom flange of the crane bridge and the top flange of the end carriage have rigid links between them to simulate the bolted connection. The strain gauge positions on the experimental crane also correspond to nodes on the numerical model.

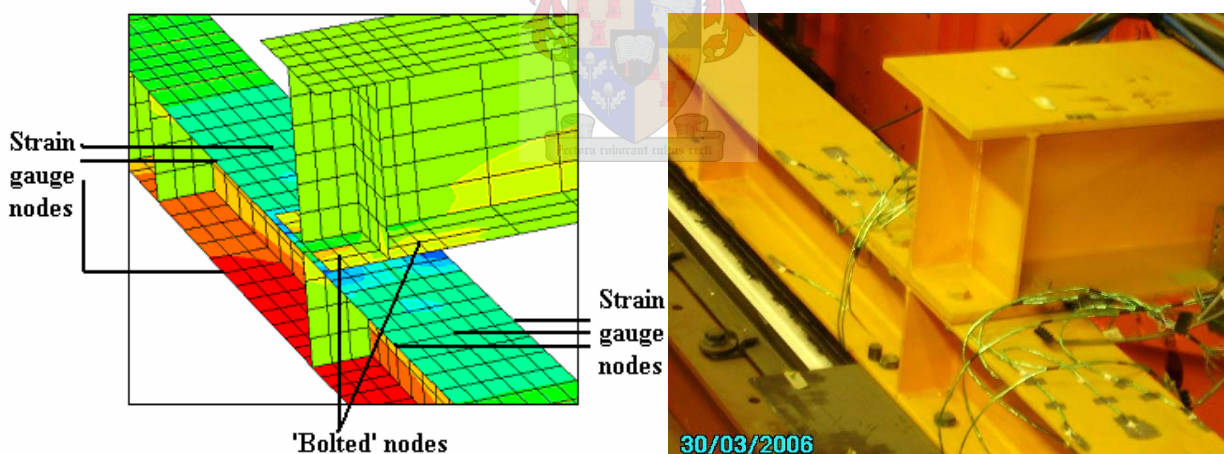


Figure 5.3: Numerical model of crane bridge to end carriage connection

Each node has three translational and three rotational degrees of freedom. The own weight effect of the crane was not investigated with this model. External vertical point loads and external horizontal point loads were applied onto the crane, to determine its behaviour under loading. The analysis consisted of 15 incremental steps for each analysis in the linear elastic domain of the material, with a modulus of elasticity of 210 GPa. These load cases and the relevant supported points of the crane and the resulting behaviour of the crane will be compared with the experimental calibration results in the next chapter.

5.2.1 Vertical load on crane bridge

A concentrated load of 50 kN was applied onto the bottom of the crane bridge to simulate the hoisting of the 5 ton payload. Figure 5.4 below indicates the maximum vertical deflections and bending stress of the crane bridge, at the specified points, due to the 50 kN concentrated load being applied at those points.

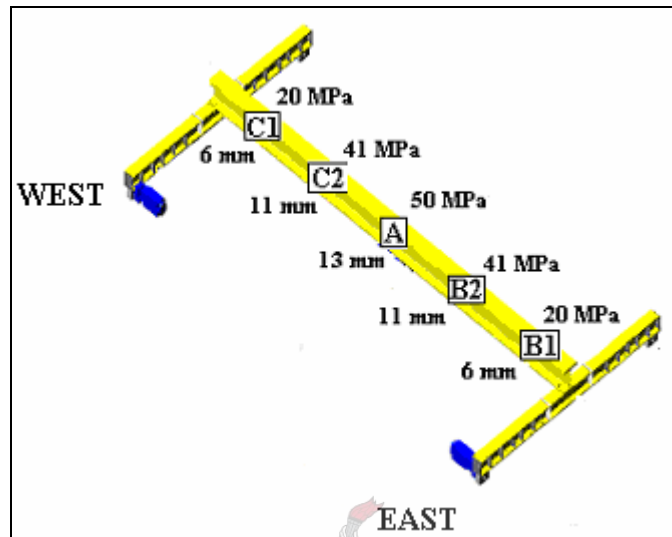


Figure 5.4: Vertical deflection and bending stress behaviour of the crane bridge

The deflection of the crane bridge due to these vertical loads, induces vertical deflections and rotation of the end carriages. The vertical deflections induce linear **compressive stresses in the top flanges** at the strain gauge positions as indicated in figure 5.5 below, for different positions of vertical loading indicated at the top of the figure. The maximum compressive stress is 58 MPa.

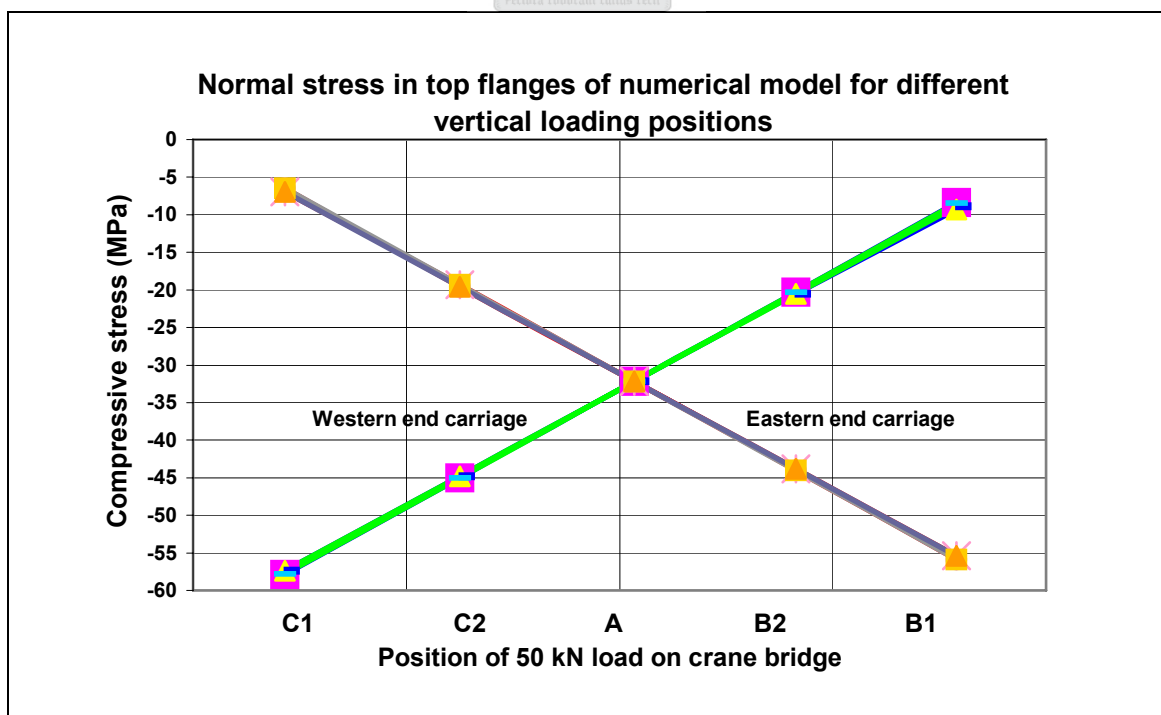


Figure 5.5: Compressive stress in top flange of end carriages

The rotation of the end carriages due to vertical load on the crane, results in lateral horizontal loads at the wheel points, which are highest when the load is at the middle of the crane bridge (position A). These maximum lateral horizontal loads at the wheels of 0.65 kN, which acts outward from the crane, cause the **tensile stress in the bottom flanges** to deviate by 18 MPa from each other, as indicated in figure 5.6 below.

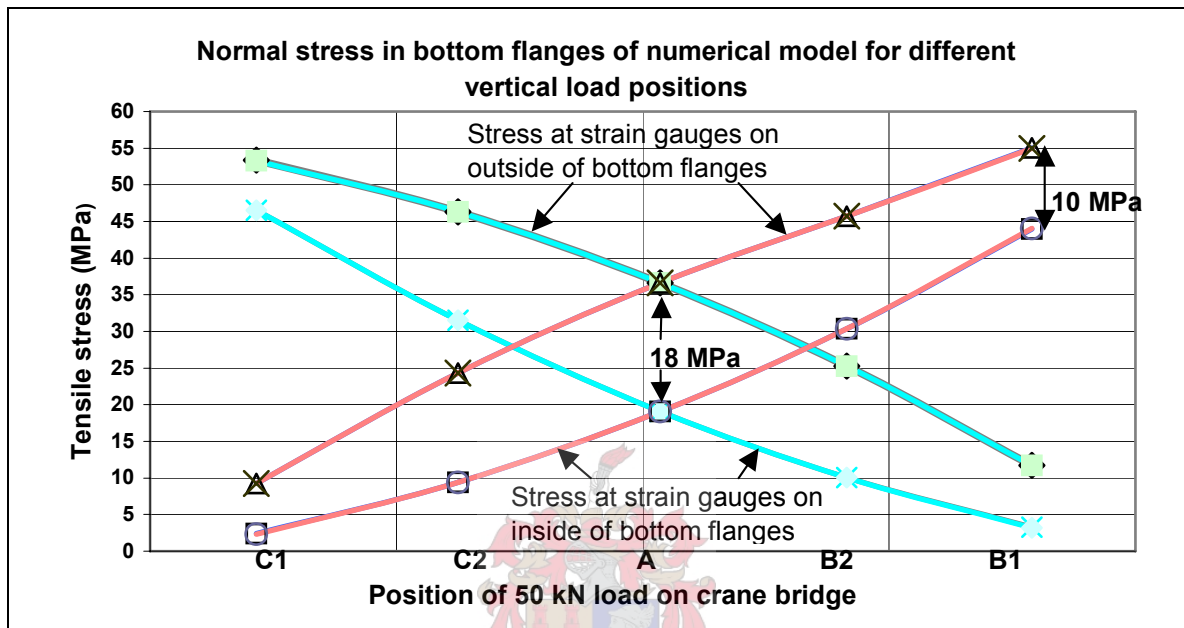


Figure 5.6: Tensile stress in bottom flanges of end carriages

It was observed that the magnitude in stress deviation in the bottom flanges due to static vertical loads, is related to the magnitude of lateral horizontal wheel loads.

5.2.2 Lateral horizontal loads on end carriage

The wheel node is eccentric in the vertical direction from the neutral axis of the end carriages. A lateral horizontal load was applied at the neutral axis of the end carriage, to determine the weak axis bending behaviour due to this force. The stress result from this load model deviated from the standard weak axis bending behaviour of a fully restraint beam, due to the top flange being restraint, while the bottom flange was not fully restrained. The stress at the top flange at the strain gauge positions was higher than in the bottom flange. This load model indicated that the actual stress response was not simplistic and that this numerical model is important to understand the stress behaviour of the crane.

The following are some of the behavioural stress patterns that were observed in the end carriages, due to a lateral horizontal load at one wheel. The normal stress behaviour in the end carriage due to a single lateral horizontal load at one wheel can be separated into two dominant behaviours, which are not necessarily exclusive. Weak axis bending behaviour in the flanges at the corresponding side of the horizontal load and warping torsional behaviour in the flanges at the opposite side, to achieve stress equilibrium at the strain gauge positions at the flanges, as indicated in figure 5.7 below.

Refer to figure 6.6 for the experimental results, that correspond to the scenario indicated below.

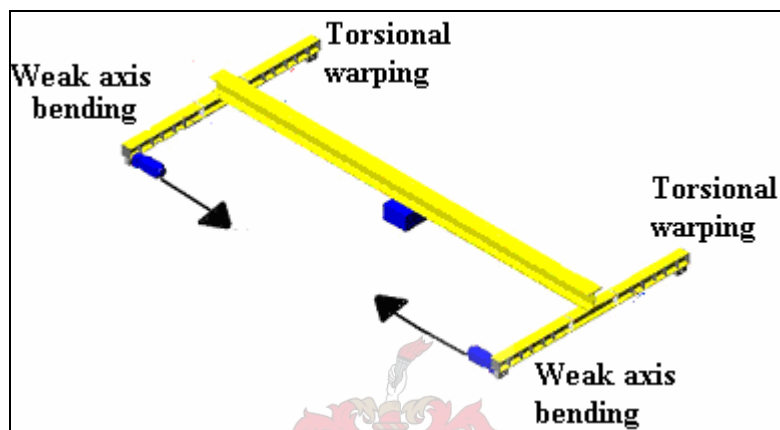


Figure 5.7: Typical stress behaviour due to lateral horizontal wheel loads

Refer to Appendix C1 for a theoretical description of these measured stress behaviours.

If all the wheels are pulled together due to lateral horizontal loads, the stress is concentrated in the bottom flanges. If the wheels on one side are pulled closer and the wheels on the other side are pulled apart due to lateral horizontal loads, the stresses are concentrated in the top flange. These stress concentrations are a result of the interaction of the weak axis bending stress and torsional warping stress in the flanges. The stress behaviour at the edges of the flanges close to a web stiffener deviates and these regions are not ideal for experimental stress measurements.

This numerical model gave insight into the stress behaviour of the crane, under vertical and lateral horizontal loading. This will help understand experimentally determined stress results in the next chapters.

Chapter 6 – Calibration of end carriage load measuring system and supporting structure

The calibration of the end carriage load measuring system and supporting structure is described in this chapter. The different configurations of externally applied wheel loads onto the end carriages of the crane for these calibrations are described. The influence of a continuous rail over a simply supported girder connection on the behaviour of the supporting structure is also investigated during the calibration of the supporting structure.

6.1 Configuration of crane during calibration process

Photo 6.1 indicates the crane's position on the laboratory floor, relative to the supporting structure, during calibration of the end carriage load measuring system.



Photo 6.1: Crane orientation on floor during calibration process

6.2 Strain data transformation

When an axial force is applied to a structure, the length of the structure changes. Strain is the ratio of this change in length from the original length. As the strain gauge is glued to the structure, any distortion will also cause a distortion of the strain gauge. The strain gauge contains conducting material and the distortion results in a change in its resistance, which can be measured by the strain gauge.

A table in the book by Louis Eder^[17] reference the Wheatstone bridge configurations for transforming actual strain data. Hooke's law states that the relationship between stress and strain is linear. This experimental investigation will be limited to this specified domain.

ϵ_n = normal strain and ϵ_b = bending strain

k (property of the specific strain gauge) = 2.14

x = change in strain per volt applied (mV/V)

E (Youngs modulus) = 210GPa

Normal stress: $\sigma_n = \epsilon_n \cdot E = 2/k \cdot x \cdot E$

Bending stress: $\sigma_b = \epsilon_b \cdot E = 2/k \cdot x \cdot E$

Shear stress can not be measured directly by the current strain gauge configuration.

Figures 6.1 below indicate the cross section of the end carriages with the general normal stress responses at the strain gauges on the flanges, for respectively, weak axis bending, strong axis bending and torsional deformation. The positive signs (+) refer to tensile normal stress and the negative signs (-) refer to compressive normal stress, measured at the strain gauges. The total absolute stress response is calculated with the following algebraic summation, referring to the symbols in figure 6.1 below. $(B + D) - (C + E) = \text{total absolute stress due to wheel loading}$.

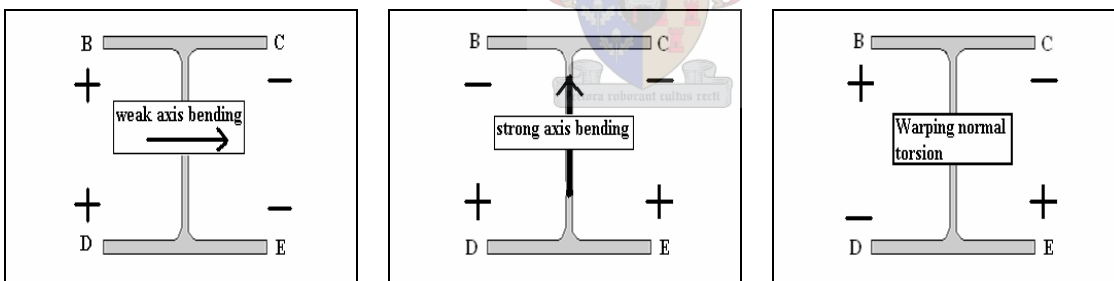


Figure 6.1: General normal stress response at strain gauges on flanges of end carriages, due to wheel loads

This algebraic summation was determined by post-processing of the experimental data. This algebraic summation causes the normal stress due to weak axis bending to be a maximum value, while the normal stress due to strong axis bending and the normal stress due to warping normal torsion to cancel each other out. By implementing this algebraic summation, the normal stress (MPa) per unit of applied lateral horizontal wheel load (kN), which causes weak axis bending, will be determined.

6.3 Calibration for measuring vertical wheel loads

Figure 6.2 below indicates the position of supporting points and load cells relative to the wheels in the vertical plane, during the calibration of the vertical wheel loads.

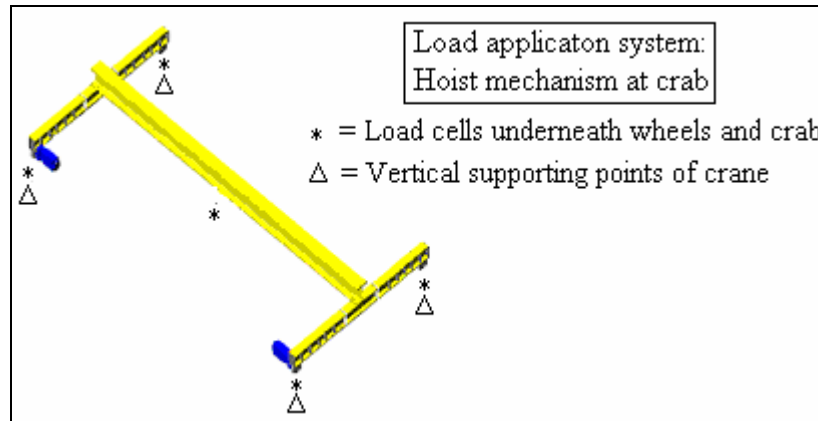


Figure 6.2: Load cells and support point positions for vertical force calibrations

Photo 6.2 shows the load cell fixed to the laboratory floor, below the center of the crane bridge, onto which the hoisting mechanism of the crane was connected. The zero reading was taken with the crane resting on top of the supports at the wheels, before the hoisting mechanism was activated. The vertical deflection at the centre of the crane bridge, reaction forces at the wheels and bending stress at the strain gauges was then measured, during the increase in force at the center of the crane bridge. The load cell in photo 6.2 was also used to verify the reaction force results at the crane wheels. The bending stress at the strain gauges was then calibrated against the reaction forces at the wheels.



Photo 6.2: Load cell bolted to floor to simulate payload hoisting

Due to the deflection of the crane bridge and end carriages under loading, rotation at the crane bridge to end carriage connection occurred, which resulted in lateral and longitudinal horizontal reaction forces at the wheels. These horizontal reaction forces influenced the normal stress behaviour at the strain gauges at the edges at the flanges. This resulted in only the bending stress data being used. A linear relation between vertical wheel loads and bending stress, for each of the wheels are defined in figure 6.3 below.

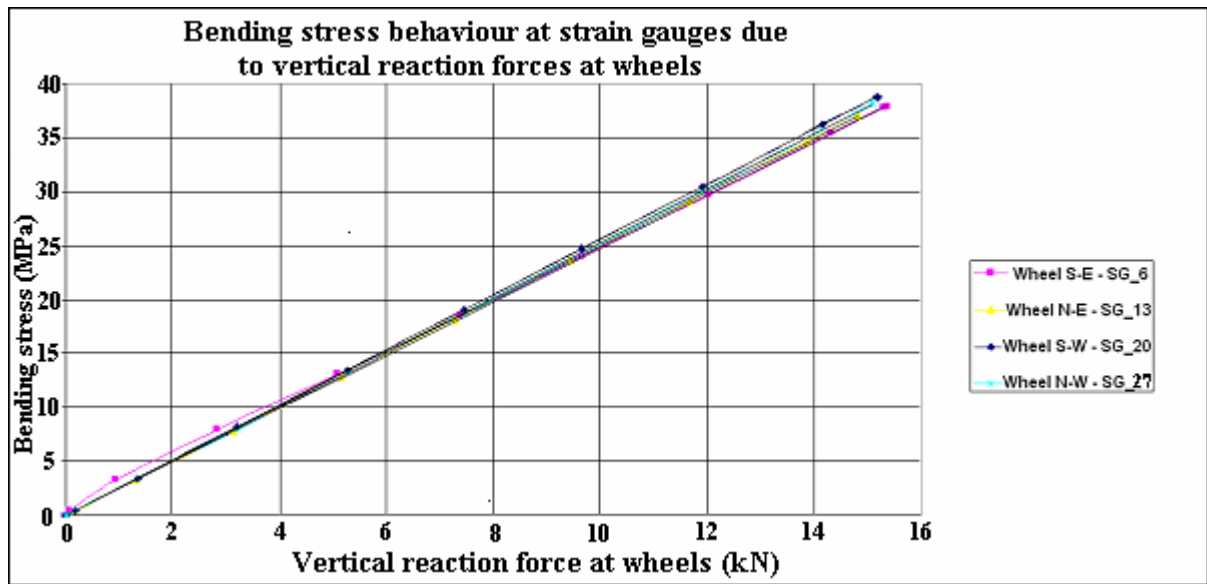


Figure 6.3: Bending stress behaviour at strain gauges

The vertical calibration results are summarized in figure 6.4 below.

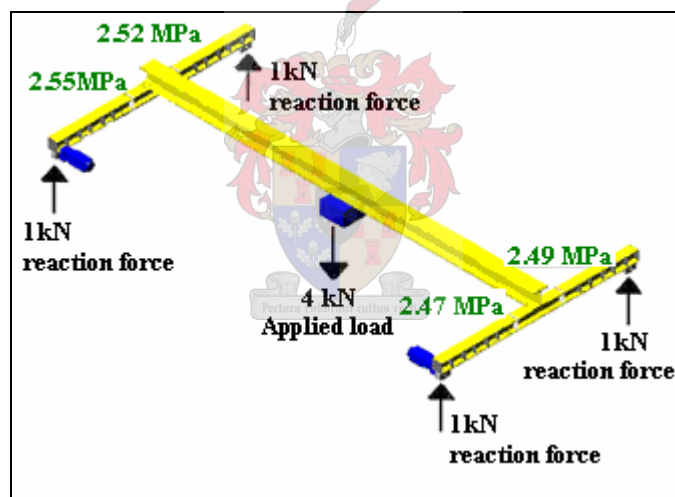


Figure 6.4: Linear elastic bending stress behaviour of end carriage load measuring system

A ratio of **bending stress** due to vertical wheel load of **2.5 MPa/kN** was used during the experimental investigation. This is a maximum deviation of 2% from the calibrated results at wheel S-W.

6.4 Calibrations for measuring lateral horizontal wheel loads

These calibrations required that there was no contact between the wheel and the rail supports underneath the wheels. Wheel to rail contact would result in frictional forces, influencing the measured strains. Figure 6.4 below indicates the position of the hydraulic jacks supporting the crane to prevent wheel to rail contact after the zero reading was taken. The orientation of the load cell

positions relative to the wheels in the horizontal plane, are also indicated. The wheels were simply pushed apart or pulled together during these calibrations, as indicated in figure 6.5 below.

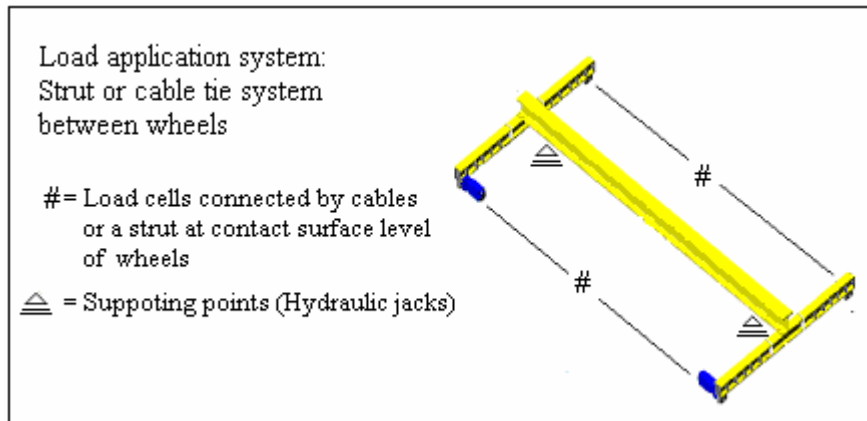


Figure 6.5: Load cells and support positions for lateral horizontal force calibrations

Photo 6.3 below indicates the point of horizontal load application just above the wheel contact surface with the crane wheel hanging above the rail, due to the lifting of the end carriages with hydraulic jacks under the crane bridge.



Photo 6.3: Crane wheel load applied with cable tie connection

6.4.1 Pulling the wheels together on a side

A tensile force was applied by means of a turnbuckle, cable and load cell, at the applicable wheel contact areas. The other wheels were deflecting away from each other, during these calibrations. The maximum force at the load cell was a tensile force of 5 kN. The normal stress results at the edges of the flanges were linear elastic, while the other strain gauges did not give any significant results.

Figures 6.6 and 6.7 are a graphic representation of the linear elastic stress behaviour, at the edges of the flanges, when the wheels of the crane are pulled together on one side. The top values next to the end carriages are the normal stress (MPa) at the strain gauges on the top flanges and the bottom values are the normal stress (MPa) at the corresponding strain gauges on the bottom flanges.

The positive values are tensile stresses and the negative values are compressive stresses. The encircled load response values are calculated with the algebraic summation, which was described in chapter 6.2.

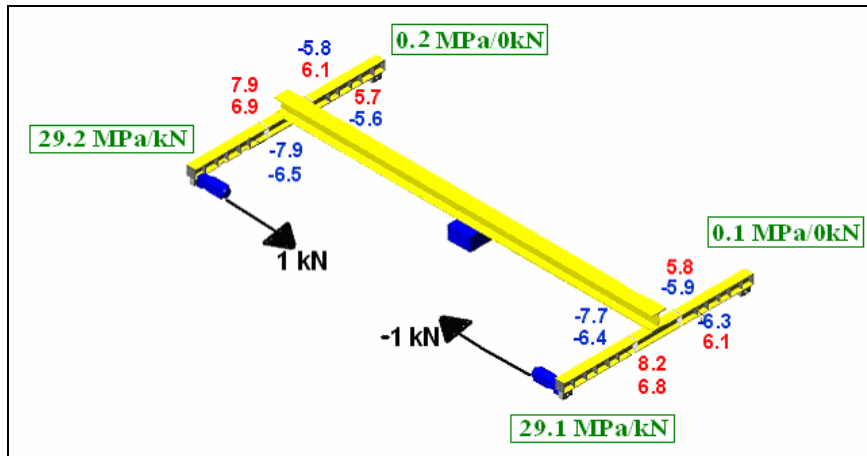


Figure 6.6: Linear elastic normal stress behaviour due to pulling southern wheels together

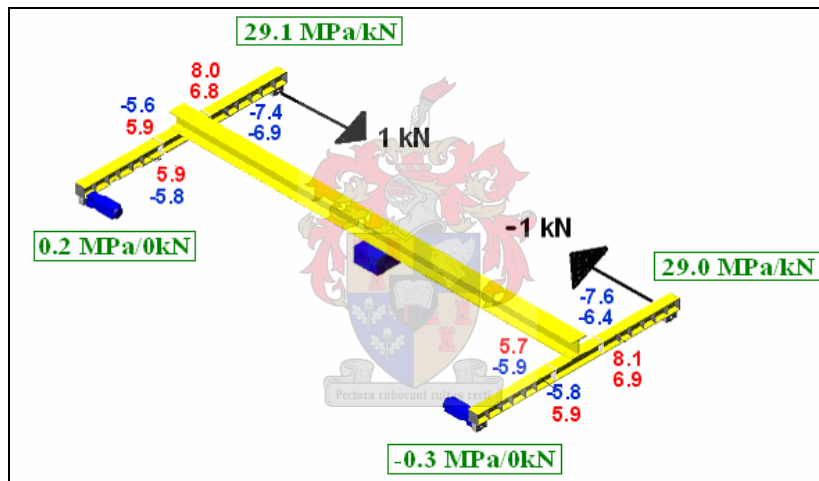


Figure 6.7: Linear elastic normal stress behaviour due to pulling northern wheels together

6.4.2 Pulling the wheels together on both sides

This calibration procedure is equivalent to the summation of the two previous calibrations. The load model that is simulated with this procedure is defined in the crane loading codes as misalignment of the rail of the supporting structure.

The loads were increased incrementally on both sides, to a maximum value of 5 kN. The end carriages were interacting in such a way that increasing the tensile force on the southern tie, caused the force in the northern tie to increase as well, due to the deflecting northern wheels pulling on the northern tie. The normal stresses are concentrated at the bottom flanges, due to the summation of the weak axis bending and warping torsional stress behaviours.

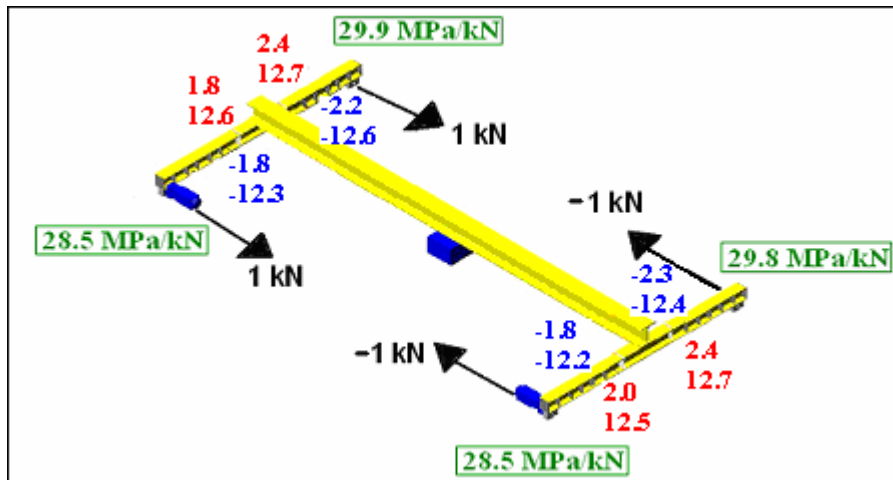


Figure 6.8: Linear elastic normal stress behaviour due to pulling on both sides

6.4.3 Pushing the wheels apart

A strut system made of cold formed lipped channel, a hydraulic jack and load cell was designed and implemented to push the wheels apart. It fits between the wheels spaced approximately 8.2 m apart, with connections close to the wheel contact surfaces. The strut system was supported vertically on its weak axis at 3rd points, to prevent sideways buckling of the strut. The stroke of the hydraulic jack of approximately 60 mm, caused the maximum applied force to be only 4 kN. Refer to figure 6.9 for the results from this calibration

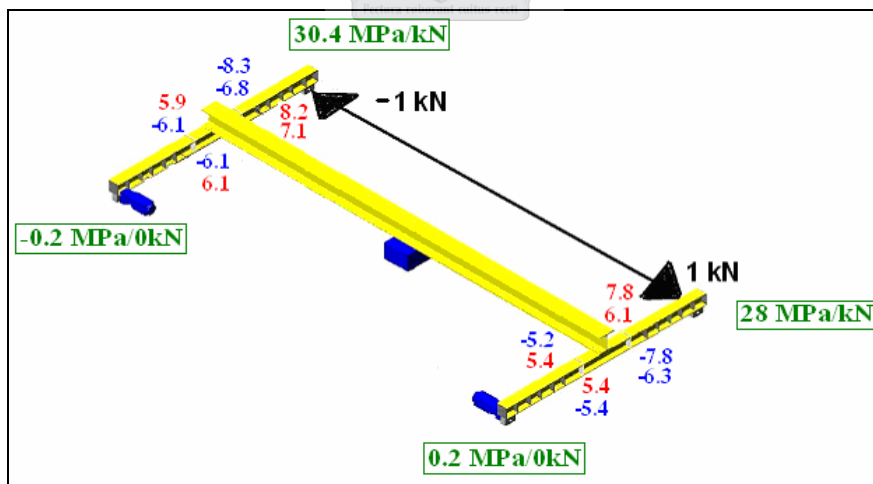


Figure 6.9: Linear elastic normal stress behaviour due to pushing northern wheels apart

6.4.4 Pulling and pushing the wheels

The load model that is simulated with this procedure is defined as skewing of the crane. This calibration is a quasi-static process which cause relative lateral horizontal deviation of the end carriages, while the crane loading code define skewing to be induced by longitudinal acceleration of

the crane, which will result in longitudinal end carriage deviation. Figure 6.10 below indicate the stresses being concentrated at the top flange of the end carriages.

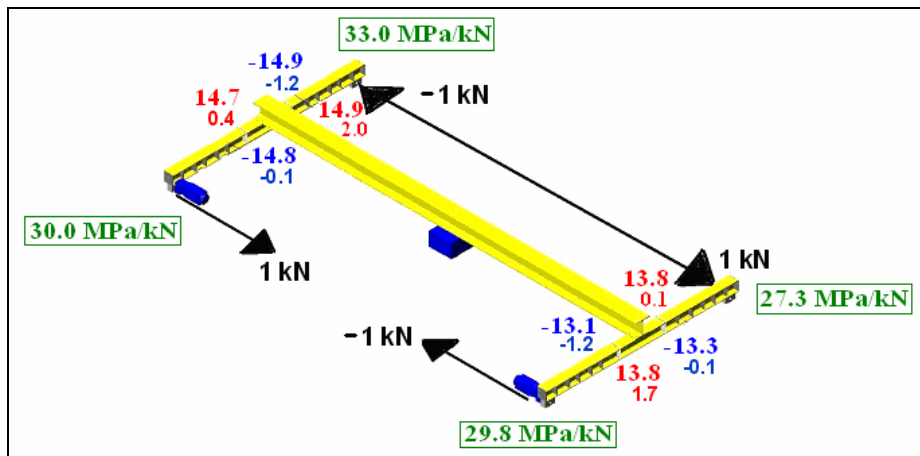


Figure 6.10: Linear elastic normal stress behaviour due to pulling and pushing the wheels

An average maximum force of only 2.5 kN could be induced, due to the pulling of the wheels together, caused the other wheels to push away from each other. The hydraulic jack was being pulled at, and resulted in the stroke being less effective. During this calibration procedure, the largest lateral deflection behaviour was observed.

6.4.5 Summary of lateral horizontal calibrations

The previous loading situations on the end carriage load measuring system and its results, which is a summation of the weak axis bending stress behaviour, are summarized in the table below.

Calibration procedures	Wheel S-E	Wheel S-W	Wheel N-E	Wheel N-W	Average
Pulling southern side	29.1	29.2	~	~	29.1
Pulling northern side	~	~	29.0	29.1	29
Pulling together on both sides	28.5	28.5	29.8	29.9	29.2
Pushing northern side	~	~	28	30.4	29.2
Pulling and pushing together	29.8	30	27.3	33	30

Table 6.1: Summary of calibration coefficients

A ratio for normal stress at strain gauges vs. lateral horizontal wheel force of **29 MPa/kN**, will be implemented during the experimental investigation in the next chapters. This is a deviation of about 1%, from the average result of all the lateral horizontal calibration results.

6.5 Calibration for longitudinal horizontal wheel loads

These calibrations were implemented to determine the influence of longitudinal forces at the wheel contact surface. Figure 6.11 below indicates the orientation of the cable tie system.

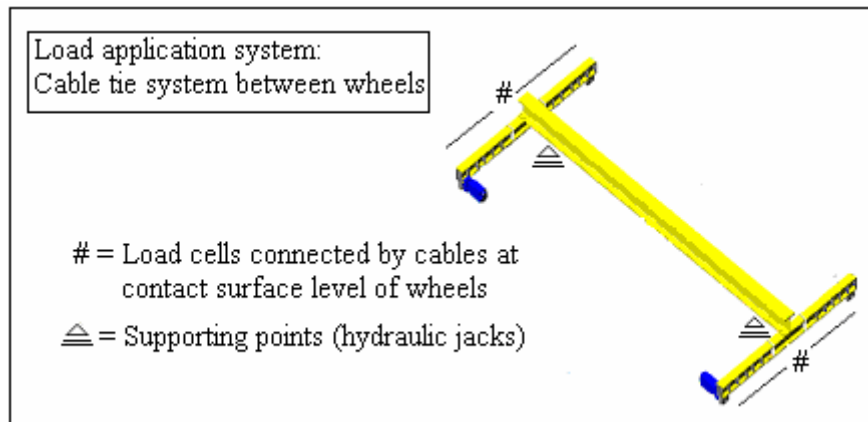


Figure 6.11: Load cells and supporting positions for longitudinal horizontal force calibrations

The maximum force applied in this calibration, can be compared with the maximum longitudinal horizontal force that the electrical motors can induce. An axial compressive stress ratio of **0.13 MPa/kN** was determined at the web of the cross section.



6.6 Calibration results of crane compared with results from numerical model

The bending stress result of the experimental calibration for **vertical wheel loads** is compared with the results from the numerical model, in table 6.2 below.

Experimental results MPa/kN	Numerical results MPa/kN	Deviation %
2.51	2.56	2

Table 6.2: Summary of vertical wheel load calibrations

The average normal stress results obtained from the experimental calibration for **lateral horizontal wheel loads** is compared with the results from the numerical model, in table 6.3 below.

Type of lateral horizontal loading situation	Experimental results MPa/kN	Numerical results MPa/kN	Average deviation %
Pulling the wheels together on one side : Top flange	7.9	5.4	14
Bottom flange	6.6	7.3	
Pulling the wheels together on both sides Bottom flange	12.5	13.2	6
Pulling and pushing the wheels: Top flange	14.1	11.0	28

Table 6.3: Summary of stress results due to lateral horizontal wheel loads

If these results are used in the algebraic summation described in chapter 6.2, the comparison in results due to **lateral horizontal wheel loads** are indicated in table 6.4 below.

	Experimental summation MPa/kN	Numerical summation MPa/kN	Deviation %
Pulling one side	29.0	25.4	14
Pulling both sides	29.2	26.8	9
Pulling and pushing	30.0	24.0	25

Table 6.4: Summary of lateral horizontal wheel load calibrations

The normal stress results from the experimental calibration for **longitudinal horizontal wheel loads** are compared with the results from the numerical model, as indicated in table 6.5 below.

	Experimental results MPa/kN	Numerical results MPa/kN	Deviation %
Top flange	-0.29	-0.21	38
Bottom flange	0.56	0.44	27
Web	0.14	0.13	7

Table 6.5: Summary of stress results due to longitudinal horizontal wheel loads

6.7 Applying direct loads on supporting structure

The behaviour of the supporting structure will be described by its deflection at mid-span and reaction force response due to calibrated loads at mid-span. An experimental wheel load application system was designed for this purpose. The system consisted of a hydraulic jack that was fixed to the reinforced concrete floor and a load cell that was fixed to a semi-circular steel wheel on top of the rail and crane girder. The hydraulic jack was used to pull downwards on the load cell and a maximum vertical wheel load of 100 kN was applied safely onto the top of the rail, as is indicated in figure 6.12 below.

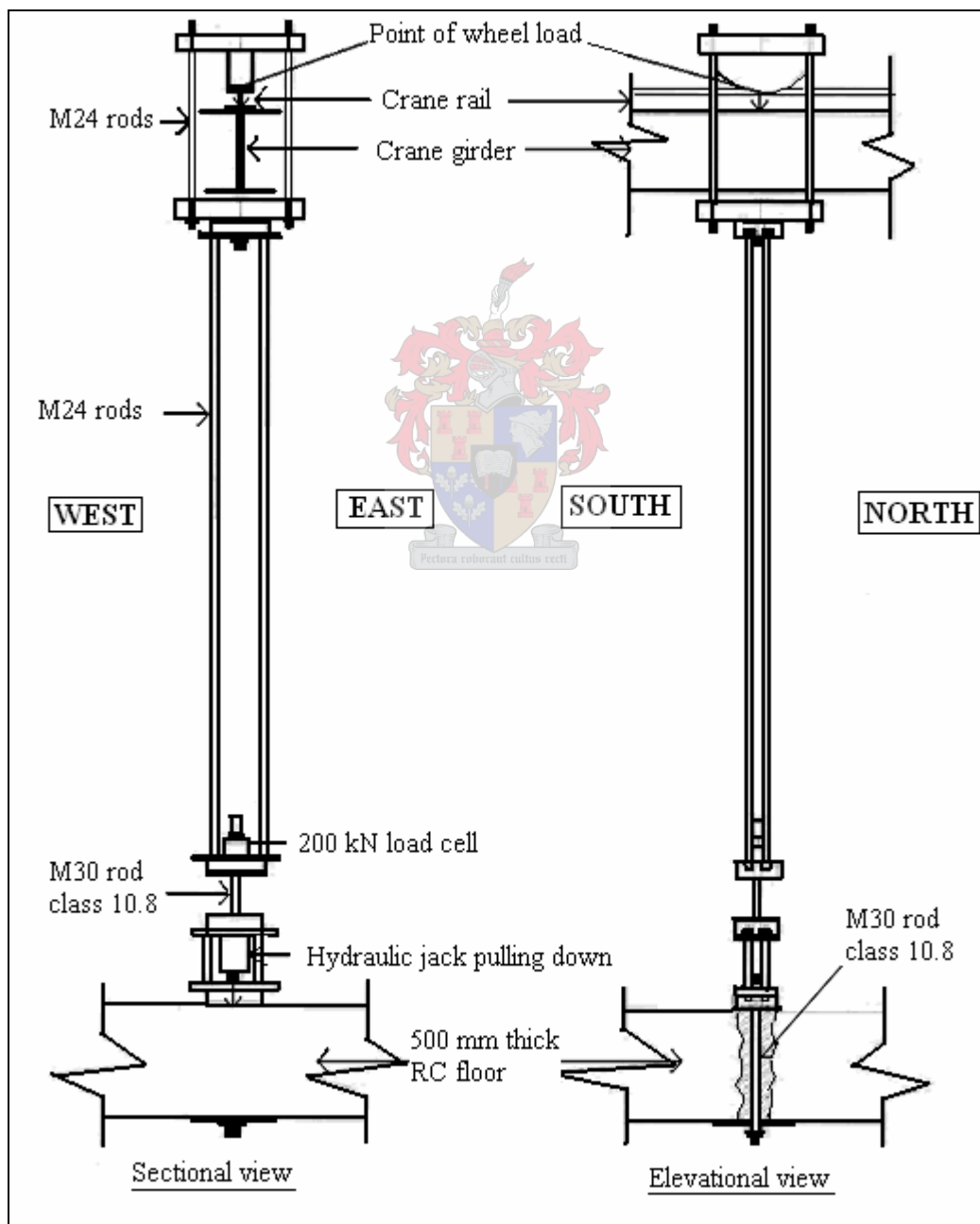


Figure 6.12: Calibrated vertical wheel loads directly onto supporting structure

Deflections of the crane girder were measured with linear variable displacement transducers (LVDT's) that were independently positioned, onto the crane girder, as shown in photo 6.4 below.



Photo 6.4: LVDT's measuring deflection of girders

If the vertical wheel load is eccentric, lateral rotation of the girder is possible. Deflection measurements were performed on both sides of the wheel load, to determine the average deflection of the girder.

The experimental investigation of the influence of a continuous rail over a simply supporting girder connection was also investigated. This information was important for the experimental verification of a PhD students numerical model of the supporting structure.

6.7.1 Behaviour of supporting structure under vertical loads

These loads are quasi-static in nature, while the wheel loads due to the crane are dynamic in nature. The zero reading is taken when the load application system is unloaded. The deflection due to the own weight of the structure and the deflection due to the weight of the load application system is not taken into account. Figure 6.13 on the next page indicates the reference points on the supporting structure used during the experimental investigation and the position of the separate wheel loads at mid-span of the crane girders. Each test was repeated at least three times to achieve reliable results.

The influence of a bolted rail joint splice at position A14 on the supporting structure's load response is also investigated. The top surface of the rail at the splice position is uneven (± 2 mm), due to imperfections in the supporting girders, onto which the rails are bolted. The influence of this unevenness on the vertical and lateral horizontal wheel forces will be described in chapters 7 and 8.

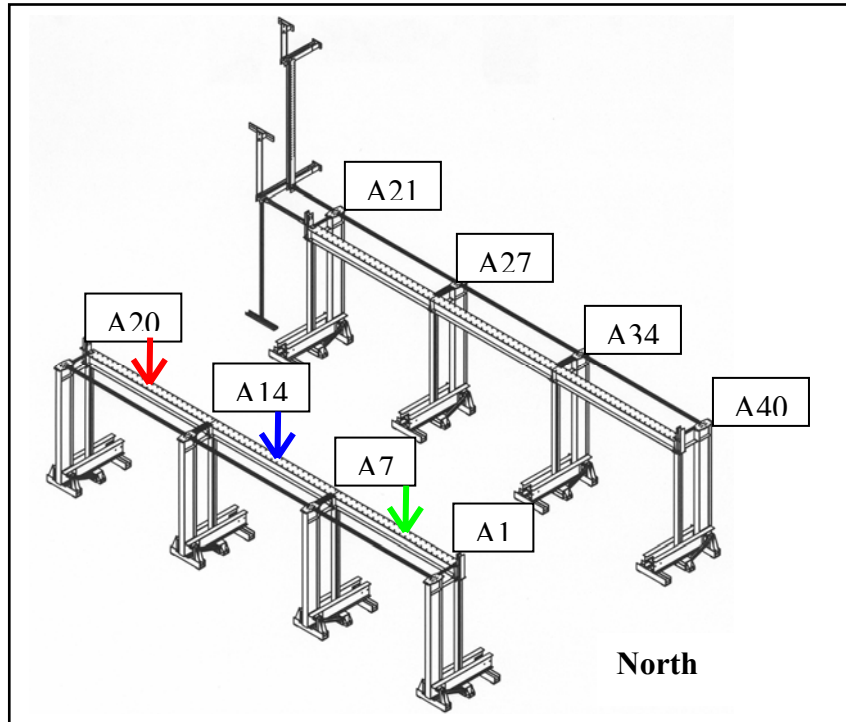


Figure 6.13: Position of individually applied vertical wheel loads

The top 3 lines in the figure 6.14 below indicate deflection measurements on the top flanges of the crane girders. Girders A1-A7 and A14-A20 behaved similar under loading as would be expected, with 3 mm deflection at 100 kN. The stiffest girder is A7-A14 with 2.6 mm deflection at 100 kN loading.

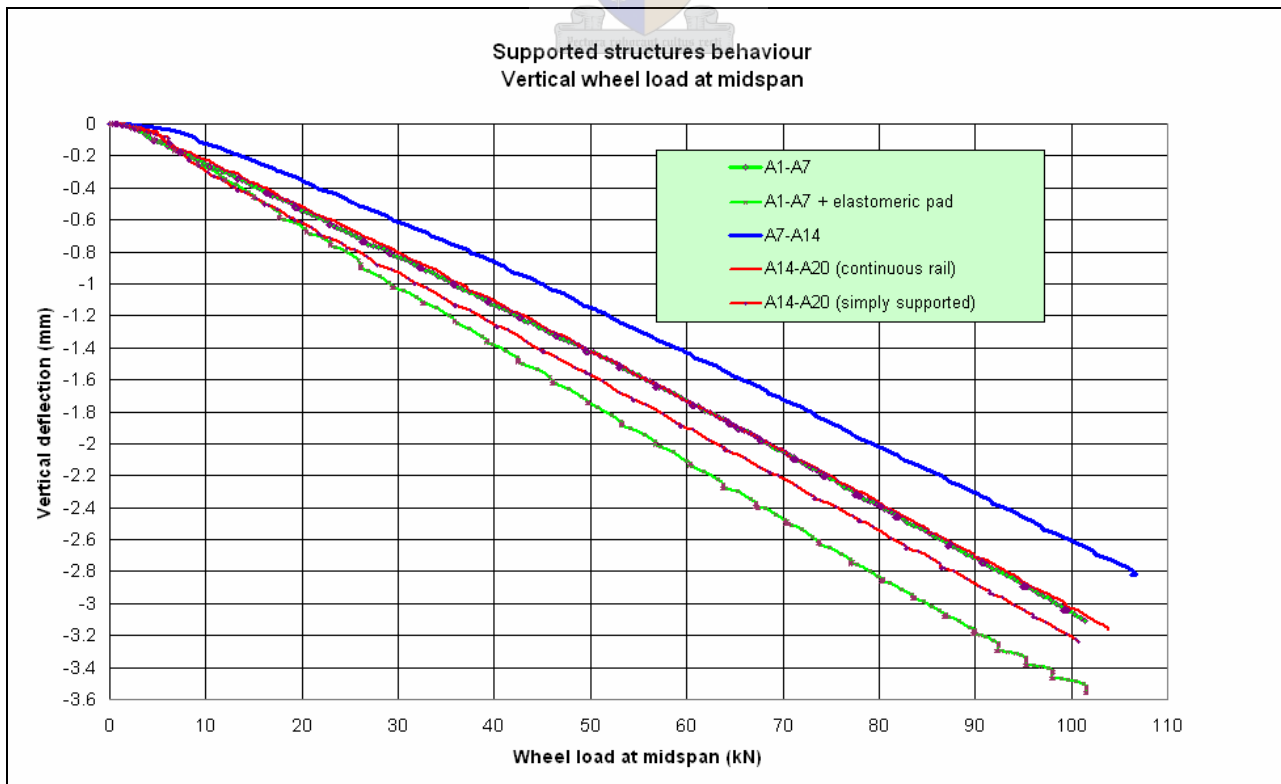


Figure 6.14: Vertical deflection behaviour of supporting structure

The relative vertical deformation due to the elastomeric pad at A1- A7 is 0.6 mm at the point of wheel load application. If the rail splice at A14 is loosened and the load is again applied, the most flexible girder is A14-A20 with 3.2 mm deflection. The rotational stiffness at that connection decreases and results in 8% higher deflections than with a fixed rail splice. This relates to relative vertical strain deformation of 8.5% of the elastomeric pad itself.

The crane supporting columns experience linear elastic strain deformation under axial loads and a deflection of 0.34 mm was measured at a loading of 50 kN in column A14.

The measured reaction forces at the crane supporting columns are indicated in table 6.6 below.

The highlighted cells indicate the main loaded crane supporting columns.

Load at mid-span of crane girder	Reaction force in crane supporting column			
	A20	A14	A7	A1
A1 – A7	~	-0.4	56.0	43.0
A7 – A14	-2.8	54	52.6	-3.8
A14 – A20 (Rail splice in position)	44	58.3	-2.3	~
A14 – A20 (Rail splice removed)	46.5	53.6	~	~

Table 6.6: Reaction forces measured in crane supporting columns

These results indicate that the response of the structure due to a single quasi-static wheel load at mid-span is influenced by the rotational stiffness of the connections. Table 6.6 is an important reference for interpreting the reaction force results from the simultaneous wheel loads due to the experimental crane traversing the crane girder in the longitudinal direction.

The main deflection results of the supporting structure under loading, is due to the following: 67 % of the measured deflection of the rail is due to the crane girder's beam bending, 17 % is due to the vertical strain of the elastomeric pad and 16 % is due to axial strain of the crane supporting columns.

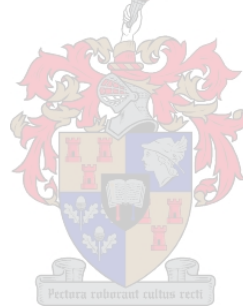
The means for quantifying the influence of a rail splice on the behaviour of the system, is by comparing vertical deflections measured at the centres of the girders and also by comparing the reaction forces measured underneath the supporting columns. The influence of a rail splice on the deflections measured at mid-span of the girders can be described as 7 % increase in vertical deflections, when the rail splice is removed. The influence of a rail splice on the reaction force measured at the supporting column closest to the rail splice, can be described as 5 % decrease in measured reaction force, when the rail splice is removed.

6.7.2 Behaviour of supporting structure under lateral horizontal loads

The semi-circular wheel of the load application system in the previous section, was modified to also apply lateral horizontal forces onto the rail, at the mid-span positions. A turnbuckle and calibrated loadcell system was implemented, to pull the rail and supporting girder, towards the wall of the laboratory. The lateral restraining rods of the supporting structure were calibrated during these loading tests.

Lateral horizontal loads at the rail cause a rotational response from the crane girder, so the accuracy of direct deflection measurements is limited. An approximate lateral horizontal deflection of 0.7 mm occurs at the top of the rail at mid-span, when a lateral horizontal force of 10 kN is applied.

In this chapter the mechanisms involved in the calibration of the crane were described and the results obtained, were compared with the results from the numerical model. The behaviour of the supporting structure was also described. The crane will now be positioned on top of the supporting structure, and the system will now be exposed to the load models specified in literature.



Chapter 7 - Regular loads on overhead crane and supporting structure

During normal use of overhead cranes, the crane and supporting structure are subjected to regular loads at the crane wheels. The forces that are measured at the payload and the columns of the supporting structure and the loads that are measured at the crane's wheels during these normal crane operations, will be determined experimentally.

7.1 Forces due to own weight of crane

The influence of the own weight of the crane had to be determined, before experiments with the crane and payload could be performed. Refer to figure 3.3 on page 16, for the position of the load measuring equipment in the supporting structure, from which data will be used for describing the experimental wheel load results.

The own weight of the crane of 22.4 kN, is determined in Appendix A. This means that the vertical load at each of the 4 wheels is 5.6 kN, when the crab is stationary at the middle of the crane bridge. A zero reading is taken when the crane is lifted of the supporting structure. The crane is then placed on the southern side of the supporting structure as indicated in figure 7.1 below and allowed to travel 8.6 m in both the northern and southern direction, while reaction forces in the supporting columns are measured.

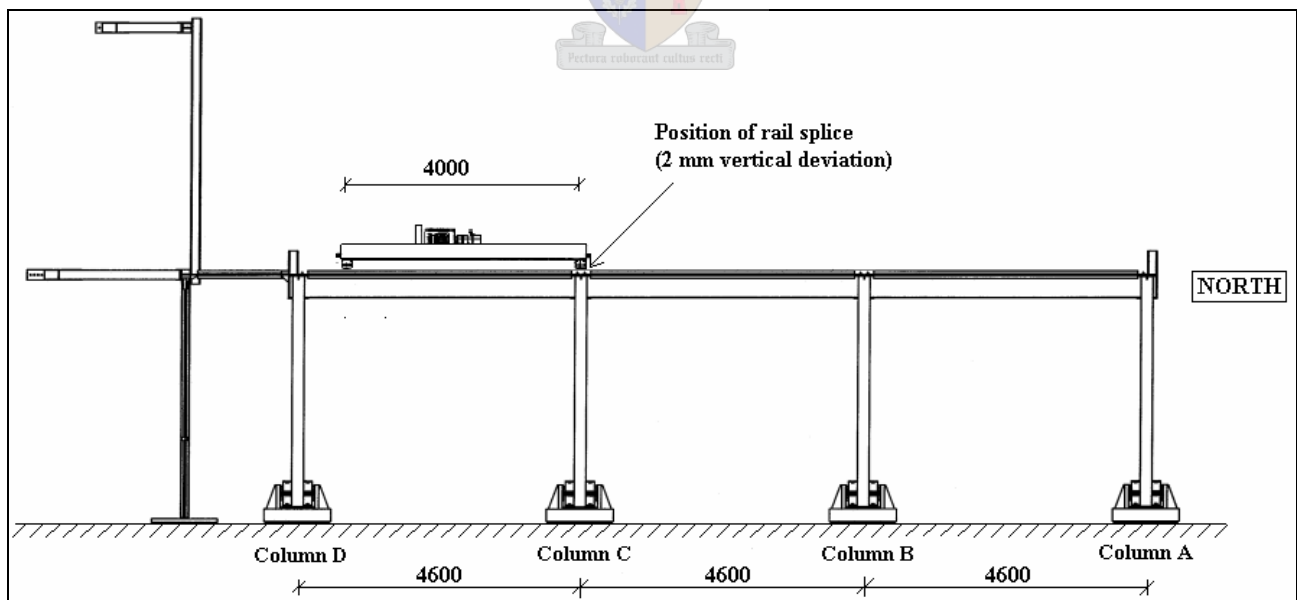


Figure 7.1: Position of crane at start of longitudinal travel experiments

Figure 7.2 below shows the reaction forces measured at the supporting columns of the supporting structure, indicated in figure 7.1 above, as the crane traverses the runway,

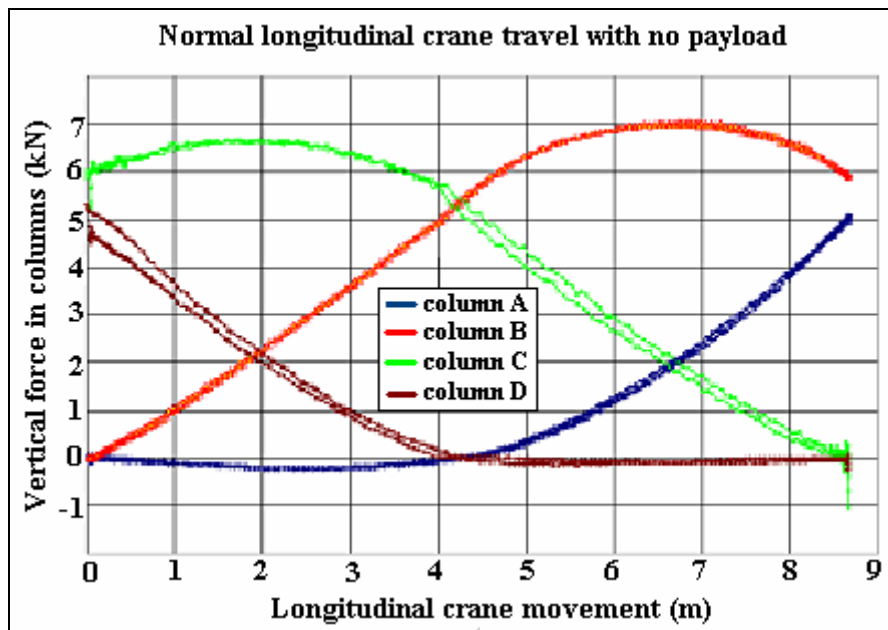


Figure 7.2: Vertical reaction forces in columns when no payload is handled

A maximum force of 7 kN at column B occurs after about 7 m of longitudinal travel.

The lateral horizontal wheel loads are largest when the crane wheels move over the mid-span positions of the crane supporting girders. Figure 7.3 below indicates the largest lateral horizontal wheel loads measured when no payload is handled, during normal longitudinal crane travel.

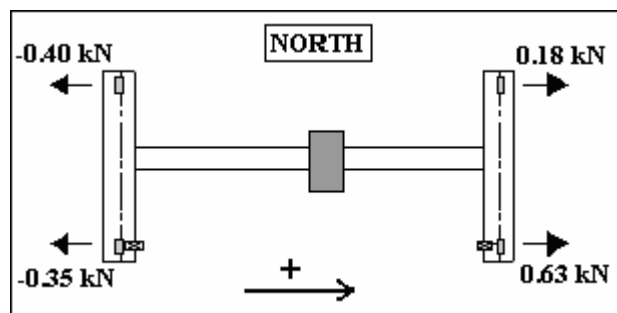


Figure 7.3: Lateral horizontal wheel loads when no payload is handled

7.2 Forces and loads due to hoisting and lowering of payload

Hoisting the payload at various crane and crab positions was performed. The maximum wheel load behaviour during hoisting of the payload is described.

The payload clears the ground after one second. The hoist drive control system ensures the use of a steady creep speed for the first 5.5 seconds, then the hoisting accelerates, which causes the

maximum dynamic response of 1.05 in the system. The force measured at the payload and the loads measured at the respective crane wheels during payload hoisting, are indicated in figure 7.4 below.

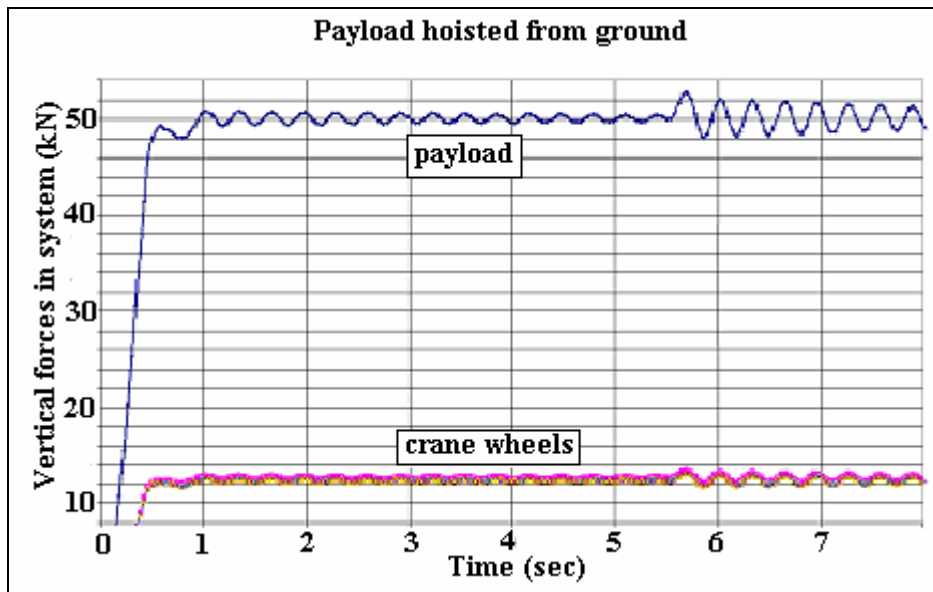


Figure 7.4: Dynamic response due to payload hoisting from the ground

When the payload hoisting is stopped at a height of 1.2 m, the maximum dynamic response is 1.07. The maximum measured vertical vibration frequency of 4.25 Hz occurs when the payload is hoisted at the eccentric payload position. This is 24 % higher than when the payload is hoisted at the mid-span crane bridge position (3.4 Hz).

The weight of the payload induces not only vertical wheel loads, but also lateral horizontal wheel loads. The lateral horizontal loads at the wheels have a similar dynamic response to that of the vertical wheel loads. Figure 7.5 below indicates the maximum measured lateral horizontal wheel loads during hoisting of the payload.

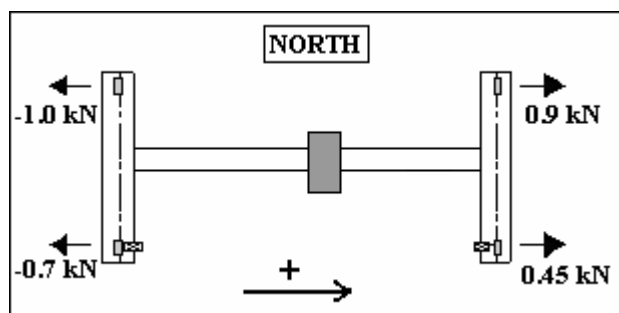


Figure 7.5: Maximum lateral horizontal wheel loads due to normal payload hoisting

The existing lateral horizontal wheel loads due to the own weight of the crane and its electrical motors when a zero reading is made, influences the lateral horizontal force equilibrium results during payload hoisting.

When the payload lowering is initiated during normal crane operation, as indicated in figure 7.6 below, a maximum dynamic factor of 1.11 is determined, when the payload is lowered at the center of the crane bridge.

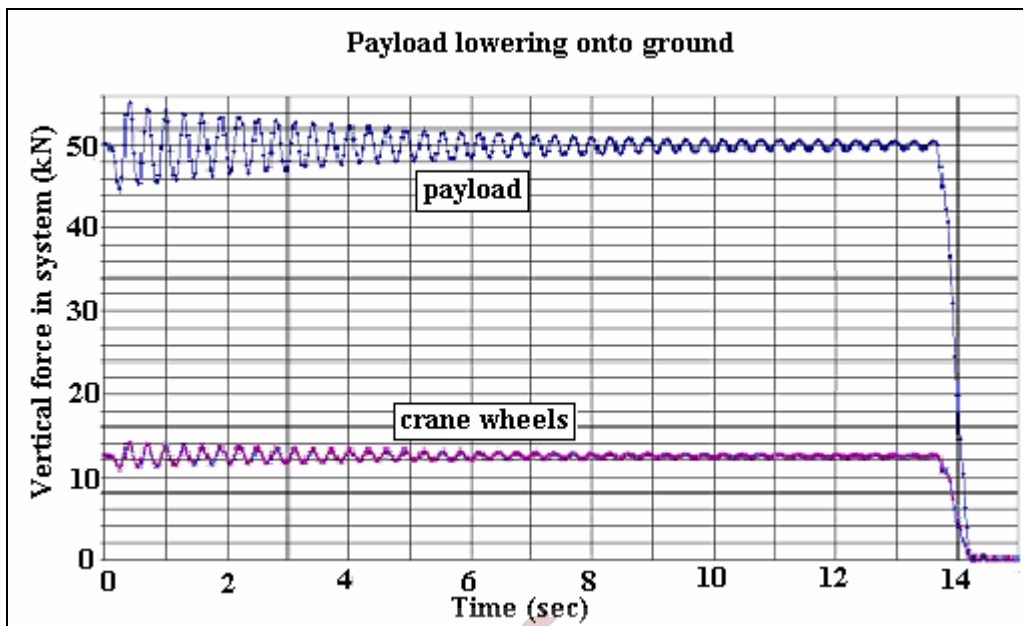


Figure 7.6: Dynamic response due to payload lowering onto the ground

The relative position of the crane on the supporting structure does not influence the dynamic response substantially, due to the stiffness of the supporting structure.

7.3 Forces and loads during longitudinal travel of crane with payload

7.3.1 Crab at middle of crane bridge

This is the most symmetrical load configuration for the crane handling the payload. A zero reading is taken before the payload is hoisted from the ground. The payload is then hoisted and data capturing starts after about 1 minute, to allow vibrations induced by hoisting to subside. When the crane bridge traverses longitudinally with the payload, the largest vertical reaction force of 22 kN is measured at the internal supporting columns. When a crane wheel traverses the rail splice after 4 metres of longitudinal travel, the determined vertical dynamic response factor is 1.02 with a highly under damped vertical vibration frequency of 3.2 Hz during the next four metres of longitudinal travel. The outwards lateral horizontal forces at the wheels increase by 0.5 kN at each wheel as the rail splice is traversed, but are damped after another 1 metre of longitudinal travel. The maximum measured lateral horizontal loads when the crane traversed the rail splice are indicated in figure 7.7 on the next page.

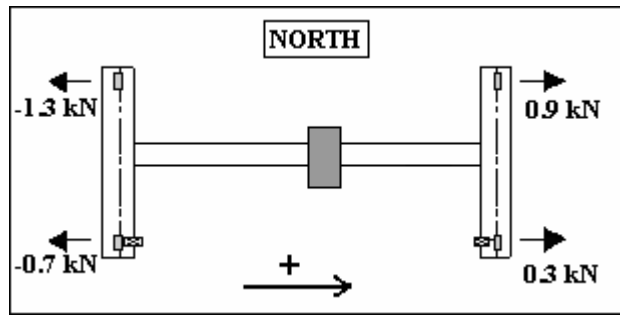


Figure 7.7: Lateral horizontal loads at uneven rail splice

The deviation from lateral horizontal force equilibrium of the system is mainly due to the initial wheel forces, which are neglected when a zero reading is taken, before the experiment starts. The electrical driving motors also add lateral horizontal forces onto the system, which could influence the equilibrium of the lateral horizontal wheel loads of the crane. The largest gradual deviation in lateral horizontal wheel loads occurs, when the crane changes its direction of longitudinal motion.

7.3.2 Crab at eccentric position on crane bridge

When the payload is hanging at the most eccentric crane bridge position (position B1), refer to figure 4.5, the vertical loads at the wheels closest to the payload are highest. The zero reading was taken with the crab already at the eccentric position, for practical reasons. Figure 7.8 below indicates the forces measured in the supporting structure and the loads at the wheels as the crane traversed longitudinally. Note the dynamic response as the crane wheel traverses the rail splice after 4 metres.

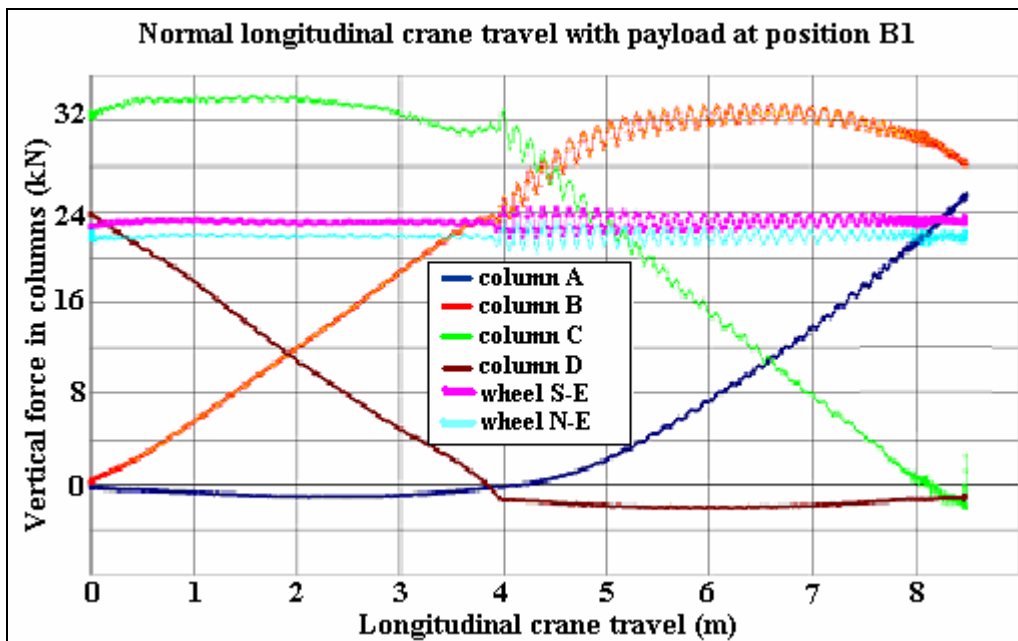


Figure 7.8: Vertical forces during longitudinal crane travel with eccentric payload

The largest vertical force of 34 kN was measured at the internal columns. The determined dynamic response factor is 1.04 when the highly loaded crane wheel traverses the rail splice with an under damped vibration frequency of 4.2 Hz.

The measured lateral horizontal loads were smaller than expected. They were not more than 1.0 kN, due to the smaller deflection of the crane bridge with the eccentrically hoisted payload.

7.4 Loads during lateral travel with payload

The crane was positioned in the centre of the supporting structure, with the crab and payload at position C1; refer to figure 4.5. A zero reading was taken with payload on the ground and then the payload was hoisted. The crab was allowed to traverse the crane bridge in both directions during this experiment. The soft-start/stop mechanism allows slow initial lateral acceleration and no lateral end-buffer impact of the crab.

The vertical loads at the crane's wheels are constantly changing, due to the changing payload position. At the same time lateral horizontal loads are transferred to the supporting structure, which are influenced by the acceleration or deceleration of the crab, as well as the rolling resistance at the crab's wheels on the bottom flange of the crane bridge. The rolling resistance at the crab's wheels are related to the own weight of the crab, the weight of the payload and the frictional resistance at the crab's wheels.

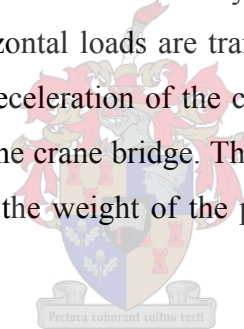


Figure 7.9 on the next page indicates the vertical loads at the wheels of the crane, as the payload is moved from C1 on the western side to B1 on the eastern side and back again to C1. Refer to figure 4.5 for orientation, relating to these points on the crane bridge. The crab starts moving laterally after 6 seconds and then for the next 9 seconds is only allowed to move slowly, due to the soft-start mechanism. The crab then accelerates and moves laterally until the soft-stop mechanism at the opposite side forces the crab to decelerate and finally stop. The crab is then stationary for 10 seconds before it starts moving in the opposite direction.

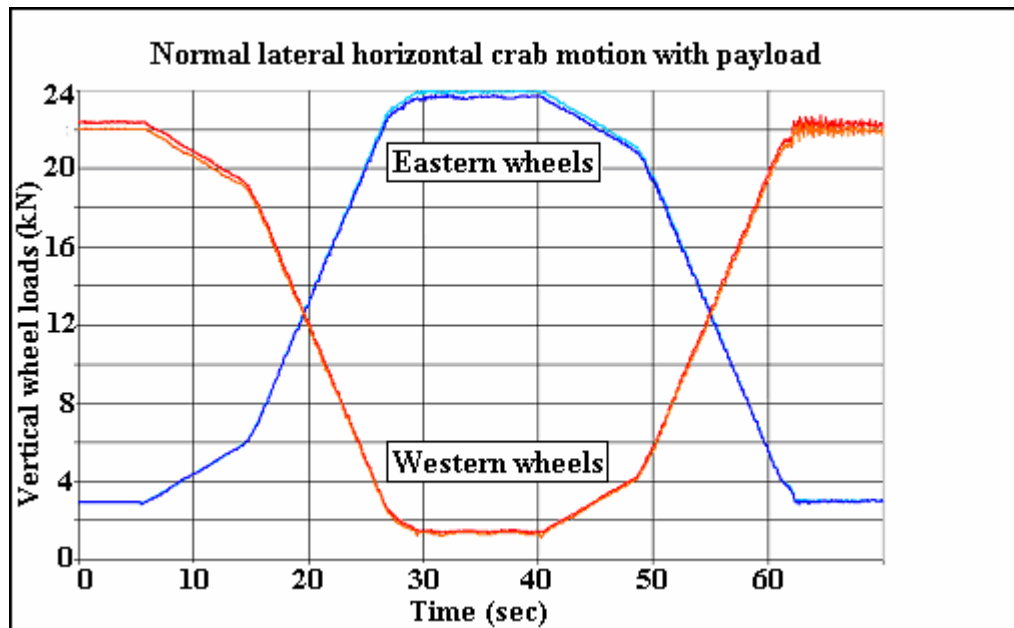


Figure 7.9: Vertical loads at wheels, due to lateral traversing of crab with payload

These vertical loads are statically determinable and can be calculated very accurately for any position of the crab and payload by using equilibrium of vertical forces. The lateral horizontal forces are not so easily determined, because these forces are induced by the lateral horizontal component of the force in the cable by which the payload is hoisted. The increase in payload height decreases the maximum possible amplitude of the pendulum action of the payload during swinging. As a result the maximum lateral horizontal forces occur when the crab is accelerating with the payload hanging low, as indicated in figure 7.10 below. This graphic representation of data is from the same experiment in figure 7.9 above.

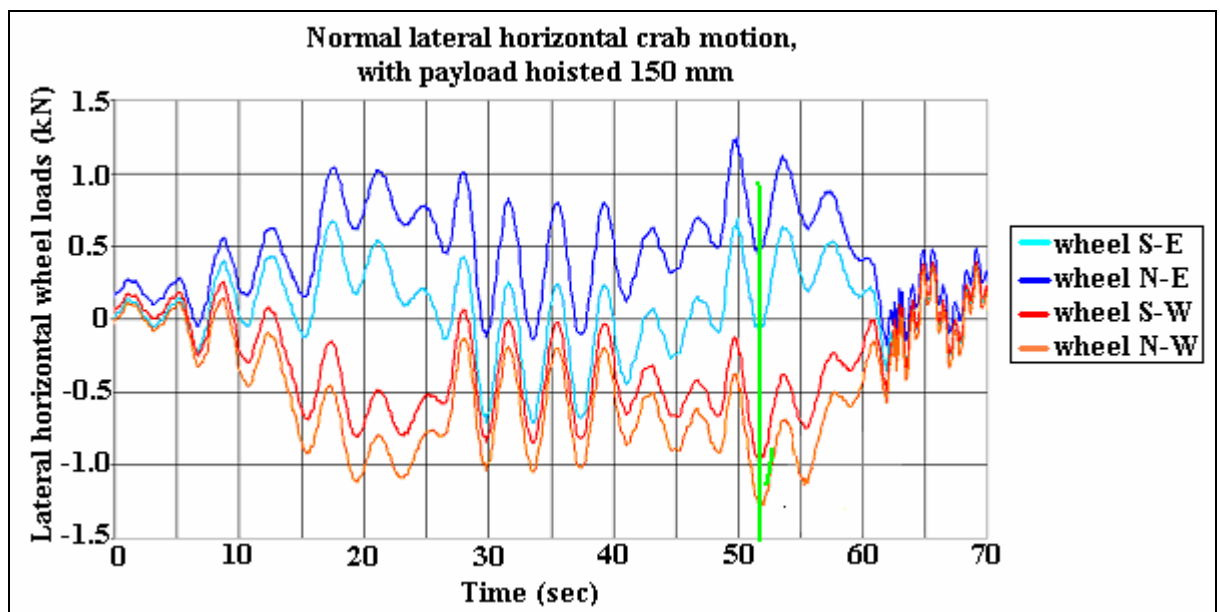


Figure 7.10: Lateral horizontal wheel loads due to crab's motion with payload hanging low

The maximum lateral horizontal wheel load of 1.3 kN and the other simultaneous occurring wheel loads from figure 7.10 on the previous page at the green line, due to the acceleration of the crab, are indicated at the relevant wheels of the crane in figure 7.11 below.

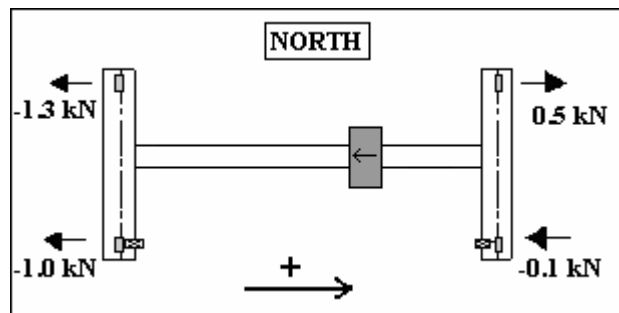


Figure 7.11: Maximum lateral horizontal wheel loads due to crab's acceleration

The regular wheel loads at the crane wheels were determined experimentally. The vertical wheel loads are normally statically determinable. Experimental equilibrium of the maximum lateral horizontal wheel loads is not easily achieved, due to the dynamic behaviour of the system.

The behaviour of the crane under the different types of regular loads can be described as follows. During payload hoisting and lowering, the load behaviour at the wheels is under-damped, dynamic loads. During longitudinal crane travel without a payload on a smooth surface, the vertical wheel loads are constant, while the lateral horizontal wheel loads vary more. If the crane traverses an uneven rail splice during longitudinal travel with a payload, the vertical and lateral wheel load behaviour becomes dynamic, with the lateral horizontal wheel loads being damped better by the system.

Chapter 8 - Exceptional loads on overhead crane and supporting structure

The supporting structure and the crane itself are subjected to exceptional loads at the crane wheels and forces induced onto the supporting structure, when the acceleration and deceleration of the crane, crab and/or payload are higher than those accelerations specified as normal in chapter 4.3. The lack of proper maintenance of the crane's driving motors and alignment of the rails of the supporting structure, can also lead to exceptional loads on the system. These exceptional forces at the payload and the supporting structure and the exceptional loads at the crane's wheels will be determined experimentally.

8.1 Loads due to hoisting the payload to maximum height

In a normal industrial production line the payload would only be lifted a minimum clear height from the ground, so that the shortest possible translational route is followed by the payload to the desired new location.

An accelerometer was fixed onto the payload to measure the relative change from gravitational acceleration of 9.8 m/s^2 and the load cell measured the force deviation in the hoisting cable, due to the own weight of the payload of 50.3 kN.

When the payload of the experimental system is hoisted to the maximum clear height of 2.2 m between bottom of the payload and ground level, a mechanism at the crab causes the hoisting process of the payload to be deactivated electrically. This decelerates the payload to a sudden stop, which causes visible vibrations of the crane and payload; the vibration was determined to be at a frequency of 4.5 Hz, and lasted for at least 10 seconds. During this sudden stop of the payload, a maximum dynamic force of 57.3 kN and deceleration of 1.3 m/s^2 is measured. The total relative acceleration that the system experienced was 11.1 m/s^2 with a dynamic load factor of 1.14. A linear relation between the relative acceleration of the payload and dynamic response of the system is indicated in figure 8.1 on the next page.

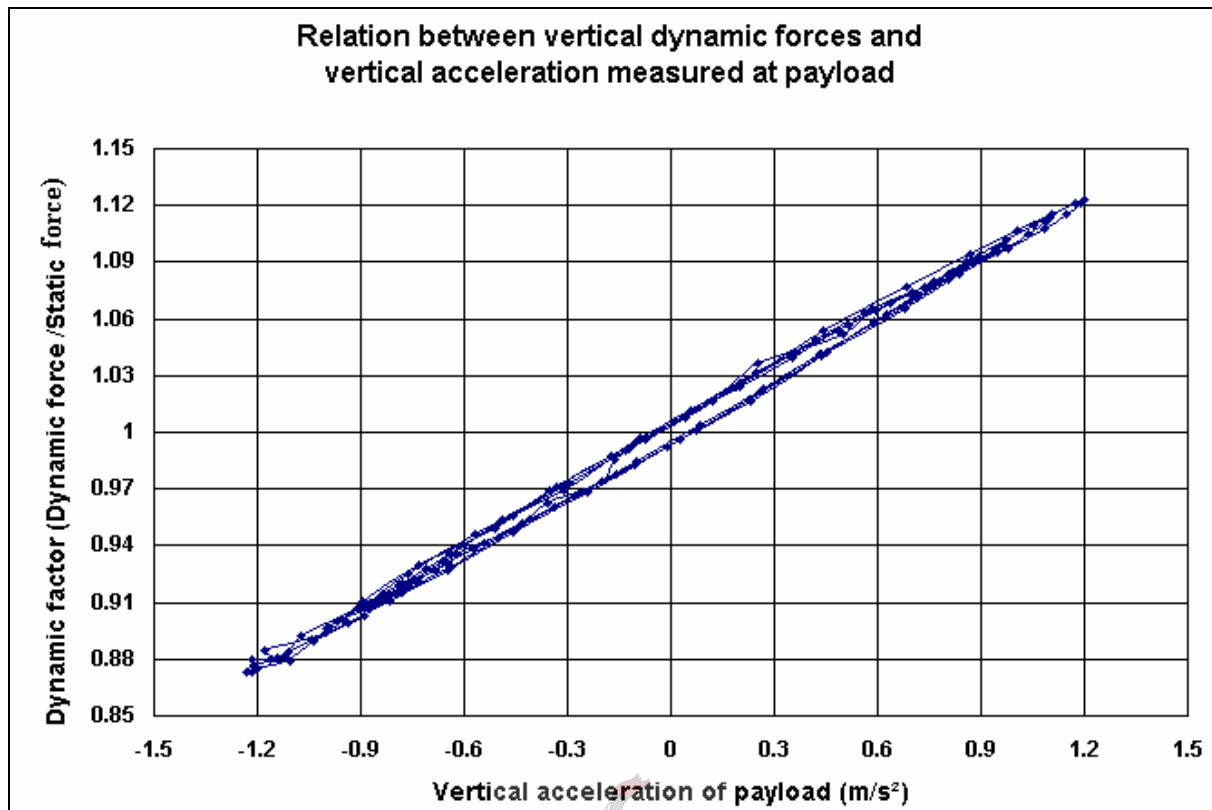


Figure 8.1: Linear relation between acceleration and dynamic response of crane

8.2 Forces due to longitudinal buffer impact

In the design of overhead crane supporting structures provision is made for endstops to prevent the crane from running off the rails. The force due to this impact is an accidental load model, which can occur due to human error or due to electrical malfunction of the driving motors or the safety switches at the end of the runway. Elastomeric buffers on the crane or hydraulic shock absorbers on the endstops are mechanisms for absorbing the impact forces. The bracing system of the supporting structure must then transmit these forces to the ground or to a rigid point. Photo 8.1 below indicates the compression of the elastomeric buffer on the crane, during impact.

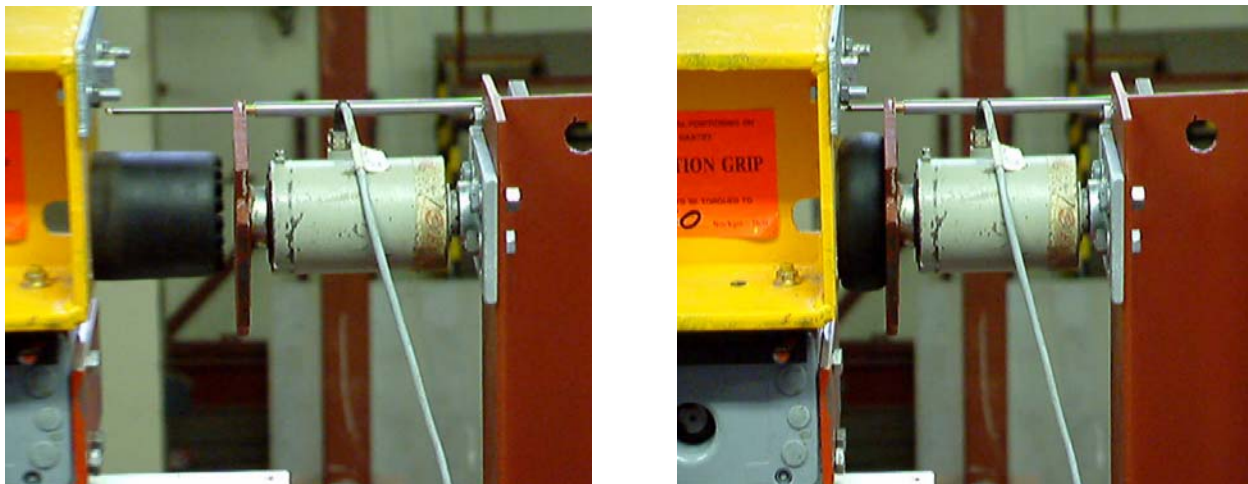


Photo 8.1: Elastomeric buffer compression during impact

The maximum compression of the elastomeric buffer of 60% is measured from the endstop using a LVDT.

During a buffer impact test there are a number of longitudinal impacts due to the electrical motors continuing to drive the crane bridge through a step-down function to decrease power gradually to the driving motors. When this step-down function was deactivated, these secondary impacts decreased. Shortly after the first longitudinal impact, high vertical forces were also measured at the payload, due to the hinged connection causing the payload to swing. Figure 8.2 below indicates the average critical force measured at the two load cells on the endstops. The deviation in vertical force measured at the payload is also indicated.

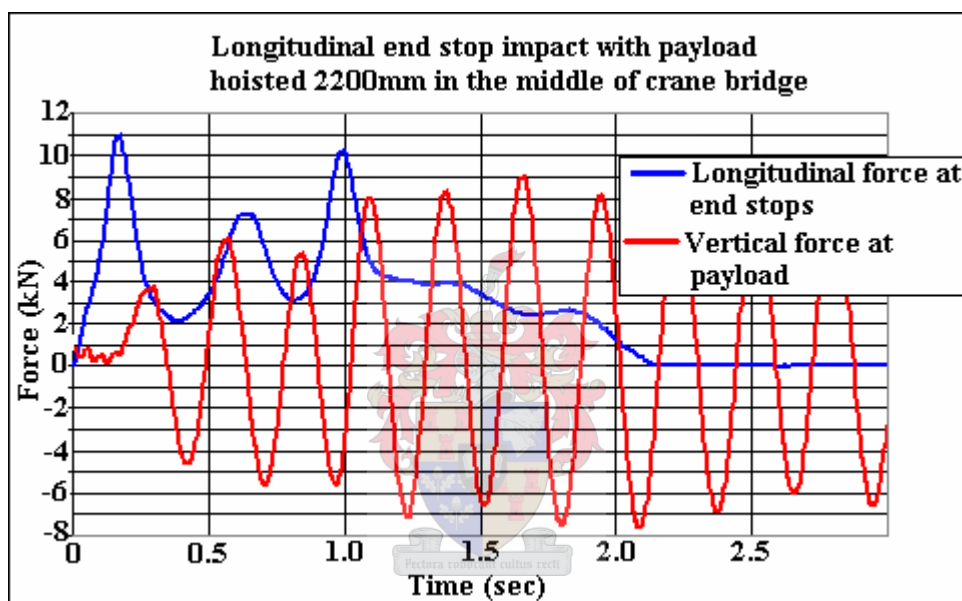


Figure 8.2: Longitudinal force at end-buffers and vertical force at payload

This measured vertical force at the payload deviates by 2 % from the total vertical load that is measured at the wheels of the crane. Note the frequencies of the endstops (2.5 Hz damped) and swinging payload (3.6 Hz undamped) response. Resonance could have severe effects.

The longitudinal impact forces at both end stops are not exactly symmetrical despite efforts to achieve this. As a result lateral horizontal loads at the wheels are also generated after the impact.

The table below indicates the summary of the maximum longitudinal impact forces at the end stops.

Payload height above ground	No payload	150 mm	2200 mm
Maximum force at end stop (kN)	7.3	10.5	11.0

Table 8.1: Summary of longitudinal impact forces

Increasing the height of the payload did not increase the impact forces substantially. This is due to the fact that the payload is free to swing during the impact.

8.3 Forces induced by electrical driving motors

The crane accelerates longitudinally due to the driving force exerted by the electrical motors at the southern wheels. These longitudinal wheel loads are difficult to measure directly in the supporting structure, due to the lateral restraints that would also absorb some of these forces. These forces were measured indirectly, by fixing the crane with cables onto the load cells at the end stops. The crane then pulled on the load cells, by attempting to move southwards. The measured longitudinal forces were 1 kN, due to the own weight of the crane, causing frictional resistance at its wheels. When the payload was then also hoisted, these longitudinal forces increased due to the higher wheel loads increasing the frictional resistance at the crane wheels. Literature states that the longitudinal wheel load is 10% of the static vertical wheel load per rail. The experimental results are compared against this linear relation in figure 8.3 below.

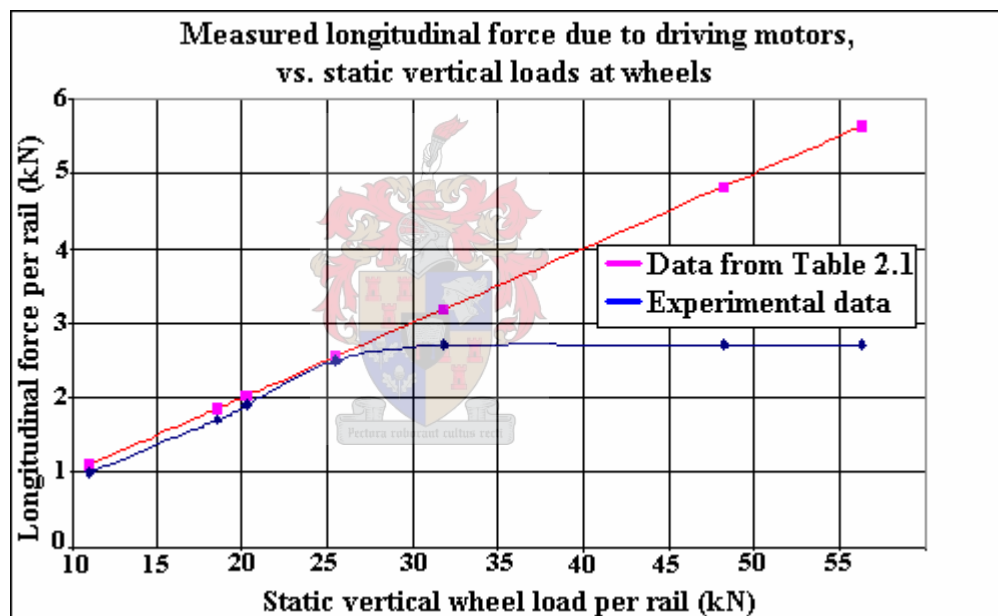


Figure 8.3: Longitudinal force per rail

When the static vertical wheel load at the 2 wheels on one rail increased above 28 kN, the measured longitudinal force did not increase above 2.7 kN per rail. The power output from the 0,55 kW electrical motors is the determining factor of the maximum longitudinal forces measured.

8.4 Loads due to eccentric payload hoisting from the ground

If a crane is operated incorrectly by not positioning the crane and crab exactly above the payload when hoisting of the payload starts, the oblique hoisting will induce a horizontal forces into the crane system. If these horizontal forces are larger than the frictional resistance at the wheels of the crane or crab, the crane system will adjust itself to achieve equilibrium of forces.

The hoisting eccentricity of 0.3 m of the 50 kN payload was investigated experimentally, with the relative position of the eccentricity indicated in figure 8.4 below.

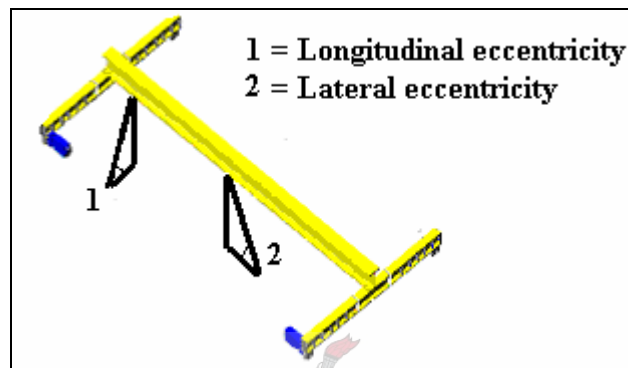


Figure 8.4: Orientation of eccentric hoisting of payload

When hoisting the payload from position 1, the maximum lateral horizontal loads of 1.8 kN are measured at the crane wheels, due to the end carriage closest to the payload moving first longitudinally, until the crane is above the payload. An accelerometer was also fixed onto the crab to measure the lateral acceleration of the crab. When hoisting of the payload at position 2, the crab experiences an acceleration of 8 m/s^2 and a deceleration of 14 m/s^2 in the lateral direction until the crab stops above the payload. This acceleration is 13 times faster than that which the electrical motor of the crab can induce. A maximum lateral horizontal load of 1.0 kN is measured at the crane wheels. A large vertical dynamic force of 58 kN is also measured at the payload, due to the steady creep speed hoisting mechanism not functioning during this lateral eccentric hoisting.

8.5 Loads due to deactivated electrical motor

If the electrical driving motors of an overhead travelling crane are not properly maintained, malfunction is a possibility, which will result in one end carriage lagging behind the other during acceleration of the crane. This situation was experimentally investigated by deactivating an electrical driving motor of the experimental crane. With only one electrical driving motor working, the crane was still able to traverse the runway with relative ease. In an industrial environment a crane with a failed electrical motor could easily be operated without the operator being aware thereof, if the rail to wheel contact surface is smooth.

When the crane moves in the longitudinal direction, the lateral horizontal wheel loads are a result of these kinematic longitudinal forces not being in equilibrium. These lateral horizontal loads at the wheels act as a horizontal force couple, which can also be described as a horizontal force moment around the centre of gravity of the system. The relative position of the centre of gravity of the crane and payload and the spacing and number of crane wheels influence these lateral horizontal wheel loads. The orientation of horizontal wheel loads due to a horizontal force moment around the centre of gravity of the system is indicated in the figure below, when one electrical driving motor is deactivated.

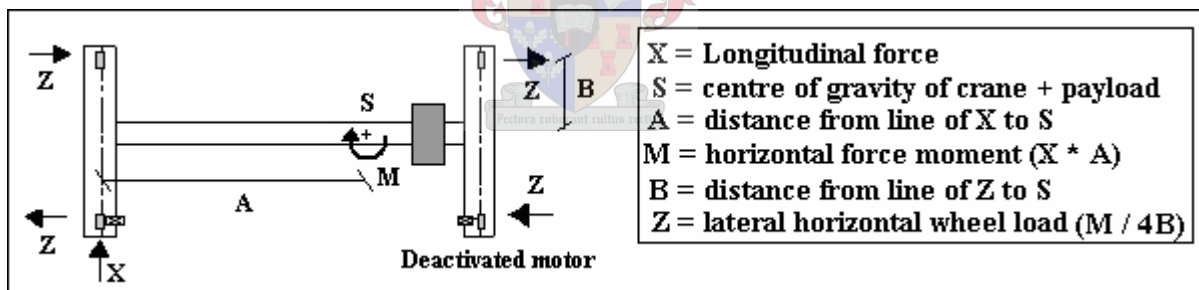


Figure 8.5: Skewing force mechanism when an electrical motor is deactivated

When the crane accelerated longitudinally with a deactivated electrical motor, a difference in relative longitudinal position of the end carriages was experimentally determined with the encoders on the two end carriages, by subtracting the relative distances traversed by the two end carriages from each other.

Figure 8.6 below indicates the loads measured at the wheels of the crane due to the deactivated electrical motor, during only acceleration and deceleration of the crane. The maximum lateral horizontal wheel loads at the green line on figure 8.6 are indicated at the crane wheel positions, when the crane accelerates. When the crane then decelerates, the wheel loads change orientation and when the crane comes to a halt, there are still some static wheel loads occurring.

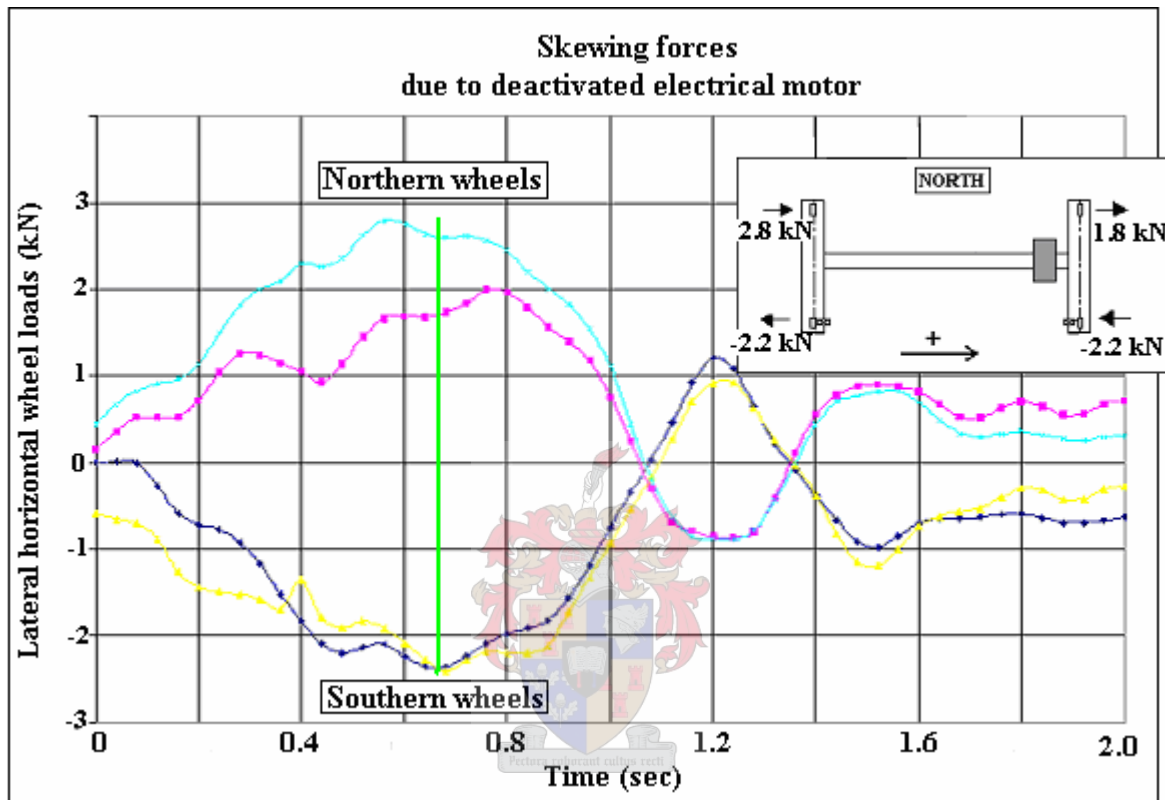


Figure 8.6: Lateral horizontal loads due to deactivated electrical motor

Figure 8.7 on the next page shows the longitudinal end carriage deviation that was determined during the same experiment as indicated in figure 8.6 above, when the crane accelerates and decelerates with a deactivated electrical motor.

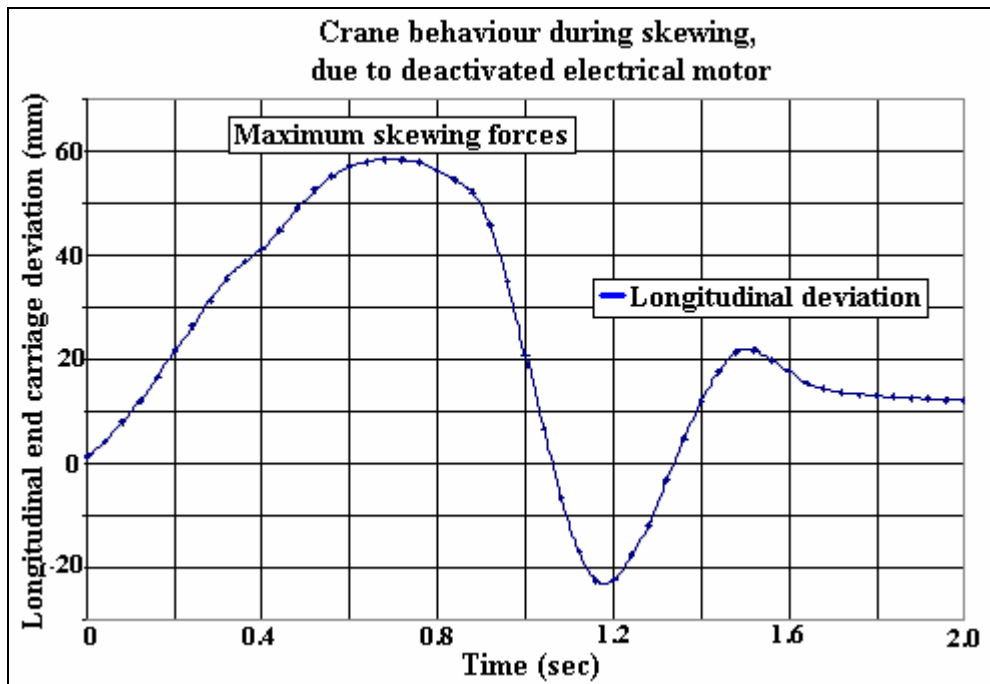


Figure 8.7: Longitudinal end carriage deviation resulting in skewing

From the above it is visible that these wheel loads are dynamic in response and that the lateral horizontal wheel loads are damped after longitudinal acceleration and deceleration stops. This is because the oscillating force behaviour is dramatically decreased, when the crane comes to a halt.

The normal functional crane is compared experimentally with the crane with a deactivated electrical motor. If the crane bridge accelerates and then immediately decelerates within 3 seconds with the payload at the maximum eccentric position as indicated in figure 8.6 above, the results are summarized in the table below.

Number of driving motors working	Longitudinal distance travelled by crane in 3 seconds	Max. longitudinal deviation in end carriage positions	Average skewing forces
2	400 mm	27 mm	0.8 kN
1	250 mm	66 mm	2.1 kN

Table 8.2: Influence of deactivating an electrical motor on acceleration behaviour of crane

The payload's pendulum behaviour during deceleration of the crane also induces external horizontal forces into the crane, which counteracts the initial lateral horizontal loads at the wheels, in an attempt to achieve lateral horizontal force equilibrium. The further the payload is positioned away from the center of the crane bridge, the higher these lateral horizontal forces are, due to the position of the center of gravity of the crane system being influenced by the payload position (refer to

figure 8.5 above). The crane also experiences a third lateral horizontal load response, in order for equilibrium of the system to be achieved in the longitudinal direction.

The largest lateral horizontal wheel loads of 2.8 kN were induced by the payload swinging when the crane decelerates. The position of the payload and the relevant lateral horizontal wheel loads are indicated in the figure below. If the crane traversed in the opposite direction these forces are equivalent in magnitude and opposite in direction, after the crane decelerated.

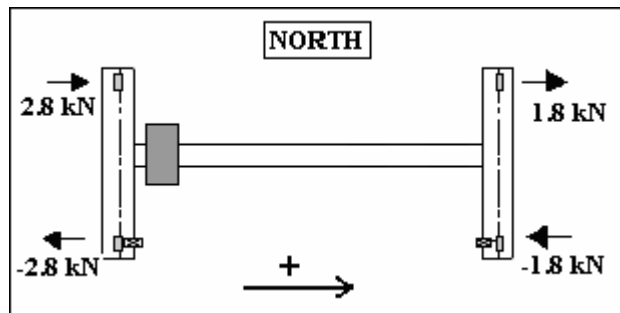


Figure 8.8: Critical lateral horizontal wheel loads

If the wheel at the deactivated motor has a maximum vertical wheel load, that wheel is unable to traverse the uneven rail splice (refer to figure 7.1), due to the frictional resistance at that wheel. The one end carriage moves longitudinally, while the other is restrained in the longitudinal direction. This resulted in skewing loads that could be investigated and also the visible elastic torsional deformation of the end carriages. This observation was recorded by a video camera, and can be seen on the attached DVD. Figure 8.9 below indicates the skewing forces that were measured.

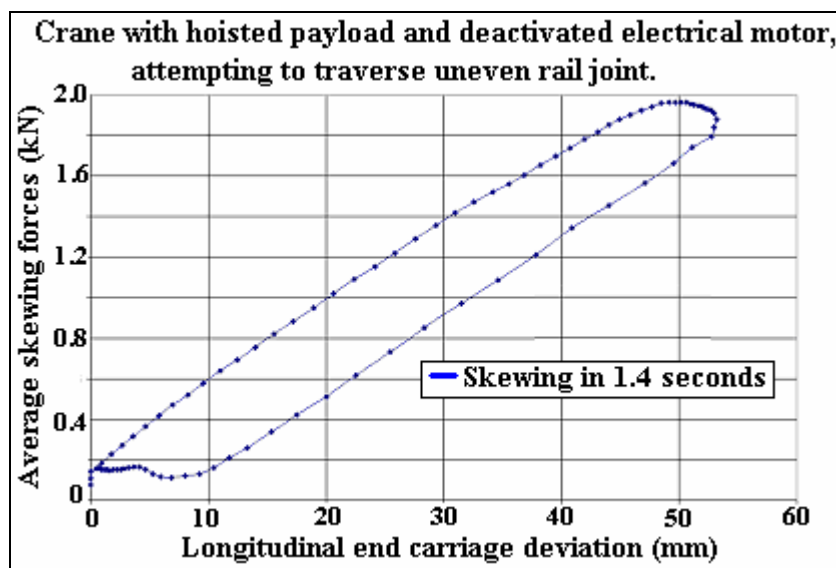


Figure 8.9: Skewing behaviour due to static crane, restraint longitudinally at a wheel

The maximum average skewing loads occur at the point of maximum longitudinal end carriage deviation. After this point is reached, the end carriage that moved longitudinally accelerates in the opposite direction, to achieve longitudinal force equilibrium.

8.6 Loads due to misalignment of supporting structure

If the supporting structure is not properly aligned within certain parameters based on the length of the crane bridge, the supporting structure is defined as being misaligned. The supporting structure under experimental investigation has the functionality that the lateral restraints of the girder can be modified to adjust the alignment of the supporting structure. An LVDT was positioned to measure the lateral displacement of the rail at the position of the lateral restraint that was modified.

These loads could occur on an actual overhead crane if the foundation of a supporting column rotates in such a way, that there is lateral deflection at the top of the columns. This could be induced by unstable soil conditions or excavation in the vicinity of the crane's supporting structure.

8.6.1 Quasi-static loads due to misalignment

To simulate this loading situation, the supporting structure was modified in the lateral horizontal direction up to 15 mm with the crane stationary on the supporting structure and one of its wheels close to the lateral restraint that was to be modified. The lateral deflection of the rail and the lateral horizontal wheel loads were measured. These experiments were performed to isolate the forces induced by misalignment of the supporting structure, onto the static crane.

These experiments were performed on the crane only as well as on the crane with hoisted payload. When no payload is hoisted, the lateral wheel load due to deflection of the rail is linear for the first 7mm of lateral displacement. After that the behaviour becomes non-linear, as the wheels start to slip laterally, due to the static frictional resistance being overcome at the wheels. If the payload is hoisted no wheel slip occurs, due to the high vertical wheel loads. This resulted in the lateral wheel load due to deflection staying linear for the whole experiment. The results of these two experiments at 10 mm of lateral deflection of the rail inwards as indicated in figure 8.10 below are compared, with the larger wheel loads occurring when the payload is hoisted.

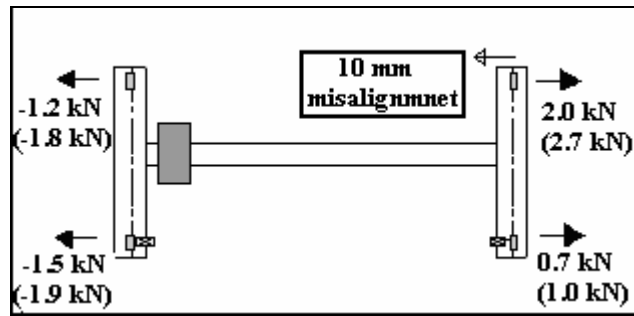


Figure 8.10: Maximum lateral horizontal wheel loads without payload (with payload hoisted)

The maximum lateral wheel load (kN) per millimeter of static lateral horizontal misalignment is **0.27 kN/mm**.

8.6.2 Kinematic loads due to misalignment

The position of the crane when the zero reading is taken and the point of misalignment of the supporting structure are indicated in the figure 8.11. The crane is now allowed to traverse the supporting structure with the misaligned rail and lateral horizontal wheel loads are measured.

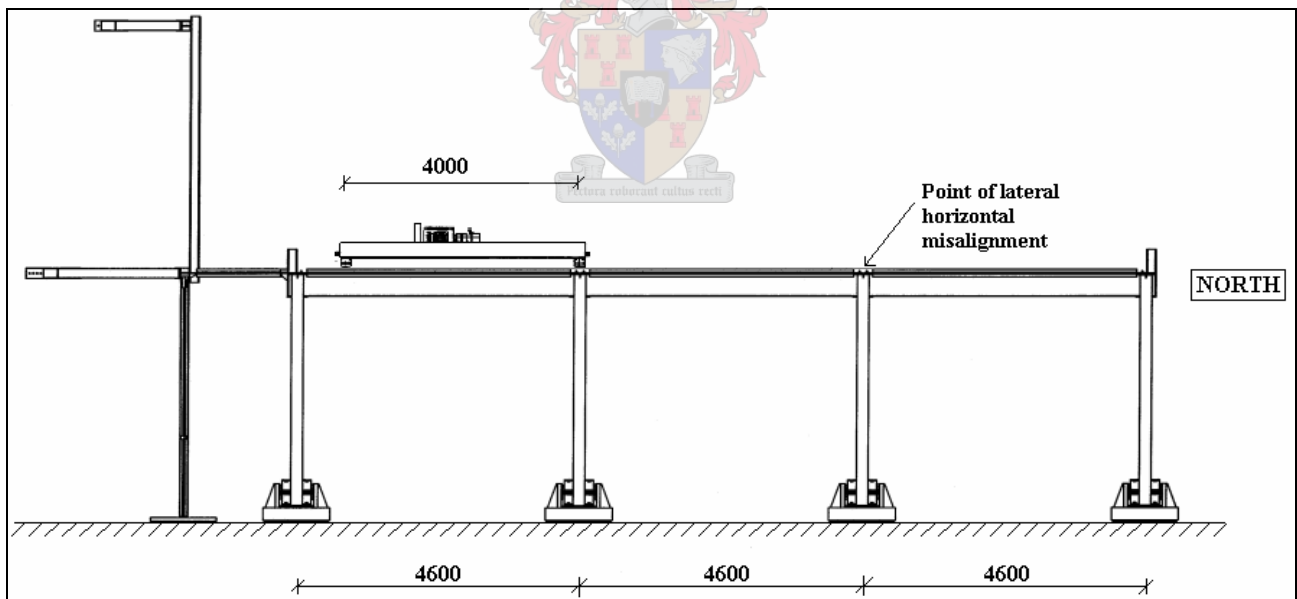


Figure 8.11: Configuration of system at start of misalignment investigation

The lateral horizontal wheel loads caused by misalignment of the supporting structure are influenced by the existing magnitude and direction of lateral horizontal wheel loads, the direction of longitudinal travel and the direction of misalignment. The maximum lateral horizontal wheel loads were measured during inward misalignment of the crane, with southwards longitudinal crane travel.

Figure 8.12 below indicates the lateral horizontal wheel load behaviour as the crane traversed the supporting structure with the payload at the centre of the crane bridge, with the supporting structure inwardly misaligned by 10 mm. The maximum lateral horizontal wheel loads and their orientation are also indicated.

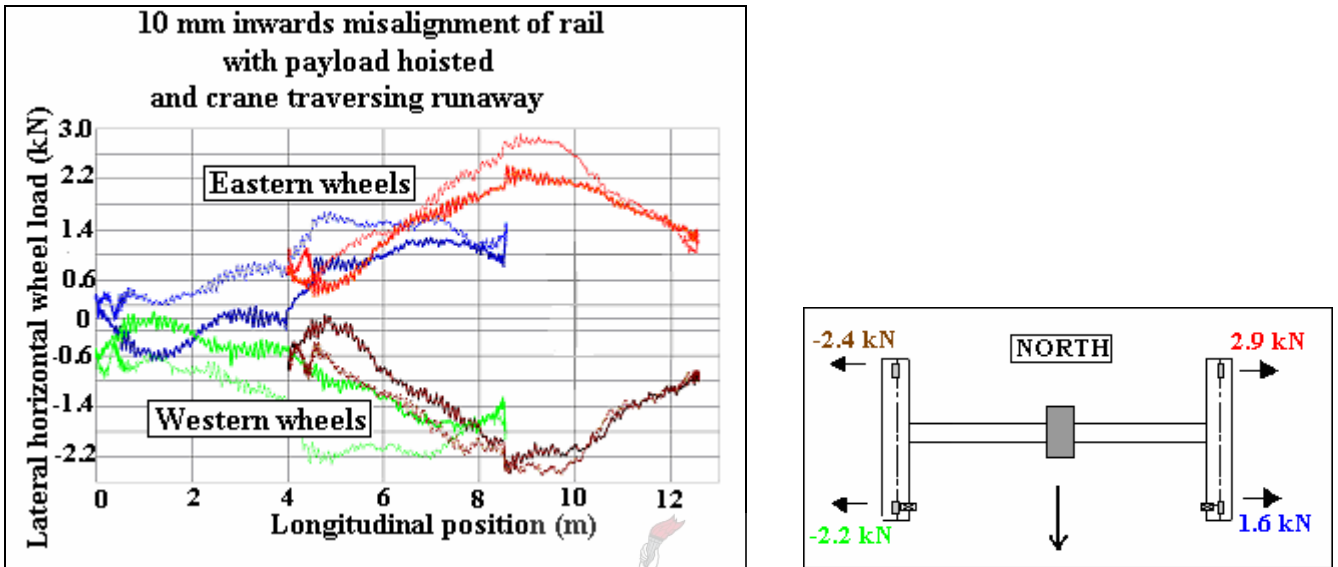


Figure 8.12: Maximum wheel loads measured during inward misalignment

The maximum kinematic wheel load measured per millimeter of lateral misalignment is **0.29 kN/mm**.

With an eccentrically positioned payload, the lateral horizontal forces are not higher than with the payload at the center of the crane bridge. This indicates that the vertical wheel load does not influence the lateral horizontal wheel loads due to misalignment, but are rather influenced by the existing lateral horizontal wheel loads due to deflection of the crane bridge.

The exceptional forces at the payload and the supporting structure and the exceptional loads at the crane's wheels were determined experimentally.

Chapter 9 – Summary of wheel loads and crane characteristics

In this chapter the experimental results due to regular loads and exceptional loads onto the supporting structure are summarized. These critical wheel loads are compared with the loads determined by implementing the load models in SABS 0160 -1989 and EN 1991-3 for a class 2 crane with similar geometric characteristics and load carrying capacity. The general crane characteristics from this research report, during normal crane operation, is compared with the relevant information from literature.

The table below is a summary of the experimental investigation in the previous two chapters, with regards to the **wheel loads**. The shaded cells indicate the highest wheel loads measured during this experimental investigation.

Regular wheel loads due to	Vertical wheel load (kN)	Maximum lateral horizontal wheel load (kN)	
7.1. Own weight of crane	5.2	0.6	
7.2. Hoisting and lowering of payload (A)	13.9	1.0	
7.3. Longitudinal travel with payload (B1)	24	1.3	
7.4. Lateral travel with payload (B1)	24	1.3	

Exceptional wheel loads due to	Vertical wheel load (kN)	Maximum lateral horizontal wheel load (kN)	Longitudinal horizontal force per end carriage (kN)
8.1. Hoisting payload to maximum height	14.4	1.1	~
8.2. Longitudinal buffer impact (A)	14.8	1.5	11.0
8.3. Electrical driving motors	~	~	2.7
8.4. Eccentric hoisting of payload	14.5	1.85	~
8.5. Deactivating an electrical motor (skewing)	~	2.8	~
8.6. Misalignment (inwards)	~	0.29 kN/mm	~

Table 9.1: Summary of critical experimental wheel loads

Figure 9.1 on the next page indicates the crane position where the highest vertical forces in the supporting structure and the largest lateral horizontal wheel loads occur, during longitudinal crane travel, with the zero point reading taken with the crane positioned as indicated in figure 7.1.

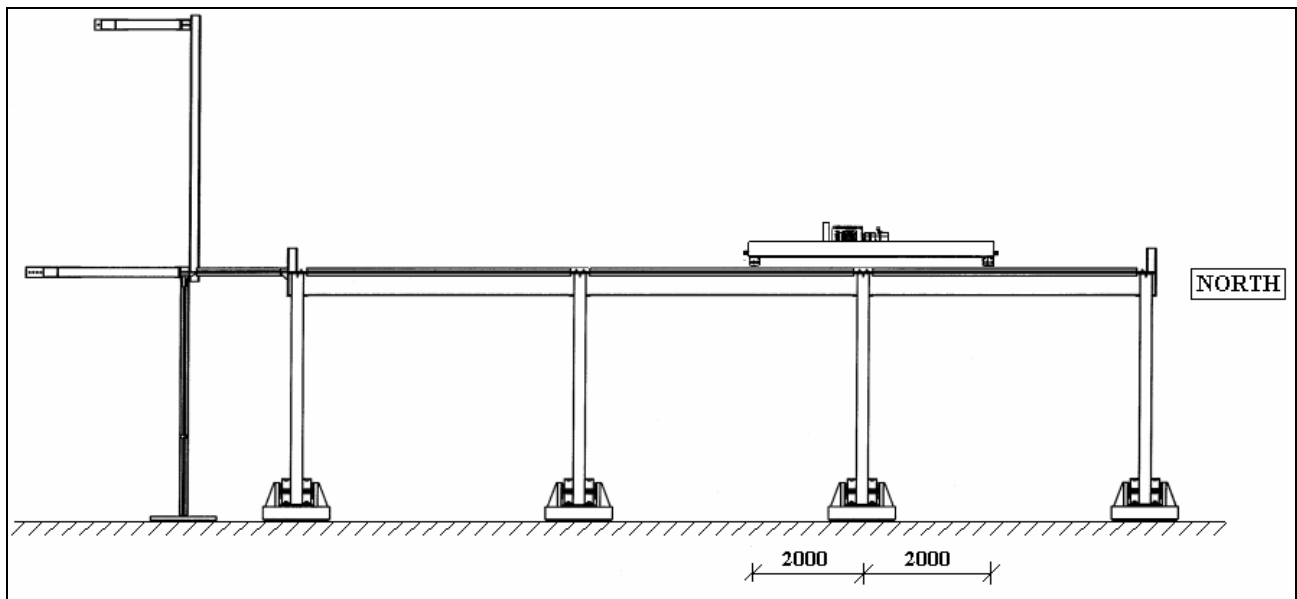


Figure 9.1: Position of crane for largest forces and wheel loads on system

Table 9.2 below compares the maximum experimentally determined wheel loads in the 3 main directions. The wheel loads measured in the experimental investigation are compared against the wheel loads as per SABS 0160 load models and the newly proposed SANS 10160 as adopted from EN 1991-3. Refer to Appendix E for the wheel load calculations. The wheel load calculation results from SABS 0160 and SANS 10160 closest to the experimental results, are highlighted.

Critical dynamic forces (kN)	Experimental results	SABS 0160	SANS 10160
Vertical wheel loads			
Maximum	28.7	34	32.5
Minimum	5.7	6.8	5
Lateral horizontal wheel loads			
Due to acceleration of crab	1.3	1.3	1.3
Misalignment	2.9	2.2	2.2
Skewing due to acceleration of crane, defective electrical motor, wheel guide mechanism	2.0	3.2	2.7
	2.8	~	~
	~	~	6.5
Longitudinal horizontal force per rail			
Electrical driving motors	2.7	5.6	1.9
Force on each end stop	11	21 or 11.2	22.7

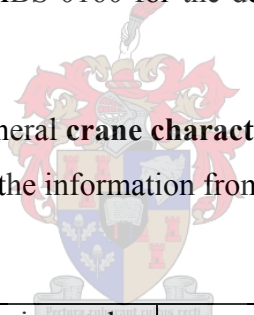
Table 9.2: Comparison of results from the experimental investigation with crane load models from SABS 0160 and newly proposed SANS 10160

For the vertical wheel loads, SANS 10160 gives a more accurate and detailed description of the dynamic wheel load behaviour, as compared to SABS 0160.

For acceleration of the crab and misalignment of the crane and gantry, the results from SABS 0160 and SANS 10160 are similar, because no major modifications in SANS 10160 occur. The results for acceleration of the crab correlate very well against the experimental results. The theoretical results for misalignment of the supporting structure are lower because the lateral horizontal wheel loads due to the static weight of the crane and payload are not taken into account. The description of skewing behaviour in SANS 10160 is more detailed than in SABS 0160. No theoretical load model for a defective electrical driving motor occurs and the theoretical forces due to the guide force mechanism seem disproportionately high.

For longitudinal horizontal wheel loads, SANS 10160 makes reference to the longitudinal drive force, which is dependant on the output of the electrical driving motors, which makes it a more accurate method. The load model in SABS 0160 for the determination of the impact forces on the end stops is the most accurate.

Table 9.3 below is a summary of the general **crane characteristics** from this research report, during normal crane operation, compared with the information from literature made mention of in chapter 2.



	Experimental results	Frank Taylor ^[6]	A.Z.Al-Garni ^[7]
Maximum acceleration (m/s ²):			
longitudinal	0.2	0.37	0.3
lateral	0.5	~	0.3
vertical	1.0	~	0.5
Maximum speed (m/s):			
longitudinal	0.55	0.534	2.0
lateral	0.45	~	1.0
vertical	0.075	~	0.5

Table 9.3: Comparison of general crane characteristics with similar information from literature

Table 9.3 above is indicative of the fact that there are many different types of cranes implemented in industry today, and it emphasises the fact that crane classification relates kinematic properties of different cranes. The boundary limits between the different crane classes could however be further refined, in terms of exact limits for speed and acceleration of cranes.

Some of the assumptions made in literature on crane models will be commented on, with regards to the results and observations from this experimental investigation.

The mechanical model of J.W. Auernig & H. Troger^[8] :

- Neglected elastic deformation of the crane and all the elements were assumed infinitely stiff.

Comment: This assumption is in direct contrast to the basis on which the experimental wheel loads were determined in this research report.

- The change in rope length, due to swinging of the load, was neglected.

Comment: The influence of the shortening of the hoisting cable on the dynamic behaviour of the system, was determined experimentally (+/- 6% higher vibration frequency).

Lee, Ho-Hoon^[9] :

- Developed a system to help guide the crane in the longitudinal direction, so as to decrease the pendulum action of the payload.

Comment: This pendulum action of the payload has a substantial influence on the skewing forces that the crane can be exposed to. Implementing this system on overhead cranes that function at high-speeds will definitely help to decrease the lateral horizontal wheel loads, which these cranes will experience.

R. Karmakar & A. Mukherjee^[10] made the following assumptions, to solve the mathematical crane model, which they developed.

- Critical dynamic loading occurs when the crab is at mid-span of the crane bridge.

Comment: When the payload is hoisted at the center of the crane bridge, the vertical deflections of the crane are highest, which means that it is the least stiffest scenario. The largest dynamic loading was measured with the crab and payload hoisted at the most eccentric position on the crane bridge. This is in contrast to the assumption from literature.

- This model neglects shear deformation of the system.

Comment: Direct experimental shear measurements on the crane were not performed. Theoretical shear stress calculations were done. Refer to table C3 in Appendix C for a summary of theoretical stress results.

Chapter 10 – Conclusions relating to behaviour of system

The behaviour of the crane and its supporting structure will be described in terms of the behaviour of the measured wheel loads. Conclusions on skewing and misalignment behaviour based on the results from the experimental wheel load investigation will be made.

10.1 Description of behaviour of system

A 2 dimensional diagram will be used to indicate the influencing factors on the behaviour of the overhead crane and its supporting structure. The system is stiffest if the payload is eccentrically hoisted. During hoisting of the payload, the shortening of the cables results in further stiffening of the system.

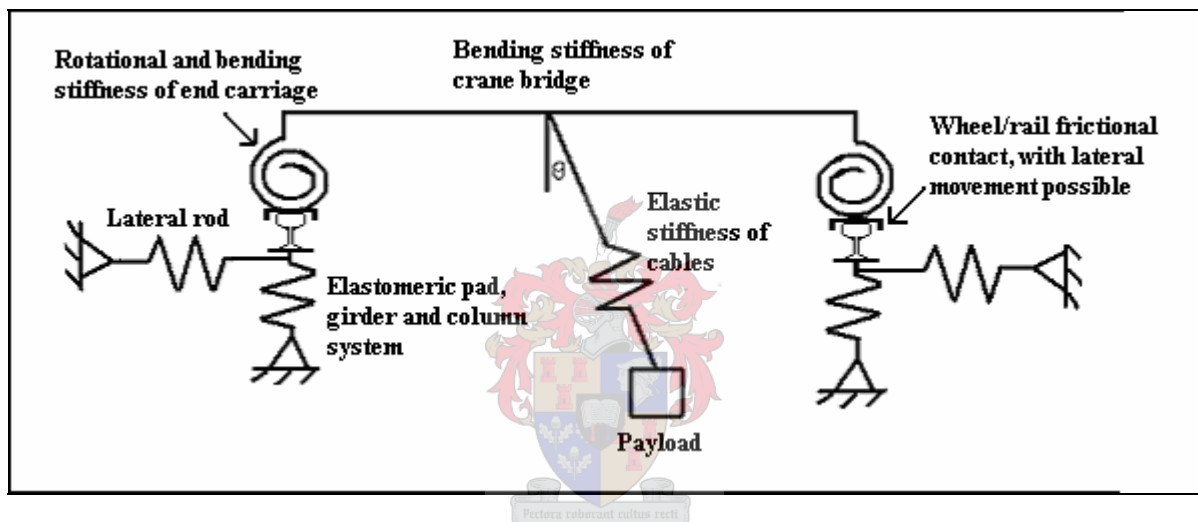


Figure 10.1: Diagram indicating aspects influencing dynamic behaviour

During vertical payload hoisting and longitudinal crane travel over an uneven surface, the forces at the crane's wheels are defined as dynamic forces with a harmonic behaviour, which experience an under-damped decaying oscillation.

During lateral horizontal crab travel the forces at the wheels are dynamic forces, which are dependant on the frictional resistance at the crab's wheels and are influenced by the vertical position of the payload. The longer the hoisting cable is, the higher the lateral horizontal wheel loads are, due to the increased rotation angle occurring during swinging of the payload.

During longitudinal crane travel over a smooth surface, the kinematic vertical forces at the wheels are constant. The lateral horizontal forces are less constant and dynamic peaks occur which have a damped response, when the payload is allowed to swing longitudinally. This damped response is due to the gap between the wheel flanges and the railhead, allowing the wheels to translate laterally, and in doing so, energy is dissipated through friction at the wheels and through deformation of the crane

end carriages. The highest vertical and lateral horizontal reaction forces under regular wheel loads on the supporting structure occur when the crane bridge moves directly over the internal supporting columns. The wheels of the crane are then closest to a specific restraining point and as a result the reaction forces are maximum at that instance.

10.2 Description of skewing behaviour

Skewing behaviour of the crane is influenced by the longitudinal equilibrium of the crane system, relative to the centre of gravity of the system. When the electrical driving motors are working correctly during normal longitudinal crane motion, there are no large lateral horizontal wheel loads if the payload is eccentric and the crane accelerates. When the crane decelerates, the swinging eccentric payload causes the highest lateral horizontal wheel loads, during normal longitudinal crane travel.

End buffer impact, uneven rail splice connection, eccentric hoisting of payload, longitudinal swinging payload and defective electrical driving motor are the load models during which skewing behaviour was observed.

10.3 Description of misalignment behaviour

The crane normally experiences outward lateral horizontal wheel loads, due to the vertical deflecting crane bridge, forcing the crane's wheels outwards. Inward misalignment is acting opposite to these lateral horizontal wheel loads. This indicates that the lateral horizontal wheel loads due to the weight of the crane and payload need to be included in the crane design process.

10.4 Possible future research

The wheel spacing on the crane can be decreased, which should result in larger reaction forces in the supporting structure. The influence thereof on the lateral horizontal forces of the system, and the possible influence on the skewing behaviour can also be investigated.

The supporting structure can be modified to a portal frame, by connecting rafters that are purpose made to the top of the supporting structure. 'Springs' must be inserted at the base of the supporting system and the lateral restraints can then be released. This will allow a supporting structure, with a variable lateral stiffness. The influence of the lateral stiffness of the system on the wheel loads of the overhead crane and supporting structure can then be investigated.

A calibrated numerical crane model can be used for determining the behaviour during various possible scenarios, which fall outside the capabilities of this experimental system.

References

1. SABS 0160, clause 5.7, South African Bureau of Standards, Private Bag X191, Pretoria, South Africa, 1989
2. South African Institute of Steel Construction Handbook, Chapter 10, PO Box 291724, Melville, 2109, South Africa, 2006
3. Gorenc B.E. – Crane Runway Girders, Australian Institute of Steel Construction, PO Box 6366, North Sydney, NSW 2059, 1983
4. Crane Aid, Code of practice for crane testing and maintenance inspections, Unit 20.12, Trostre Business Park, Llanell, Carmarhenshire, SA14 9UU, 1980
5. South African Structural Steelwork Specifications for Construction, 1st Edition, Section 8.6.2, South African Bureau of Standards, Private Bag X191, Pretoria, South Africa, 2000
6. Frank Taylor, Validation of virtual crane behaviour, through comparison with a real crane. Source: ASME 2002 Design Engineering Technical Conference, Montreal, Canada, DETC2002/CIE-34391, October, 2002,
7. Al-Garni,A.Z. (King Fahd Univ. of Petroleum and Minerals, Saudi Arabia), Optimal control of overhead cranes, Source: Control Engineering Practice, v 3, n 9, p1277-1284, ISSN:0967-0661 CODEN: COEPEL, Sept,1995
8. J.W. Auernig (Technische Univ, Vienna, Austria) ; H. Troger
Time optimal control of overhead cranes, with hoisting of load
Source: Automatica, v 23, n 4, p.437-447, July 1987
9. Lee, Ho-Hoon (Departement of Mechanical Engineering, Tulane University)
A new approach for the anti-swing control of overhead cranes with high-speed hoisting.
Source: International Journal of control, v76, n 15, p1493-1499, October 2003

10. R. Karmakar and A. Mukherjee

“Dynamics of electric overhead traveling cranes. A bond graph approach.”

Mechanical Engineering Department, Indian Institute of Technology,

Source: Mechanism & Machine Theory, v 25, n 1, p29-39, 1990

11. Karl Hoffmann, An Introduction to Measurements using Strain Gages, Hottinger Baldwin

Messtechnik, Im tiefen See 45, 64293, Darmstadt, GERMANY, 1989

12. Louis Eder, Instruments for Engineering Measurements, 29 Van Riebeeck Street, Gerdview,

Germiston 1401, SOUTH AFRICA, 2000

13. E.C. Glauser, Torsion in structures – An engineering approach, Springer – Verlag, 1966



Appendix A – Own weight of crane and crab

During the experimental investigation of the crane wheel loads, the own weight of the crane was not included in these wheel load measurements. These loads and their influence on the strain gauges on the end carriage load measuring systems, had to be determined. The end carriages were supported vertically at various points during the calibration of the end carriage load measuring system, as indicated in the photo below.



Photo A1: End carriage supported, to cancel out stress effects due to crane's own weight

A zero reading was then taken and the crane was then lifted from these supports and then placed onto the crane's wheels on top of the rail supports. The crane would then deflect due to gravity, and would result in stresses due to these deformations. The total absolute bending stress induced by the crane's own weight, was determined to be **12.8MPa**. Refer to figure C2, for the sectional properties of the end carriages.

The average measured axial force in the flanges:

$$\begin{aligned}\text{Force} &= (\text{average stress at flanges}) \times (\text{area of flanges}) \\ &= 12.8 \text{ MPa} \times (14.2 \text{ mm} \times 205.2 \text{ mm}) &= & 37.3 \text{ kN}\end{aligned}$$

The average stress at the corners of the flanges is lower than the bending stress measured at the centre of the flanges.

$$\begin{aligned}\text{Stress ratio} &= 0.5h / (0.5h - 0.5t_{\text{flange}}) \\ &= 104.8 \text{ mm} / (104.8 \text{ mm} - 7.1 \text{ mm}) &= & 1.073 \\ &\approx 7\% \text{ stress increase at the surface}\end{aligned}$$

The corresponding bending moment occurring at the strain gauges is:

$$\begin{aligned}&= \text{Average force} \times \text{ratio} \times (\text{height of End Carriage}) \\ &= 37.3 \text{ kN} \times 1.073 \times 0.2096 \text{ m} \\ &= 8.4 \text{ kN.m}\end{aligned}$$

Refer to figure C7, on the geometric properties of the end carriages, to determine the vertical force at the wheels.

$$\begin{aligned}\text{Vertical force at wheels} &= \text{Bending moment at strain gauges} / \text{Distance to wheel} \\ &= 8.4 \text{ kN.m} / 1.5 \text{ m} &= 5.6 \text{ kN per wheel} \\ \therefore \text{Own weight of crane is } &22.4 \text{ kN, as measured by strain gauges}\end{aligned}$$

This measurement takes the weight of the whole crane into account.

The own weight of the crab could not be measured directly. It could only be determined indirectly through static equilibrium of the reaction forces when the crab is moved to the limits on the crane bridge. The crab's weight must be subtracted from that of the whole crane, which was determined to be 2.3 kN, to determine the weight of the crane bridge and end carriages as being 20.1 kN.

The weight of the components of the crane are summarized below.

Crane bridge : 10 kN

End carriages: 5 kN

Web stiffeners + driving motors ~ 6 kN

Total weight without crab = 21 kN



Appendix B – Data acquisition system

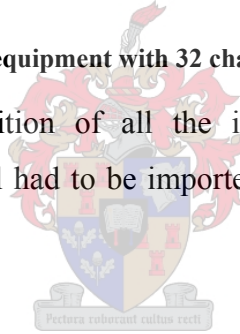
B1 Hardware and software

The photo below indicates 4 of the Spider 8 systems, which were connected to a computer system, on which Catman software was installed. This whole hardware system allowed 32 simultaneous data input channels to be imported into the Catman graphic user interface on the computer, for evaluation and to be saved on the hard drive of the computer system.



Photo B1: Spider equipment with 32 channel-input data capacity

The Catman software required definition of all the input channels and relevant calibration coefficients for each data input channel had to be imported. The input channels need to be zeroed before every experiment.



B2 Wheatstone full-bridges

The strain gauges on the end carriage load measuring system are connected to the data acquisition system, by means of Wheatstone full bridges. These connections allow transformation of the measured strain into the required type of stress.

Understanding these connections and the results that they give, are important for implementing the end carriage load measuring system. The photo and figure below indicate the full-bridge connection with two dummy gauges, which are connected to strain gauges above and below the centre of the flanges, for measuring strong axis bending strain in the end carriage load measuring system.

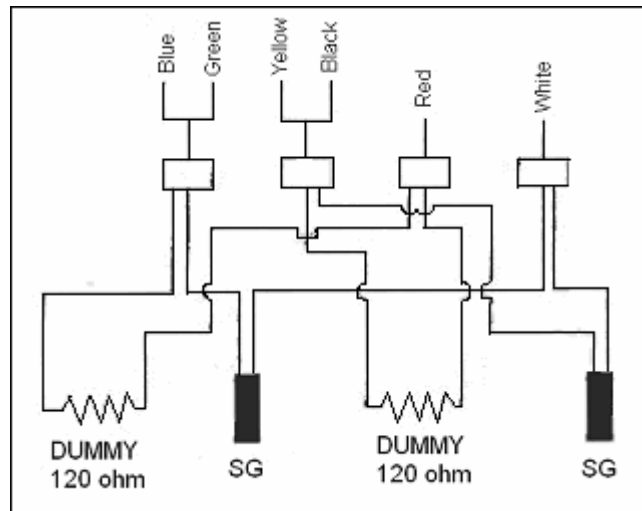
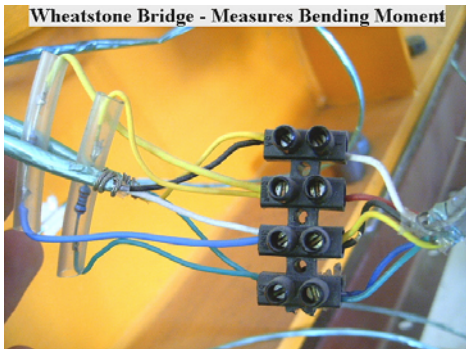


Figure B1: Photo and diagram indicating Wheatstone bridge for measuring bending strain

The photo and figure below indicate the full-bridge connection with two dummy gauges, which are connected to strain gauges above and below the edges of the flanges, for measuring average normal strain at the edges of the flanges and at the centre of the webs, in the end carriage load measuring system.

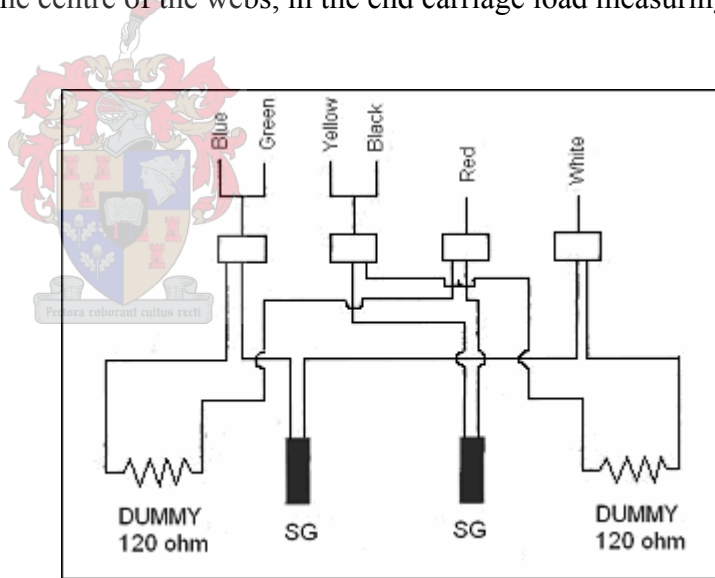
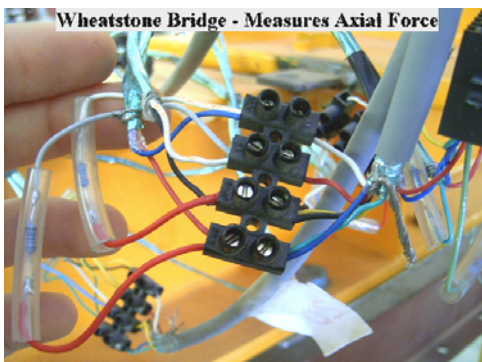


Figure B2: Photo and diagram indicating Wheatstone bridge for measuring normal strain

B3 Implementation of data acquisition system

This information is of value to people who will be doing further research on the behaviour of the electric overhead travelling crane and its supporting structure.

The different experimental data capturing systems used, are summarized in short.

Encoders are used to measure displacement and speed of the crane.

Accelerometers are used to measure acceleration of the crane, crab and payload.

LVDT's are used to measure deformation of crane and supporting structure under loading.

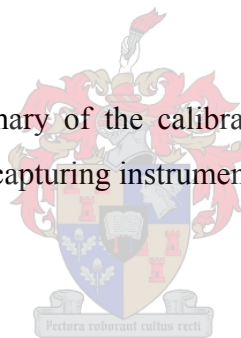
Load cells are used for calibrating end carriage load measuring system and to measure forces in the system.

Lateral supports are used to measure lateral horizontal wheel loads on the supporting structure.

Strain gauges are used to measure strains on the end carriage load measuring system, and to transform it into bending stress and normal stress.

The **end carriage load measuring system** is used to transform measured strains at the strain gauges into wheel loads at the crane.

The table on the next page is a summary of the calibrated scaling factors implemented for this experimental investigation, on the data capturing instrumentation.



Instrument	Scaling factor	Type	Range
Encoders			
• East & West	$f(x) = x * 3.92857$	2Phase1	1kHz
Accelerometers			
• East & Crab	$f(x) = x * 20000/457 * 0.950$	Full Bridge	3mV/V
• West	$f(x) = x * 20000/457 * 0.997$	-	-
LVDT's			
• Girders	$f(x) = x * 10mm / (160mV/V) * 1.062$	Half Bridge	125mV/V
• Crane Bridge	$f(x) = x * 40mm / (160mV/V) * 1.04$	-	-
• End Carriage	$f(x) = x * 40mm / (160mV/V) * 1.02$	-	-
Load cells			
• A (column A1)	$f(x) = x * 50ton / (2mV/V) * 9.575$	Full Bridge	3mV/V
• B (column A7)	$f(x) = x * 50ton / (2mV/V) * 9.668$	-	-
• C (column A14)	$f(x) = x * 50ton / (2mV/V) * 10.246$	-	-
• H (column A20)	$f(x) = x * 200kN / (2.039mV/V) * 0.974$	-	-
• 5 ton payload	$f(x) = x * 200kN / (2.mV/V) * 1.01$	-	-
• G (vertical)	$f(x) = x * 200kN / (2.039mV/V) * 0.985$	-	-
• 4 (horizontal)	$f(x) = x * 2ton / (2mV/V) * 9.790$	-	-
• E & W	$f(x) = x * 5ton / (2mV/V) * 9.775$	-	-
• D	$f(x) = x * 200kN / (2.039mV/V) * 1.029$	-	-
Lateral supports			
• Rod A	$f(x) = x * 190.0$	Half Bridge	3mV/V
• Rod B	$f(x) = x * 187.8$	-	-
• Rod C	$f(x) = x * 192.2$	-	-
• Rod D	$f(x) = x * 180.0$	-	-
• Rod F, G & H	$f(x) = -x * 190.0$	-	-
Strain gauges			
Strong axis bending stress			
6,13,20,27	$f(x) = x(mV/V) * 4 / (2 * 2.14) * 210GPa$	Full Bridge	3mV/V
Normal stress			
1-5,8-12,15-19,22-26	$f(x) = -x(mV/V) * 4 / (2 * 2.14) * 210GPa$	Full Bridge	3mV/V
End carriage load measuring system			
Algebraic computations of strain gauges			
Horizontal	Wheel S-E	$-((2+4)-(3+5)) / (29MPa/kN)$	
	Wheel N-E	$-((9+11)-(10+12)) / (29MPa/kN)$	
	Wheel S-W	$-((16+18)-(17+19)) / (29MPa/kN)$	
	Wheel N-W	$-((23+25)-(24+26)) / (29MPa/kN)$	
Vertical			
	Wheels S-E & S-W	$6 / (2.47MPa/kN) \& 20 / (2.55MPa/kN)$	
	Wheels N-E & N-W	$13 / (2.49MPa/kN) \& 27 / (2.52MPa/kN)$	

Table B1: Calibration coefficients implemented during experimental investigation

Appendix C - Theoretical model of end carriage load measuring system

The end carriage load measuring system, which was experimentally investigated, was also compared against a relative simplistic theoretical model. A fully restrained cantilever beam with similar characteristics was investigated. The reason for this, was because similar calculations in literature were used as reference. The influence of the web stiffeners was not investigated. This theoretical model is totally restrained at the end connection and load vectors are applied at the wheel position, which is free to deflect and rotate. The figure below indicates the actual and theoretical system with each of the load vectors P_x , P_y and P_z of magnitude 1 kN applied at the centroid of the theoretical model. The force moment T_z at the centroid of the theoretical model is a result of force vectors applied eccentrically to its centroid.

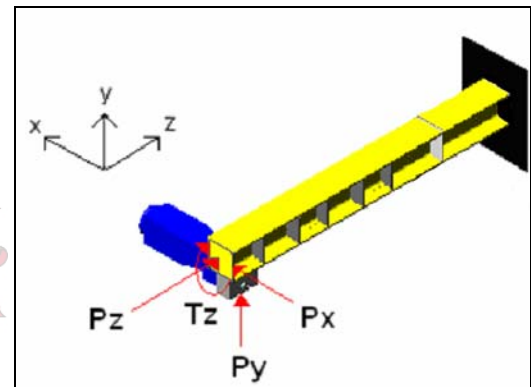


Figure C1: Theoretical investigation of end carriage load measuring system

C1 Characteristics of end carriage load measuring system

The sectional properties of the end carriage load measuring system determine its response under loading. The figure below is a sectional view of the end carriage, indicating its dimensions and sectional classification.

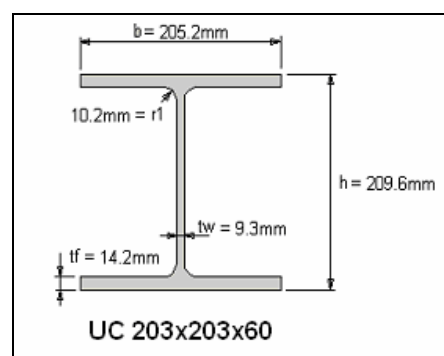


Figure C2: Sectional properties of end carriages

The structural mechanics of a universal column 203x203x60kg/meter steel section as specified in SAISCH ^[2], are as follows:

Poisson's ratio: $\nu = 0.3$

Elasticity modulus: $E = 210 \text{ GPa}$

$I_{xx} = 61\text{E}6\text{mm}^3$

$Z_{x-x} = 582\text{E}3\text{mm}^3$

$I_{yy} = 20.5\text{E}6\text{mm}^3$

$Z_{y-y} = 199\text{E}3\text{mm}^3$

Shear modulus:

$$G = \frac{E}{2(1+\nu)} = \frac{210\text{GPa}}{2(1+0.3)}$$

$$= 80.77\text{GPa}$$

Saint-Venant Torsional constant:

$$J = \frac{1}{3} \cdot (2b \cdot t_f^3 + h \cdot t_w^3) = \frac{1}{3} \cdot (2 \times 205.2\text{mm} \times 14.2\text{mm}^3 + (209.6\text{mm} \times 9.3\text{mm}^3))$$

$$= 447\text{E}3 \text{ mm}^4$$

$$\approx 475\text{E}3 \text{ mm}^4 \text{ (SAISC - Redbook)}$$

Warping Torsional constant:

$$C_w = \frac{I_f \cdot h^2}{2} = \frac{t_f \cdot b^3 \cdot h_{ave}^2}{24} = \frac{14.2\text{mm} \times 205.2\text{mm}^3 \times (209.6\text{mm} - 14.2\text{mm})^2}{24}$$

$$= 195\text{E}9 \text{ mm}^6 \text{ (SAISC-Redbook)}$$

Characteristic value of section:

$$\lambda = \sqrt{\frac{G \cdot J}{E \cdot C_w}}$$

$$= \sqrt{\frac{80.77\text{GPa} \times 475\text{E}3 \text{ mm}^4}{210\text{GPa} \times 195\text{E}9 \text{ mm}^6}}$$

$$= 9.68\text{E}-4 \text{ mm}^{-1}$$

The stress behaviour of Universal Columns under torsional loading is rather complicated and is described in the book by E.C. Glauser^[13]. The basic response can be divided into Saint-Venant torsional shear stress, warping shear stress and warping normal stress in the section. The shear stresses cannot be measured experimentally by the end carriage load measuring system, but are described for academic purposes.

Saint-Venant torsional shear stress:

The Saint-Venant torsional shear stress acts parallel to the surface of the cross section and varies linearly across the thickness of the web and flanges, as indicated in the figure below. It is the greatest in the thickest element.

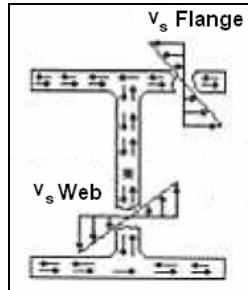


Figure C3: Saint–Venant torsional shear stress behaviour

Warping shear stress:

The warping shear stress acts constantly across the thickness of the flanges and varies along the length. As indicated in the figure below, it also acts parallel to the cross section of the flanges, and is induced if the section cannot warp freely.

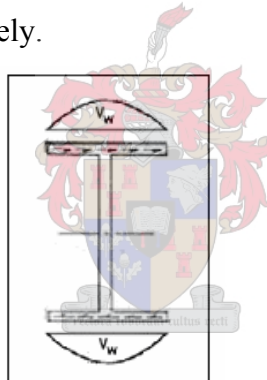


Figure C4: Shear stresses induced by warping torsion

Warping normal stress:

Direct tension and compression stresses occur in the flanges due to weak axis bending of flanges. It acts perpendicular to the cross section of the flanges, as indicated in the figure below. It also acts constantly across the thickness of the flanges and is largest at the outside fibers of the flanges.

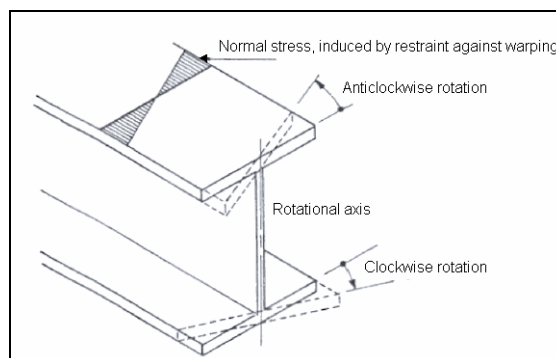


Figure C5: Warping normal stresses in the flanges

Rotational displacement function:

These torsional stresses are all a function of the rotational displacement function ϕ and its various derivatives. The function ϕ is dependant upon the type of loading as well as the end conditions of the section. The basic behaviour due to the shear forces V_f acting on the flanges, are indicated in the figure below.

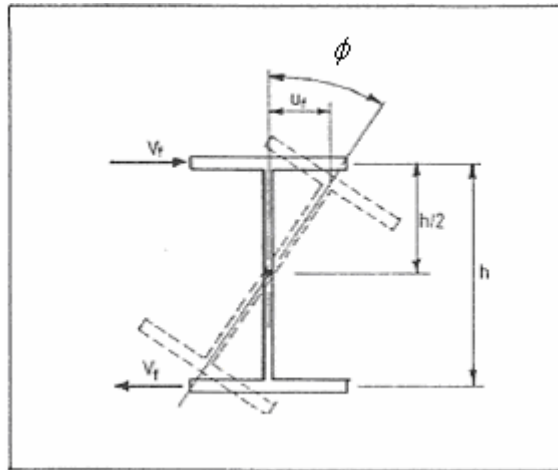


Figure C6: Bending around the z-axis due to shear forces in the flanges

The homogenous equation for torsion, based on the rotational displacement function, is defined in literature, as follows:

$$\phi = A \sinh \lambda z + B \cosh \lambda z + C + \frac{T}{2GJ} \cdot z$$

A, B and C are constant values which are influenced by z ; the relative position along the length of the cantilever beam and also the boundary conditions of the system. The rest of the variables are defined previously.

The physical meaning of ϕ and its derivatives are as follows:

$$\phi = \text{total twist of section,} \quad d\phi/dz = \text{Saint Venant torsional shear stress.}$$

$$d\phi^2/dz^2 = \text{Normal stress warping torsion} \quad d\phi^3/dz^3 = \text{Shear stress warping torsion.}$$

C2 Behaviour due to applied load vectors

The calculations, for determining the stress and strain response at the strain gauge positions on the end carriages for the different load vectors indicated in figure B3, are defined below.

C2.1 Vertical load vector

The figure below is an elevational view of the cantilever beam indicating the position of the strain gauges, the applied load vector and the orientation of the reaction forces at the restraint. The response at the strain gauges is related to these reaction forces.

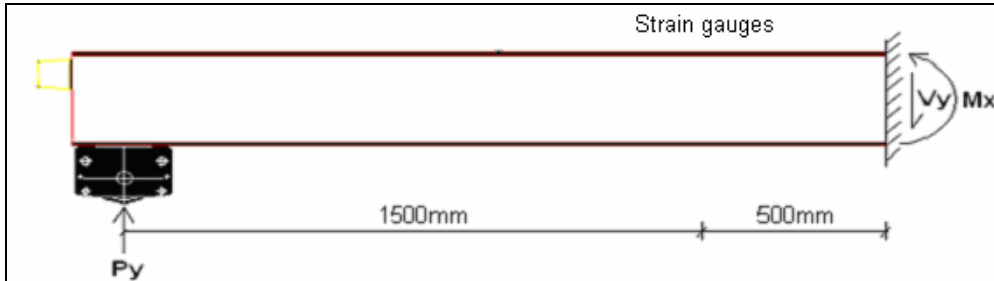


Figure C7: Elevation of cantilever beam with vertical load vector

$$V_y = P_y = 1 \text{ kN}$$

$$M_x = P_y \times 1500 \text{ mm}$$

$$\sigma_z = \frac{M_x}{Z_{x-x}}$$

$$= \frac{P_y \times 1500 \text{ mm}}{582 \text{ E}3 \text{ mm}^3}$$

$$= 2.58 \text{ MPa}$$

$$\epsilon_z = \frac{\sigma_z}{E}$$

$$= \frac{2.58 \text{ MPa}}{210 \text{ kN} \cdot \text{mm}^{-2}}$$

$$= 1.23 \text{ E}^{-2} \text{ mm/mm}$$

$$\tau_{web(max)} = \frac{P_y \times ((A_{flange} \times \bar{y}_{flange}) + (A_{web/2} \times \bar{y}_{web/2}))}{I_{xx} \times t_{web}}$$

$$= \frac{P_y \times ((205.2 \text{ mm} \times 14.2 \text{ mm} \times 97.7 \text{ mm}) + (181 \text{ mm} / 2 \times 9.3 \times 181 \text{ mm} / 4))}{61 \text{ E}6 \text{ mm}^4 \times 9.3 \text{ mm}}$$

$$= 0.57 \text{ MPa}$$

The figures below indicate an elevational view of the typical bending stress and shear stress response due to the vertical load vector, in the web of the cantilever beam.



Figure C8: Typical bending stress and shear stress response in web of cantilever beam

C2.2 Lateral horizontal load vector

The figure below is a view in plan of the cantilever beam indicating the position of the strain gauges, the applied load vector and the orientation of the reaction forces at the restraint. The response at the strain gauges is related to these reaction forces.

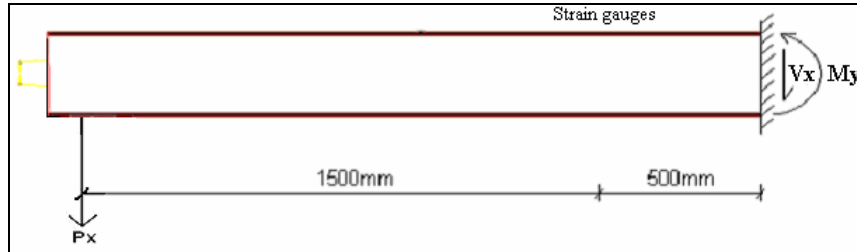


Figure C9: Plan view of cantilever beam with lateral horizontal load vector at neutral axis

$$V_x = P_x = 1 \text{ kN}$$

$$M_y = P_x \times 1500 \text{ mm}$$

$$\begin{aligned} \sigma_z &= \frac{M_y}{Z_{y-y}} \\ &= \frac{P_x \times 1500 \text{ mm}}{199 \text{ E}3 \text{ mm}^3} \\ &= 7.54 \text{ MPa} \end{aligned}$$

$$\begin{aligned} \epsilon_z &= \frac{\sigma_z}{E} \\ &= \frac{7.54 \text{ MPa}}{210 \text{ kN} \cdot \text{mm}^{-2}} \\ &= 3.58 \text{ E-}2 \text{ mm/mm} \end{aligned}$$

$$\begin{aligned} \tau_{flange} &= \frac{P_x \times (A_{flange/2} \times \bar{y}_{flange/2})}{I_{yy} \times t_{flange}} \\ &= \frac{P_x \times (205.2 \text{ mm} / 2 \times 14.2 \text{ mm} \times 205.2 \text{ mm} / 4)}{20.5 \text{ E}6 \text{ mm}^4 \times 14.2 \text{ mm}} \\ &= 2.57 \text{ E-}4 \times P_x \text{ mm}^{-2} \end{aligned}$$



The figures below indicate a view in plan of the typical bending stress and shear stress response due to the horizontal load vector, in the flanges of the cantilever beam.



Figure C10: Typical bending stress and shear stress response in the flanges of cantilever beam

C2.3 Axial load vector

The figure below is an elevational view of the cantilever beam indicating the applied load vector and the orientation of the reaction force at the restraint. The response at the strain gauges is related to this reaction force.



Figure C11: Elevational view of cantilever beam with applied load vector at neutral axis

$$\begin{aligned}\sigma_z &= \frac{P_z}{A} \\ &= \frac{P_z}{7600\text{mm}^2} \\ &= 0.132 \text{ MPa}\end{aligned}$$

$$\begin{aligned}\epsilon_z &= \frac{\sigma_z}{E} \\ &= \frac{0.132 \text{ MPa}}{210\text{kN}\cdot\text{mm}^{-2}} \\ &= 6.26\text{E-}4 \text{ mm/mm}\end{aligned}$$

C2.4 Torsional response due to eccentric load vectors

The figure below indicates the torsional moment at the centroid of the cantilever beam (T_z), due to a lateral horizontal load vector (P_x) or an eccentric vertical load vector (P_y) at the wheel. The eccentricity of P_x is constant, while the eccentricity of P_y is variable. The electrical driving motor which weighs 0.2 kN induces a constant torsional moment of 0.03 kN.m on the cantilever beam, which was excluded, due to the complexity of torsional calculations.

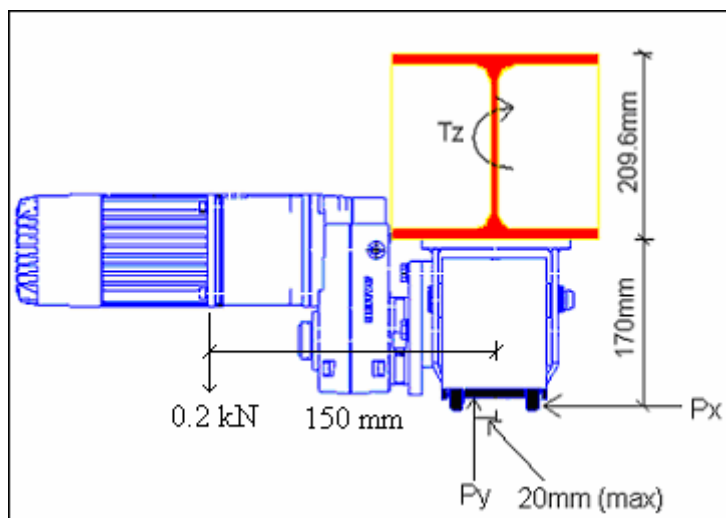


Figure C12: Lateral elevation of cantilever beam with eccentric load vectors at wheel

Differential equations for determining the torsional response of the cantilever beam based on the derivatives of the rotational displacement function, will be defined. The figure below indicates the geometric information, on which these derivations are based.

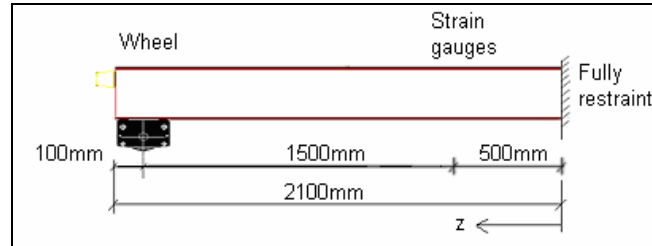


Figure C13: Dimensions of cantilever beam

λ was calculated previously as $9.68E-4/mm$.

λz , $\sinh \lambda z$ and $\cosh \lambda z$ are occurring variables in the homogeneous equation for torsion. Substituting values for z at points along the cantilever beam into these variables, give the following table with constant values, which was implemented.

Position of analysis (z)	λz	$\sinh \lambda z$	$\cosh \lambda z$
0mm at restraint	0	0	1
500mm at strain gauges	0.47	0.487	1.11
2000mm at wheel	1.878	3.193	3.35

Table C1: Values implemented in homogeneous equation for torsion

Derivation of the homogeneous equation for torsion

$\phi = A \sinh \lambda z + B \cosh \lambda z + C + \frac{T}{2G.J} \cdot z$, gives the following equations:

$$\therefore \frac{d\phi}{dz} = A\lambda \cosh \lambda z + B\lambda \sinh \lambda z + \frac{T}{2G.J} \quad \text{and} \quad \frac{d^2\phi}{dz^2} = A\lambda^2 \sinh \lambda z + B\lambda^2 \cosh \lambda z$$

The applicable boundary conditions are substituted into the relevant equations, until the constant values A,B and C are determined. For ease of reading, these calculations are not defined in detail.

At the point where the cantilever beam is restraint, $z = 0$ mm. $\phi = 0$ and $d\phi/dz = 0$.

$$\therefore B + C = 0. \quad \text{and} \quad \therefore A = -\frac{T}{2G.J.\lambda}$$

At the point where the load vectors are applied $z = 2000$ mm, $\frac{d^2\phi}{dz^2} = 0$

$$\therefore B = -0.95A = 0.95 \frac{T}{2G.J.\lambda} \quad \text{and} \quad \therefore C = -0.95 \frac{T}{2G.J.\lambda}$$

Substituting these constant values into the differential equations for torsion, result in the equations in the table below. These equations will be used to determine the torsional stresses at the position of the strain gauges ($z = 500 \text{ mm}$) and also to determine the global response to torsion.

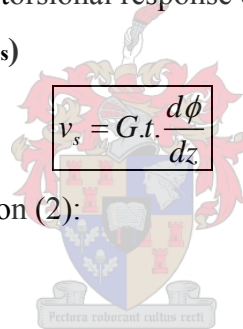
Total Twist	$\therefore \phi = \frac{T}{2G.J.\lambda} (-\sinh \lambda z + 0.95 \cosh \lambda z - 0.95 + \lambda.z)$ (1)
Saint-Venant Torsion	$\therefore \frac{d\phi}{dz} = \frac{T}{2G.J} (-\cosh \lambda z + 0.95 \sinh \lambda z + 1)$ (2)
Normal Stress Warping Torsion	$\therefore \frac{d^2\phi}{dz^2} = \frac{T\lambda}{2G.J} (-\sinh \lambda z + 0.95 \cosh \lambda z)$ (3)
Shear Stress Warping Torsion	$\therefore \frac{d^3\phi}{dz^3} = \frac{T\lambda^2}{2G.J} (-\cosh \lambda z + 0.95 \sinh \lambda z)$ (4)

Table C2: Differential equations for a torsional load on a cantilever beam

C2.4.1 Torsional stresses at strain gauge position

The following equations were obtained from literature on the subject of torsional behaviour. They are implemented to determine the torsional response due to eccentric load vectors.

Saint-Venant torsional shear stress (v_s)



Substitute above into differential equation (2):

$$\begin{aligned}
 v_s &= \frac{T.t}{2.J} (-\cosh \lambda z + 0.95 \sinh \lambda z + 1) \\
 &= \frac{P_x \times 274.8 \text{mm} \times t}{2 \times 447 \text{E}3 \text{mm}^4} \times (-1.11 + 0.95 \times 0.487 + 1) \\
 &= 0.108 \times t \text{ mm}^{-3} \\
 \therefore \text{web} &= 1.0 \text{ mm}^{-2} \\
 \therefore \text{flanges} &= 1.54 \text{ mm}^{-2}
 \end{aligned}$$

Normal stress (σ_z) due to warping torsion

$$\sigma_{z(\text{max})} = \frac{E.b.h}{4} \cdot \frac{d^2\phi}{dz^2}$$

Substitute above into differential equation (3)

$$\begin{aligned}
 \sigma_z &= \frac{T.\lambda.E.b.h}{8G.J} (-\sinh \lambda z + 0.95 \cosh \lambda z) \\
 &= \frac{P_x \times \text{ecc.} \times 9.68\text{E-}4 \text{mm}^{-1} \times 210 \text{GPa} \times 205.2 \text{mm} \times 209.6 \text{mm}}{8 \times 80.77 \text{GPa} \times 447 \text{E}3 \text{mm}^4} \times (-0.487 + 0.95 \times 1.11) \\
 &= 1.72\text{E-}2 \times \text{ecc. N.mm}^{-3}
 \end{aligned}$$

Hor. ecc = 274.8 mm : 4.72 MPa

Vert. ecc = 20 mm : 0.344 MPa

Shear stress (v_w) due to warping torsion

$$v_w = \frac{E.b^2.h}{16} \cdot \frac{d^3\phi}{dz^3}$$

Substitute above into differential equation (4)

$$\begin{aligned} v_w &= \frac{T.\lambda^2.E.b^2.h}{32.G.J} (-\cosh \lambda z + 0.95 \sinh \lambda z) \\ &= \frac{P_x \times 274.8\text{mm} \times (9.68\text{E-}4\text{mm}^{-1})^2 \times 210\text{GPa} \times (205.2\text{mm})^2 \times 209.6\text{mm}}{32 \times 80.77\text{GPa} \times 447\text{E}3\text{mm}^4} \times (-1.11 + 0.95 \times 0.487) \\ &= -0.287 \text{ MPa} \end{aligned}$$

C3 Summary of theoretical stresses

The following table indicates a summary of the stress response of the flanges and the web of the section under theoretical investigation.

Type load vector	Type of beam behaviour	Stress response (MPa/kN)
Vertical load vector (Py)	Normal stress in flanges	2.58
	Shear stress in web	0.57
Lateral horizontal load vector (Px)	Normal stress in flanges	7.54
	Shear stress in flanges	0.26
Axial load vector (Pz)	Normal stress in flanges and web	0.13
Torsional response (Tz) due to eccentric load vectors	Saint-Venant shear stress in web	1.0
	Saint-Venant shear stress in flanges	1.54
	Normal stress in flanges	4.72 and/or 0.34
	Warping shear stress in flanges	-0.29

Table C3: Summary of theoretical stress response at strain gauge positions

The following figure is a graphic representation of implementing the differential equations in table C2, along the full length of the cantilever beam. Note that the normal warping stress in the flanges is maximum, where the Saint Venant torsional response is minimum. The actual rotational response of the cantilever beam is also concave from that of the Saint Venant torsional response.

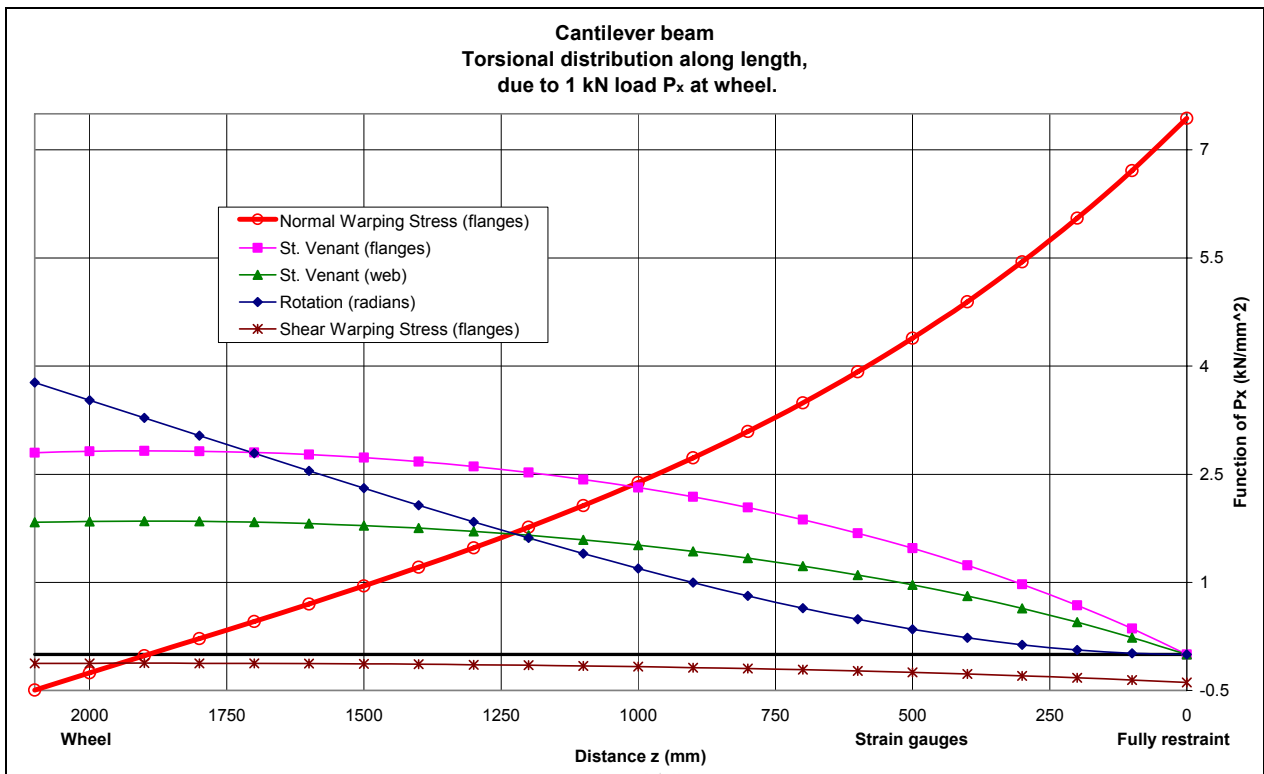


Figure C14: Torsional behaviour along length of cantilever beam

These results do not have a maximum value at the same position. This indicates that a specific point along the length of the end carriage load measuring system for measuring all the possible maximum stress results simultaneously, is not possible. The shear stress response, which can not be measured experimentally, are defined for the simplistic cantilever beam model.

These calculations indicated that torsional response is not something that can easily be solved by hand calculations. A spreadsheet must be used in which the parameters can be modified accordingly, to determine the torsional response for the specific system under investigation.

The normal stress response from these calculations can be compared to the average stress results of the experimental calibration of the end carriage load measuring system. The classification of the restraint of the actual load measuring system is not simplistic due to its physical characteristics, so these theoretical results only act as a guide in understanding the load response of the end carriage load measuring system.

These theoretical shear stresses do not influence the experimentally measured normal stresses and bending stresses.

Appendix D – Design drawings of 5 ton lead/concrete payload

The figure below indicates the reinforced concrete and lead block payload which weighs 50 kN. It was designed and built specifically for implementation in the experimental investigation of the behaviour of a 5 ton electric overhead travelling crane and its supporting structure.

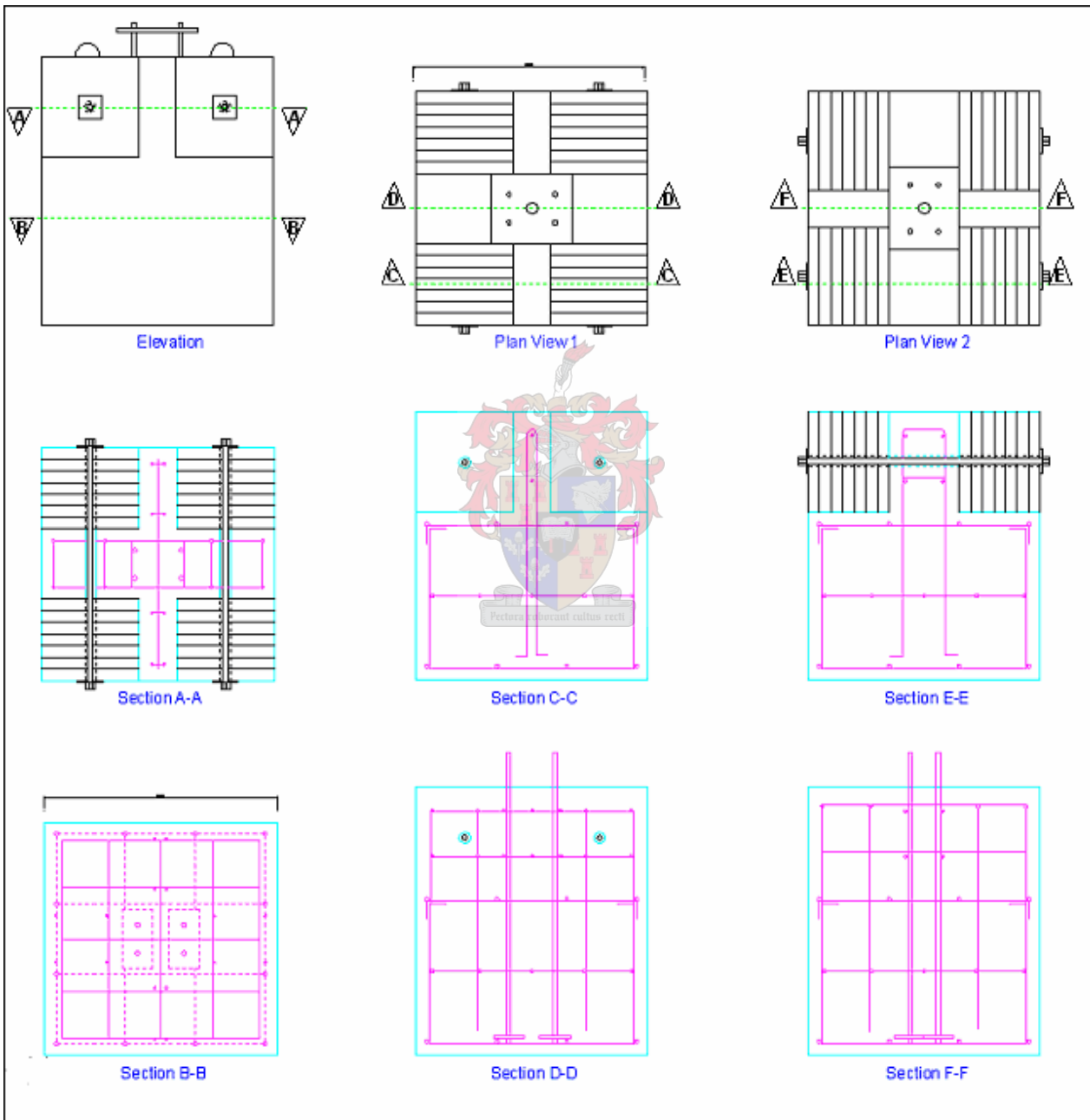


Figure D1: Design drawings of reinforced concrete for 5 ton payload

Appendix E – Wheel load calculations according to load models

SABS 0160-1989 clause 5.7: Loads due to overhead travelling cranes

Crane information required for calculations of wheel loads

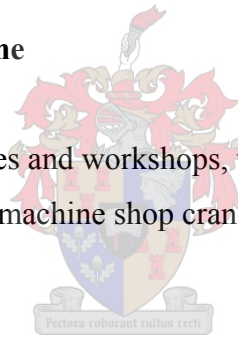
Properties of crane

Weight of crane bridge and end carriages		20.1 kN
Weight of crab		2.3 kN
Weight of payload		50.3 kN
Total number of crane travel wheels		4
Maximum vertical wheel load	V_{\max}	28.3 kN
Minimum vertical wheel load	V_{\min}	5.7 kN

5.7.2 Classification of travelling crane

Class 2 (Medium duty)

Cranes for general use in factories and workshops, warehouse cranes – intermittent operation, power station cranes, machine shop cranes or foundry cranes



5.7.3 Vertical wheel loads

Live load factor = 1.6

Impact factor for class 2 = 1.2

Unfactored maximum vertical wheel load with impact	$V_{i \max} : 28.3 \text{ kN} \times 1.2 = 34 \text{ kN}$
Factored maximum vertical wheel load, no impact	$V_{u \max} : 28.3 \text{ kN} \times 1.6 = 45 \text{ kN}$
Factored maximum vertical wheel load with impact	$V_{ui \max} : 45 \text{ kN} \times 1.2 = 54 \text{ kN}$
Unfactored minimum vertical wheel load	$V_{i \min} : 5.7 \text{ kN} \times 1.2 = 6.8 \text{ kN}$
Factored minimum vertical wheel load, no impact	$V_{u \min} : 5.7 \text{ kN} \times 1.6 = 9.1 \text{ kN}$
Factored minimum vertical wheel load with impact	$V_{ui \min} : 9.1 \text{ kN} \times 1.2 = 10.9 \text{ kN}$

5.7.4 Horizontal transverse wheel loads

Most adverse of the following:

- a) Allowance for acceleration or braking of the crab

Factor for class 2 = 0.1

Unfactored horizontal transverse wheel load $H_a : 0.1 \times (2.3 \text{ kN} + 50.3 \text{ kN}) / 4 = \mathbf{1.3 \text{ kN}}$

Factored horizontal transverse wheel load $H_{ua} : 1.3 \text{ kN} \times 1.6 = 2.1 \text{ kN}$

- b) Allowance for possible misalignment of crane wheels or gantry rails

Factor for class 2 = 0.12

Unfactored horizontal transverse wheel load $H_b : 0.12 \times (22.4 \text{ kN} + 50.3 \text{ kN}) / 4 = \mathbf{2.2 \text{ kN}}$

Factored horizontal transverse wheel load $H_{ub} : 2.2 \text{ kN} \times 1.6 = 3.4 \text{ kN}$

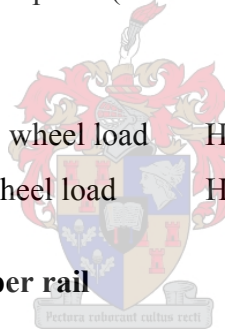
- c) Allowance for skewing of crane in plane (no roller guides present)

Factor for class 2 = 0.18

Unfactored horizontal transverse wheel load $H_c : 0.18 \times (22.4 \text{ kN} + 50.3 \text{ kN}) / 4 = \mathbf{3.2 \text{ kN}}$

Factored horizontal transverse wheel load $H_{uc} : 3.2 \text{ kN} \times 1.6 = 5.1 \text{ kN}$

5.7.5 Horizontal longitudinal force per rail



Unfactored horizontal transverse force $H_L : 0.1 \times 28.3 \text{ kN} \times 2 \text{ wheels} = \mathbf{5.6 \text{ kN}}$

Factored horizontal transverse wheel load $H_{uL} : 1.6 \text{ kN} \times 5.6 = 9 \text{ kN}$

5.7.6 Force on end stops (horizontally unrestrained payload)

Unfactored force on end stops $H_e : 22.4 \text{ kN} / 2 \text{ end stops} = \mathbf{11.2 \text{ kN}}$

EN 1991-3: Actions induced by cranes on structures

Crane information required for calculations of wheel loads

Weight

Crane bridge and end carriages	20.1 kN
Crab	2.3 kN
Payload	50.3 kN

Geometry of crane

Span of crane bridge	8280 mm
Minimum distance between hoist and rail	780 mm
Rail type	30 kg/m
Width of top of rail	57 mm
Height of rail	109.5 mm

Speeds

Steady hoisting speed	0.075 m/s
Longitudinal travel speed	0.55 m/s
Lateral crab travel speed	0.45 m/s



Guide means

Guide rollers present?	No
------------------------	----

Crane hoist

Hoist class	2
Type of hoist	hook
Is hoist free to swing?	yes

Buffers

Buffer type	Elastomeric
-------------	-------------

Wheels and wheel drives

Type of wheel drive	single
Number of single wheel drives	2
Behaviour of drive	smooth
Combination of wheel pairs	Independent

Clearance between rail and wheel flanges	6 mm
Number of wheel pairs	2
Wheel spacing	4000 mm
Coefficient of friction	0.2

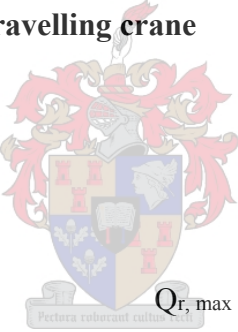
2.5.3 Vertical load form overhead travelling cranes

Dynamic factors

Hoist class of crane	HC	2
Lifting of payload (self weight)	ϕ_1	1.1
Lifting of payload (payload)	ϕ_2	1.157
Crane travelling on runway	ϕ_4	1.0
Drive forces	ϕ_5	1.25
Buffer forces	ϕ_7	1.53

2.5.4 Vertical loads from overhead travelling crane

Load case

1	Crane with payload		
	Dynamic factor ϕ_1		
	Maximum wheel load		$Q_{r, \max} : 1.157 \times 28.3 \text{ kN} = 32.5 \text{ kN}$
	Minimum wheel load		$Q_{r, (\max)} : 1.157 \times (5.7 \text{ kN} + 2.5 \text{ kN}) = 9.5 \text{ kN}$
3, 7	Crane without payload		
	No dynamic factors		
	Maximum wheel load	$Q_{r, \min} : 6.7 \text{ kN}$	
	Minimum wheel load	$Q_{r, (\min)} : 5.8 \text{ kN}$	

2.7.2 Longitudinal and transverse loads caused by acceleration and deceleration of the crane

Longitudinal forces

Drive force	K:	1.9 kN
Longitudinal force imposed by one wheel (dynamic)	$H_{L,i}$	0.96 kN
Distance between centre of mass and centre of crane when payload is at position B1:	L_s	= 2.35 m

Transverse forces

Distance from rail 1 to centre of mass	ξ_1	6.49/8.28 = 0.784
Distance from rail 2 to centre of mass	ξ_2	1.79/8.28 = 0.216
Moment caused by eccentricity of drive force	M :	1.9 kN x 2.35 m = 4.5 kN.m
Drive force	$\phi_s = 1$ (slow movement)	
	$\phi_s = 2$ (fast movement)	
	$\phi_s = 3$ (payload swings)	
Transverse forces imposed on rail 1 ($\phi_s = 1; 2; 3$)	$H_{T,1}$:	0.23 kN; 0.48 kN; 0.73 kN
Transverse forces imposed on rail 2 ($\phi_s = 1; 2; 3$)	$H_{T,2}$:	0.89 kN; 1.77 kN; 2.65 kN

2.7.3 Horizontal loads and the guide force caused by skewing

Skewing angle

Caused by clearance between rail and guidance means	α_f	= 0.0011225
Caused by wear of the rail and guidance means	α_v	= 0.001625
Caused by tolerances on rail and wheel directions	α_o	= 0.001
Total skewing angle	α	= 0.00375
Non-positive factor	f	= 0.1825

Calculations following are for two wheels, combination: Independent, Fixed/Fixed

Distance to instantaneous slide pole	h	= 4000
--------------------------------------	---	--------

Force factors

Guide force	$\lambda_{s,j}$	= 0.5
Longitudinal force on rail 1	$\lambda_{s,1j,L}$	= 0
Longitudinal force on rail 2	$\lambda_{s,2j,L}$	= 0
Transverse force on rail 1, imposed by front wheel	$\lambda_{s,1,1,T}$: $\xi_2 / 2 = 0.108$

Transverse force on rail 2, imposed by front wheel	$\lambda_{s,2,1,T} : \xi_1 / 2 = 0.392$
Transverse force on rail 1, imposed by back wheel	$\lambda_{s,1,2,T} = 0$
Transverse force on rail 2, imposed by back wheel	$\lambda_{s,2,2,T} = 0$

Forces

Guide force	$S = 6.55 \text{ kN}$
Transverse force on rail 1, imposed by back wheel	$H_{s,1,1,T} = 1.4 \text{ kN}$
Transverse force on rail 2, imposed by back wheel	$H_{s,1,2,T} = 5.1 \text{ kN}$

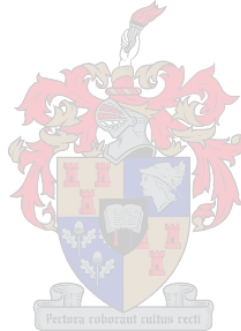
Buffer forces related to movements of the crab

Transverse for per wheel	$H_{T,3} = 1.3 \text{ kN}$
--------------------------	----------------------------

Buffer forces related to crane movement

Calculations based on a maximum deceleration of 9.81 m/s^2 .

Spring constant of buffer	$S_B = 319 \text{ kN/m}$
Buffer force per end stop	$H_{B,1} = 22.7 \text{ kN}$



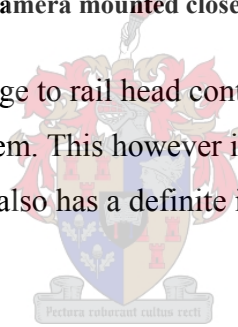
Appendix F – Video data of experiments on DVD

The photo below indicates the position of a digital camera, which was fixed onto the end carriage of the overhead crane for visual data of the interaction of the crane wheel flanges against the rail head, during implementation of the crane system.



Photo F1: A digital video camera mounted close to the wheel contact surface

The video data indicated that wheel flange to rail head contact correlated with the forces measured by the end carriage load measuring system. This however indicated that the system is complex, and that the direction of longitudinal travel, also has a definite influence on the contact between the wheel flanges and the rail head.





A journey
is usually more interesting
than the destination,



but **NEVER** loose sight of
the destination...

**AN EXPERIMENTAL INVESTIGATION
INTO THE BEHAVIOUR OF A
5 TON
ELECTRIC OVERHEAD TRAVELLING CRANE
(*EOTC*)
AND ITS SUPPORTING STRUCTURE**

Presentation for partial fulfilment of the requirements for the
degree of Master of Civil Engineering at the University of Stellenbosch



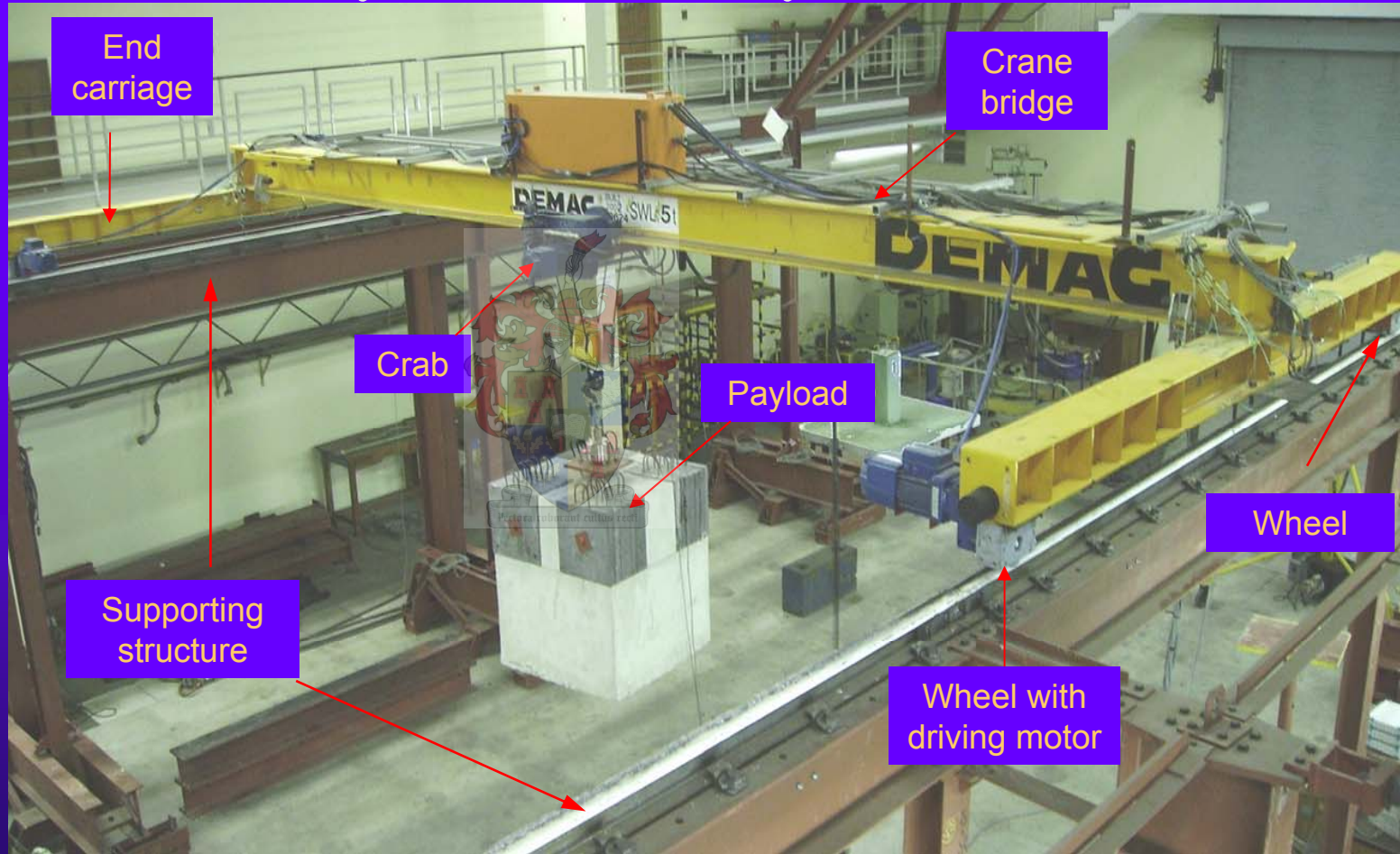
by

Johan de Lange

Promoter : Prof. P E Dunaiski

July 2004 - January 2007

EOTC research project at the Institute of Structural Engineering (ISE) laboratory at the University of Stellenbosch



Contents

- 1) Background to research on EOTC at Univ. of Stellenbosch
 - People involved in EOTC research
 - Timeline of experimental research
 - Organogram of this thesis
- 2) Crane load models of the loading codes under investigation
- 3) Description of experimental system
- 4) Behaviour of supporting structure under controlled loading
- 5) Behaviour of crane under controlled loading
- 6) Numerical modelling of overhead crane
- 7) Comparison of calibration results
- 8) Implementation of experimental crane
- 9) Comparison of accuracy of crane load models
- 10) Conclusions



1) Background to research on EOTC at University of Stellenbosch

Problems on overhead cranes : Crane wheel wear / damage

Problems on supporting structures: Metal fatigue damage

The current crane loading code modifications being implemented in the South Africa loading code:

SABS 0160 – 1989

crane load models

Eurocode 1 Part 3

(EN 1991 – 3):

Actions induced by cranes and machinery on structures

SANS 10160 - 2005 Section 10:

Actions induced by cranes and machinery on buildings and industrial structures.

A better understanding of the behaviour under loading of a variable crane system is sought, to evaluate the South African crane loading code modifications being implemented, as indicated above:

• **People involved in EOTC research**

Aspects of EOTC research

Experimental
investigation

Numerical modelling
& Best practice

Reliability analysis

Prof. Dunaiski

Prof. Retief

Hein Barnard

Trevor Haas

Juliet Warren

Pierre Viljoen

Kim McKenzie

.....

Suzanne Kolhaas

& Geoffrey Thompson

Johan de Lange

.....

.....



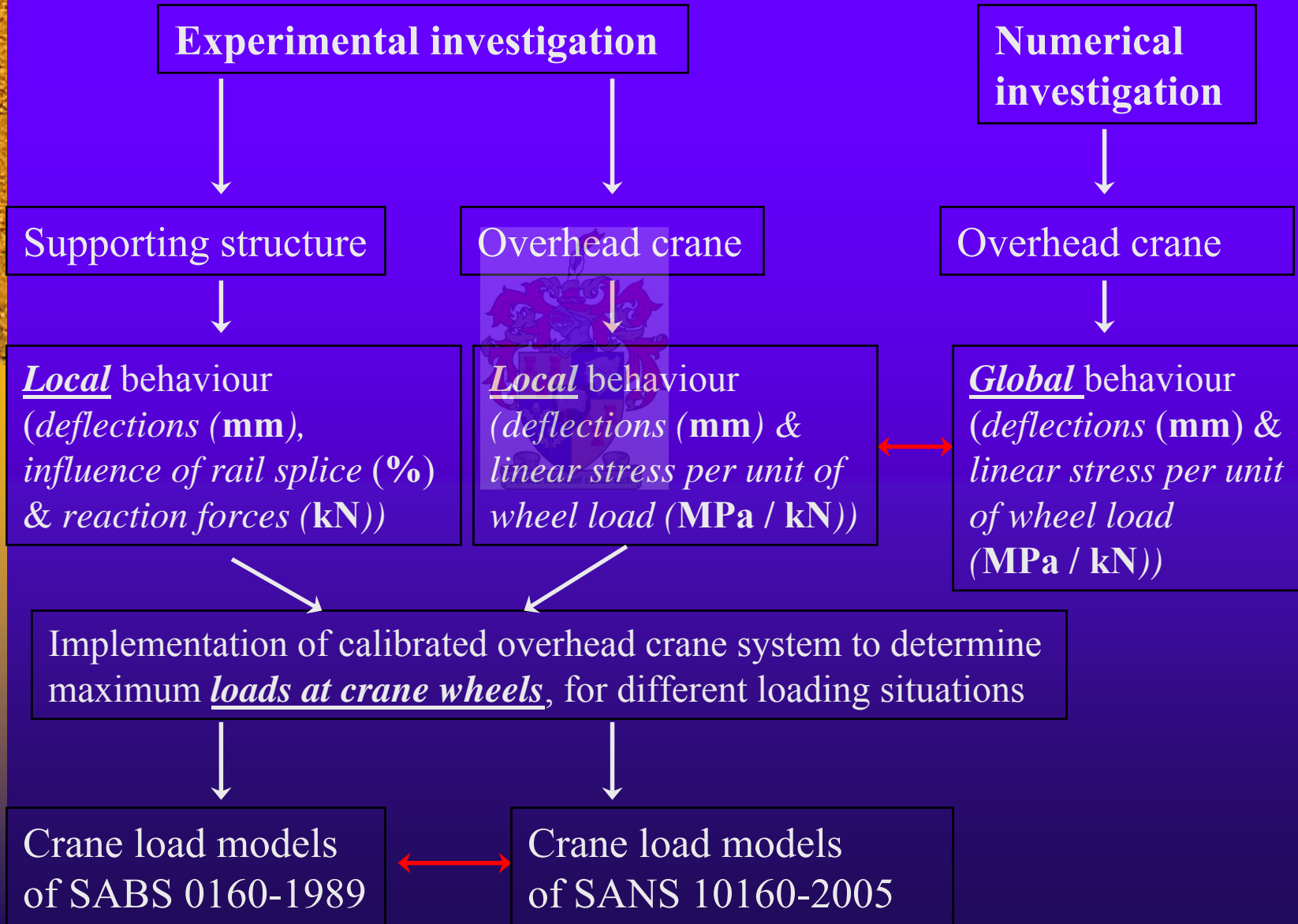


- **Timeline of experimental research**

- **2001 ~ Fabrication of crane supporting structure**
- **2002 ~ Erection of overhead crane and its supporting structure**
- **2003 ~ Installation of data capturing systems on overhead crane and supporting structure**
- **2004 to 2006 ~ Calibration of data capturing systems and experimental investigation of system**



- **Organogram of this thesis**



Contents

- 1) Background to research on EOTC at Univ. of Stellenbosch
- 2) Crane load models of the loading codes under investigation
 - SABS 0160 – 1989
 - Eurocode 1 Part 3
- 3) Description of experimental system
- 4) Behaviour of supporting structure under controlled loading
- 5) Behaviour of crane under controlled loading
- 6) Numerical modelling of overhead crane
- 7) Comparison of calibration results
- 8) Implementation of experimental crane
- 9) Comparison of accuracy of crane load models
- 10) Conclusions



2) Crane load models of the loading codes under investigation

SABS 0160 – 1989

Crane classification

Class 1- Light duty

Hand operated crane

Class 2 – Normal duty

Cranes for normal use in factories and workshops

Warehouse cranes – no continuous use

PowerStation cranes

Class 3 – Heavy duty

Warehouse cranes – continuous use

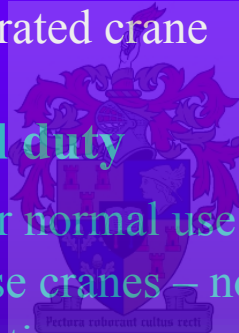
Scrap yard cranes

Foundry crane

Class 4 – Extra heavy duty


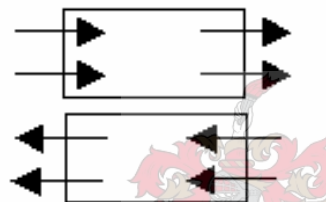
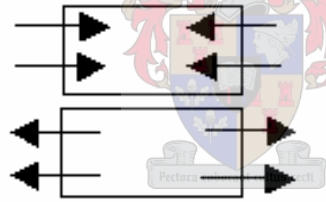
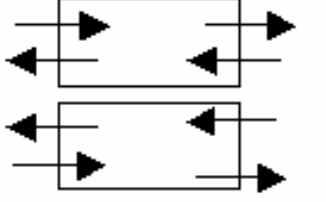

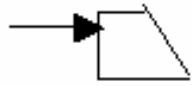
Claw cranes

Magnetic cranes



SABS 0160 – 1989

Crane load models

Type of loading	Direction of loading	Class of crane			
		1	2	3	4
Vertical loading per wheel, including impact $X_1 \cdot W$ (max. static wheel load)		$X_1 = 1.1$	1.2	1.25	1.3
Horizontal transverse forces per wheel a) Crab acceleration and braking X_2 . (Crab's weight + Load lifted)/(Number of wheels)		$X_2 = 0.05$	0.10	0.15	0.20
b) Misalignment of wheels or gantry X_3 . (Bridge's weight + C + L)/N		$X_3 = 0.05$	0.12	0.15	0.20
c) Skewing X_4 . (B + C + L)/N		$X_4 = 0.075$	0.18	0.225	0.30
Horizontal longitudinal force (acceleration and deceleration)		Force = 0.1 ($\sum W$ of line per rail)			
Force on end stops the lesser of:		Force = 1.0 (B + C) or alternatively full speed impact calculated from buffer and end stop characteristics			

Eurocode 1 Part 3 (EN 1991 – 3)

Crane loading code

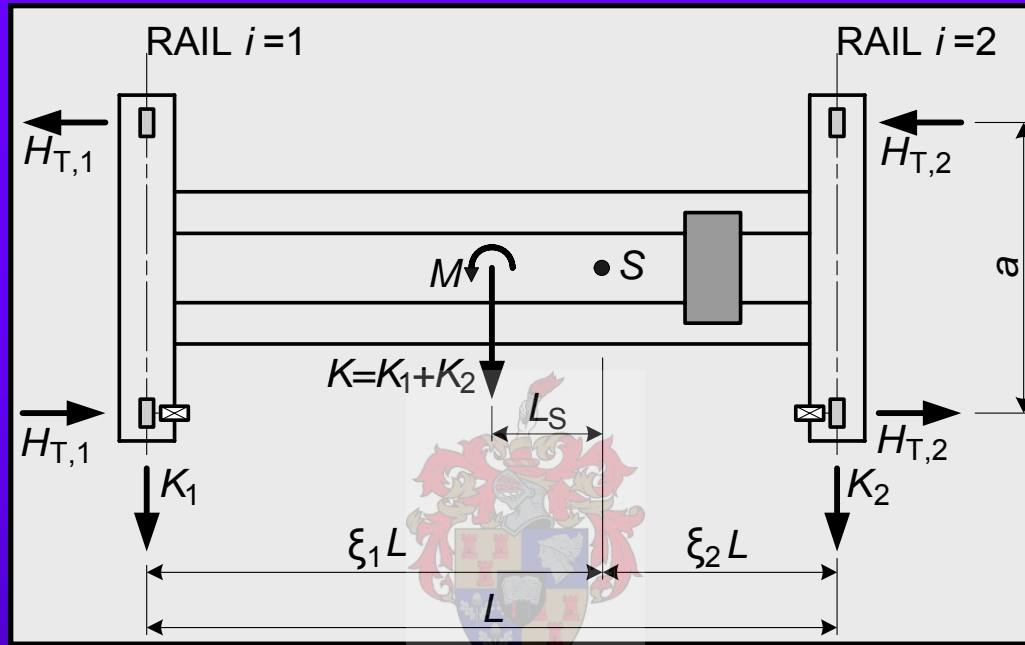
The force configurations for the load models in this crane loading code, will be referred to briefly with diagrams acting as a visual aid.

◆ Vertical loads from overhead travelling cranes

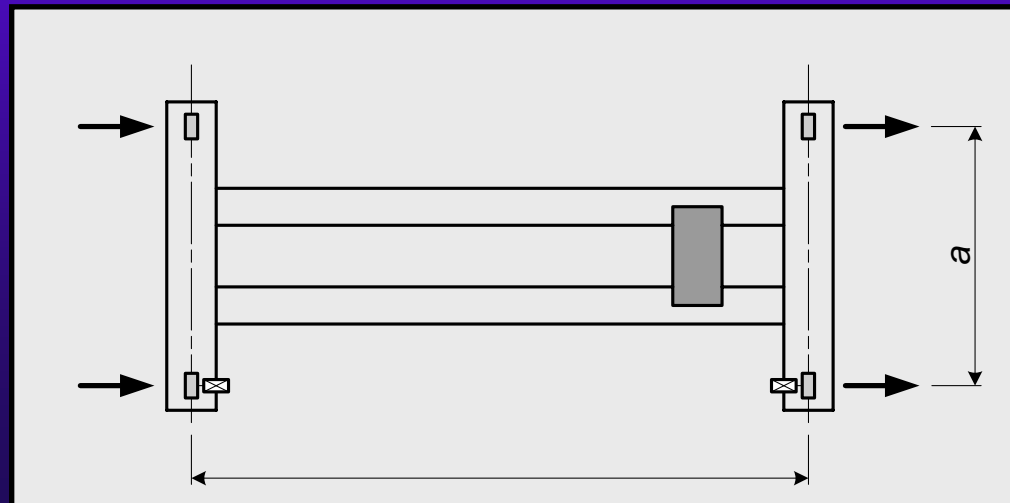


◆ Horizontal loads from overhead travelling cranes

– Acceleration and deceleration of the crane

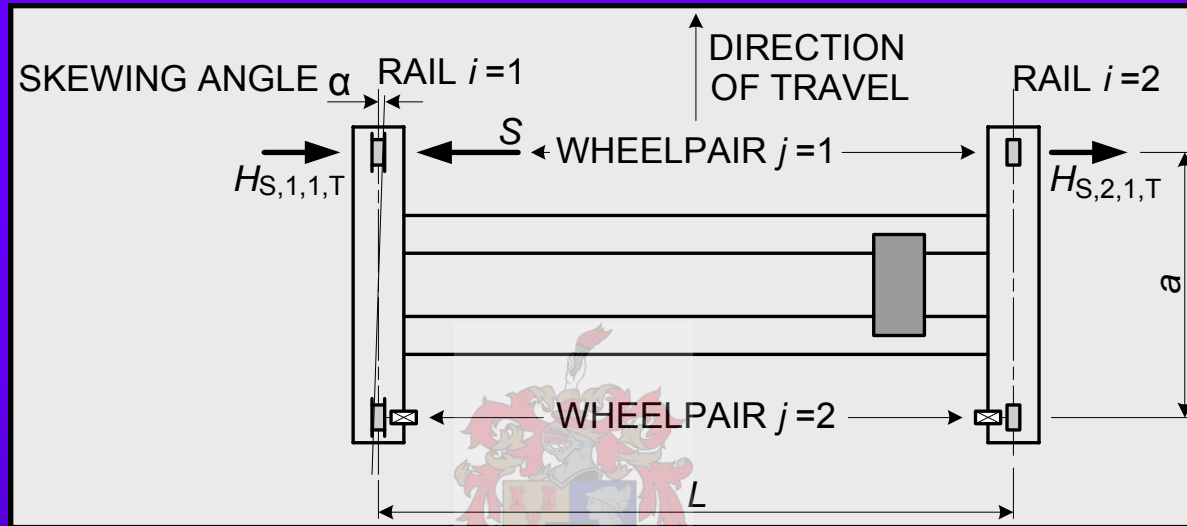


– Acceleration and deceleration of the crab

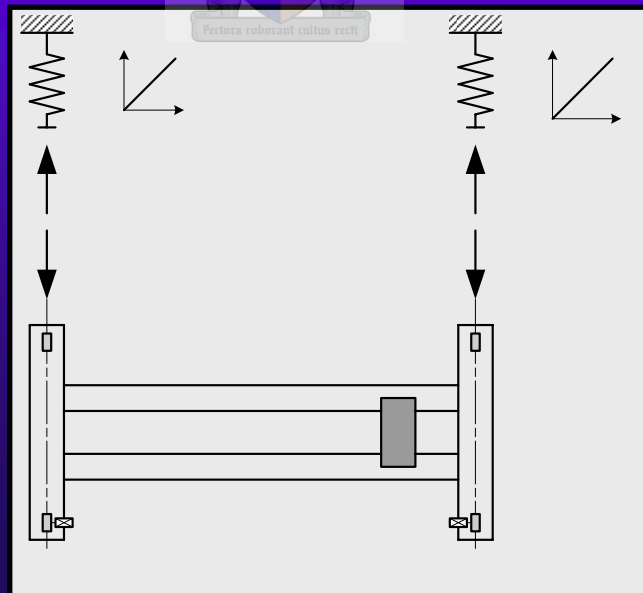


◆ Horizontal loads from overhead travelling cranes

- Skewing of the crane




- Impact on the endstops





Contents

- 1) Background to research on EOTC at Univ. of Stellenbosch
 - 2) Crane load models of the loading codes under investigation
 - 3) Description of experimental system
 - EOTC supporting structure
 - Load measuring capability of supporting structure and payload
 - Overhead crane and its instrumentation
 - 4) Behaviour of supporting structure under controlled loading
 - 5) Behaviour of crane under controlled loading
 - 6) Numerical modelling of overhead crane
 - 7) Comparison of calibration results
 - 8) Implementation of experimental crane
 - 9) Comparison of accuracy of crane load models
 - 10) Conclusions
- 

3) Description of experimental system

- **EOTC supporting structure**



Components:

Plate girders
building columns,
supporting columns,
longitudinal bracing,
lateral restraints,
elastomeric pads,
rail clips and
crane rails

Characteristics:

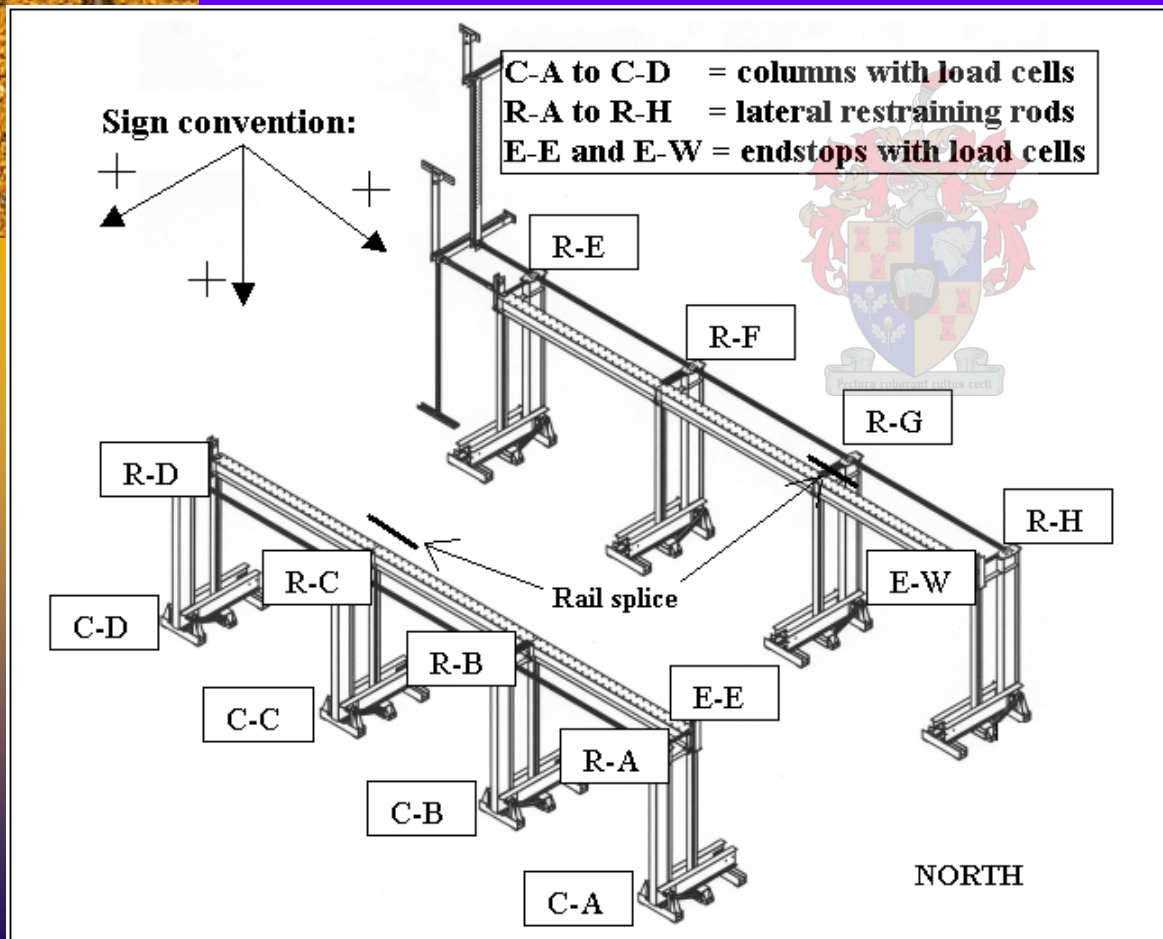
Variable column base type and lateral girder restraints.

Ability to introduce force measuring equipment into the supporting structure.



- Load measuring capability of supporting structure and payload

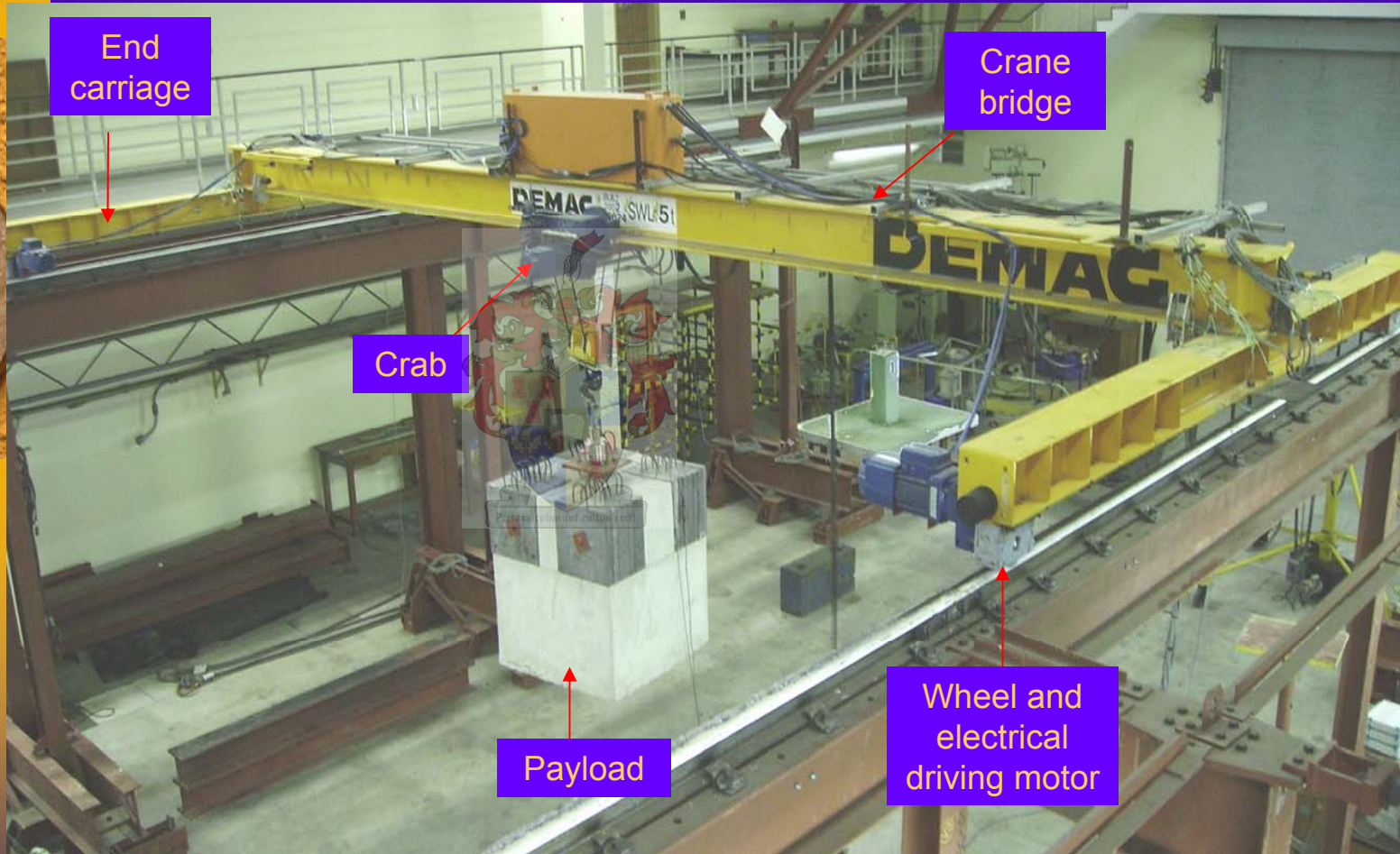
Position of force measuring equipment in supporting structure



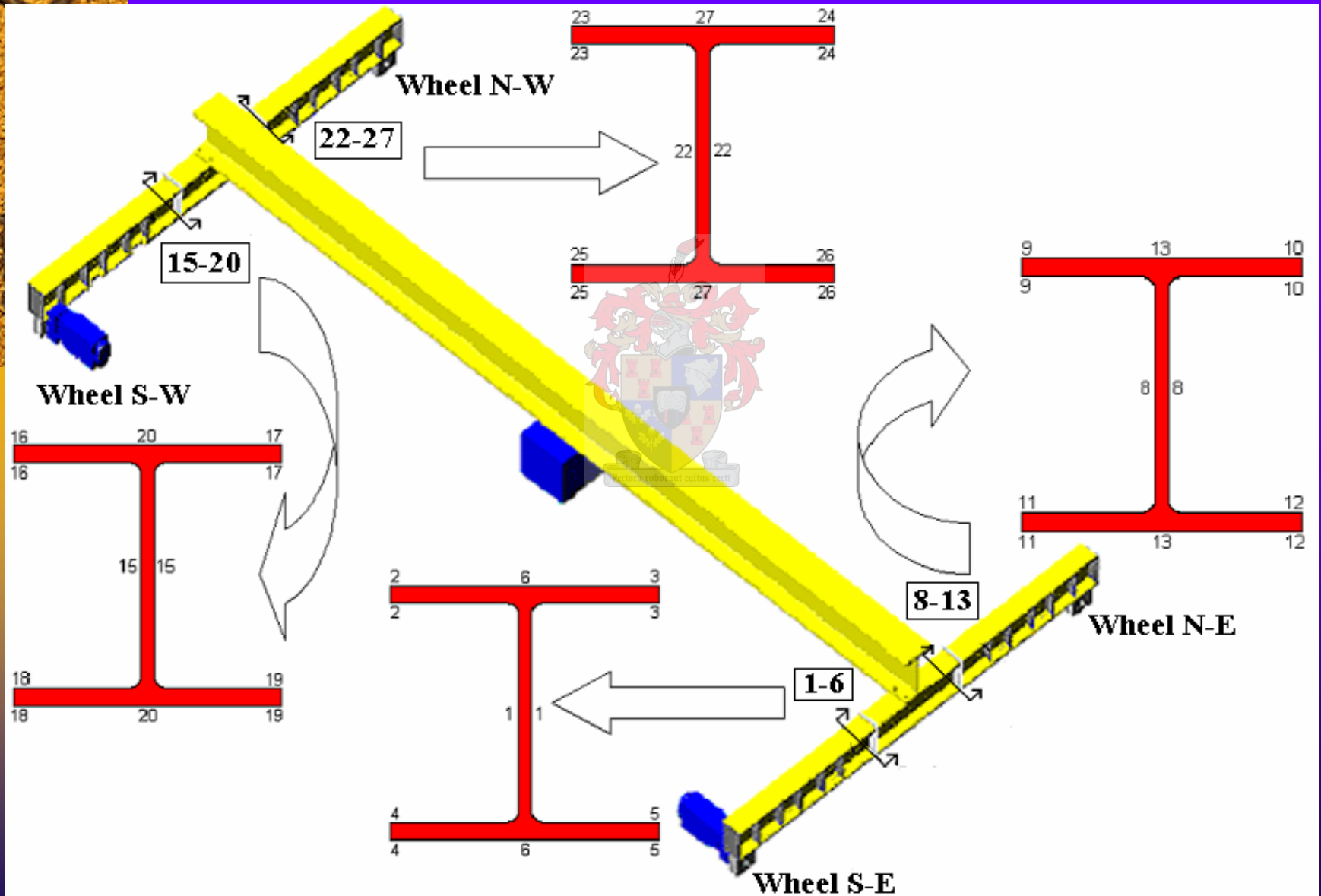
5 ton concrete/lead payload with load cell



Overhead crane and its instrumentation



- Strain gauges on end carriages of crane to measure deformations due to forces at crane's wheels.



Data acquisition instrumentation



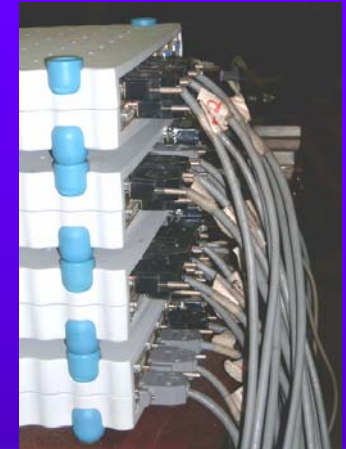
Encoders (2 off)



Accelerometers (3 off)



Spider 8 (4 off)



(32 input channels)

Fixed data capturing points:

Supporting structure ~ 14

Overhead crane ~ 29 (24 from strain gauges)

Contents

- 1) Background to research on EOTC at Univ. of Stellenbosch
- 2) Crane load models of the loading codes under investigation
- 3) Description of experimental system
- 4) Behaviour of supporting structure under controlled loading
 - Main focus
 - Results
- 5) Behaviour of crane under controlled loading
- 6) Numerical modelling of overhead crane
- 7) Comparison of calibration results
- 8) Implementation of experimental crane
- 9) Comparison of accuracy of crane load models
- 10) Conclusions



4) Behaviour of supporting structure under controlled loading

• Main focus:

The influence of a rail splice on the behaviour of the supporting structure under loading is investigated. PhD student Trevor Haas required this information to calibrate a numerical model of the supporting structure for his research.

Means for quantifying the results:

1) Compare vertical deflections measured at mid-spans

of girders.

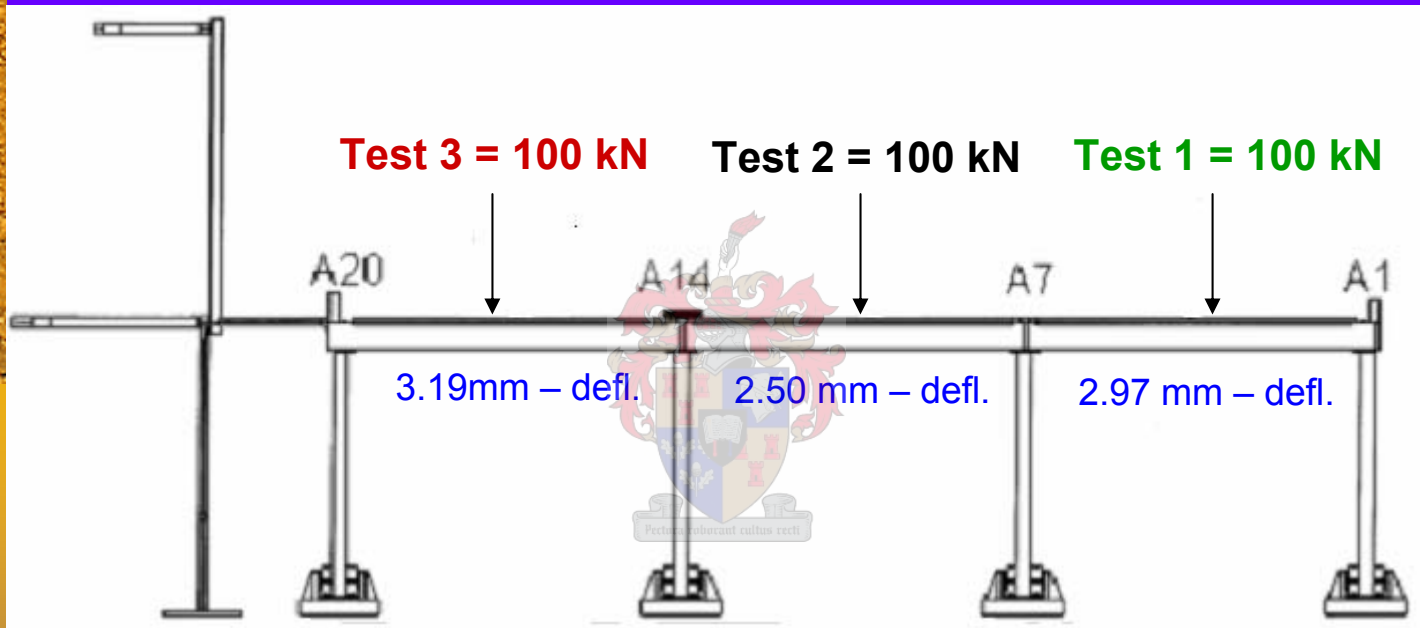


2) Compare reaction forces measured at crane supporting columns.



Experimental results

- The crane rail is continuous over A7 and a rail splice occurs at A14
- For Test 3, the **rail splice at A14** and **brace at A20** is loosened, to compare Test 1 with Test 3, which would otherwise be similar scenario's.



Test 1	~	-0.4 kN	56 kN	43 kN
Test 2	- 2.8 kN	54 kN	52.6 kN	- 3.8 kN
Test 3	46.5 kN	53.6 kN	~	~

Comments on results:

Influence on girder deflections :

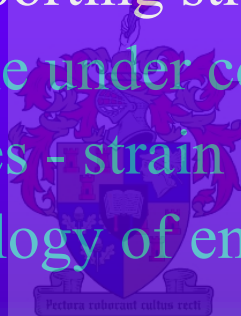
$$3.19 \text{ mm} / 2.97\text{mm} = 1.07 \text{ (7\%)}$$

Influence on reactive force distribution:

$$56 \text{ kN} / 53.6\text{kN} \sim 1.05 \text{ (5\%)}$$

Contents

- 1) Background to research on EOTC at Univ. of Stellenbosch
- 2) Crane load models of the loading codes under investigation
- 3) Description of experimental system
- 4) Behaviour of supporting structure under controlled loading
- 5) Behaviour of crane under controlled loading
 - Basic principles - strain gauges
 - Cantilever analogy of end carriage load measuring system
 - Parameters influencing experimental results
 - Results
- 6) Numerical modelling of overhead crane
- 7) Comparison of calibration results
- 8) Implementation of experimental crane
- 9) Comparison of accuracy of crane load models



5) Behaviour of crane under controlled loading

- Basic principles

- ◆ Strain gauges

When a force is applied to a structure, it undergoes deformation.

Strain is the ratio of this relative deformation of the structure.

As the strain gauge is glued to the structure, any distortion will also cause a distortion of the strain gauge.

The strain gauge contains conducting material and the distortion results in a change in its resistance, which can be measured by the strain gauge.

- ◆ Stress measurements

σ = stress (MPa)

ϵ = strain (mm/mm)

E = Elasticity modulus of steel ~ (210 000 MPa)

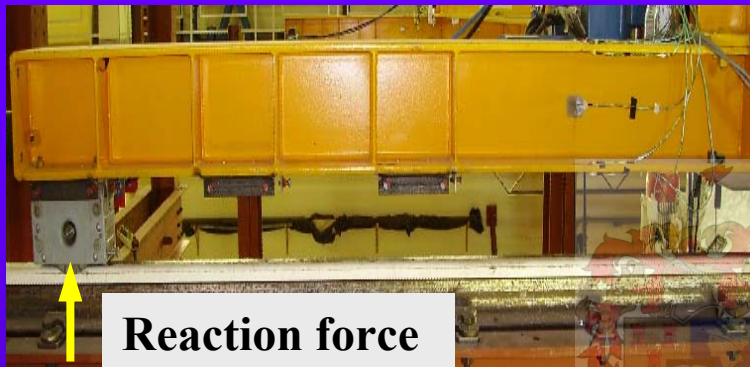
Hooke's law states that the relationship between stress and strain is linear.

$$\sigma = \epsilon \cdot E$$



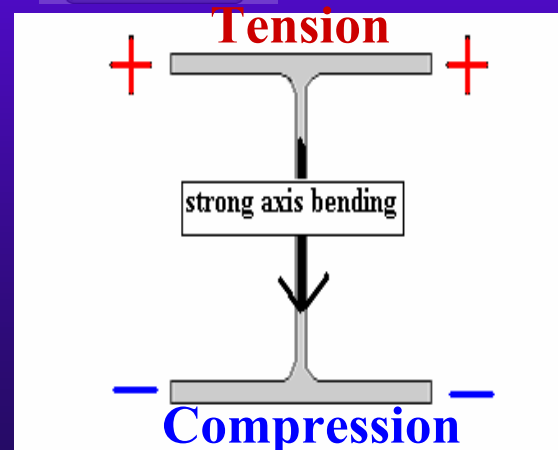
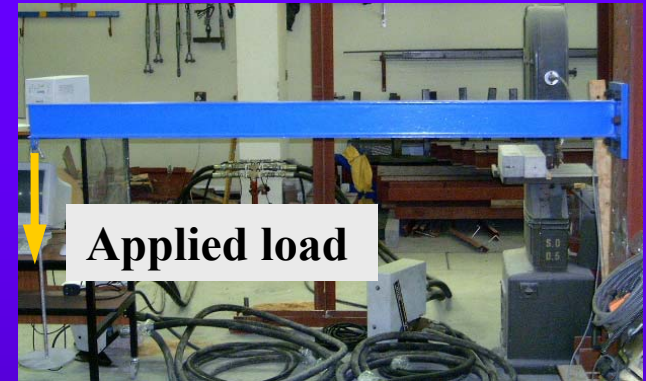
- Cantilever analogy of end carriage load measuring system

End carriage



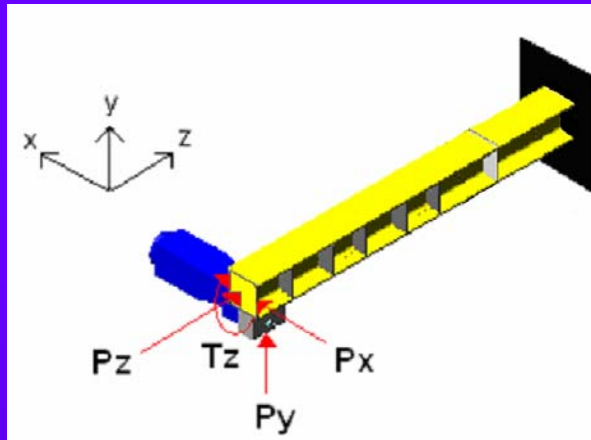
vs.

Cantilever beam



Normal stress behaviour in cross-section of cantilever beam

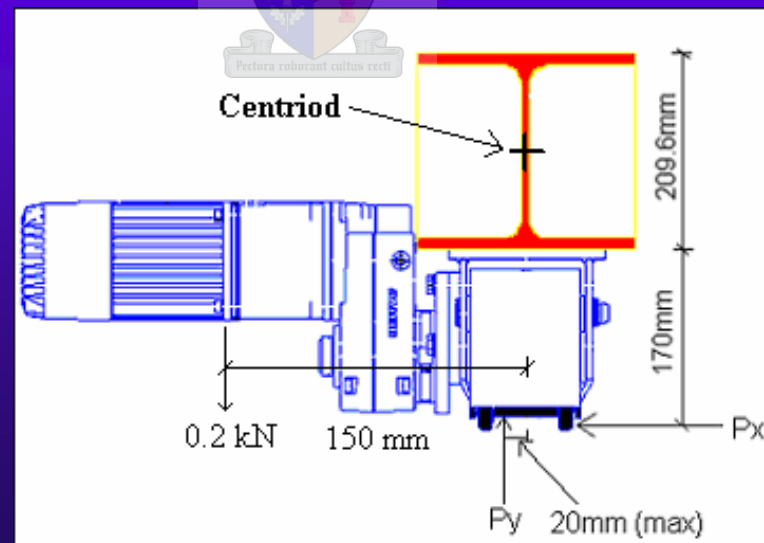
- Parameters influencing experimental results



Cantilever beam is fully restrained at an end

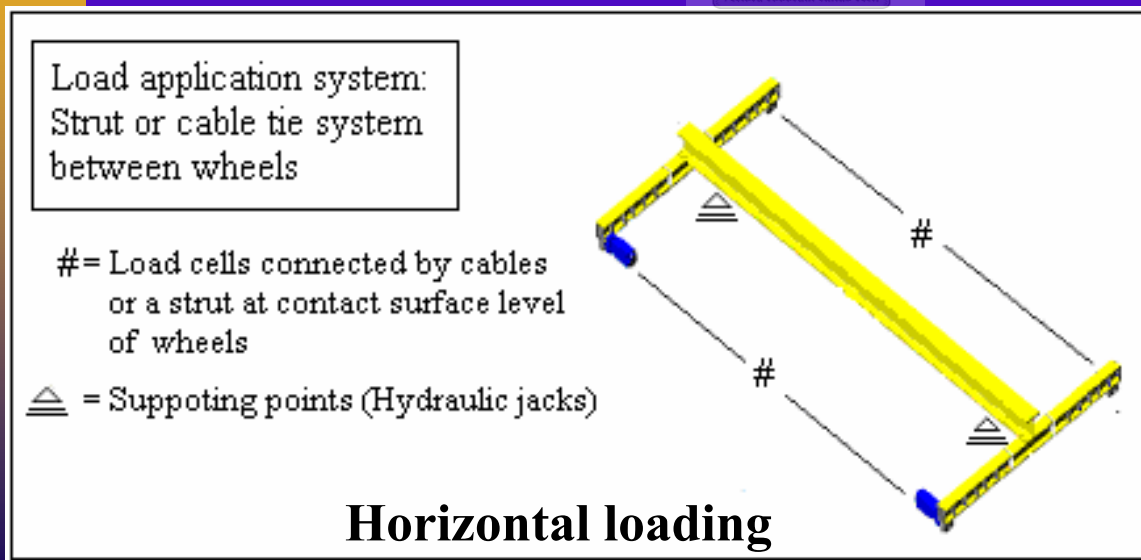
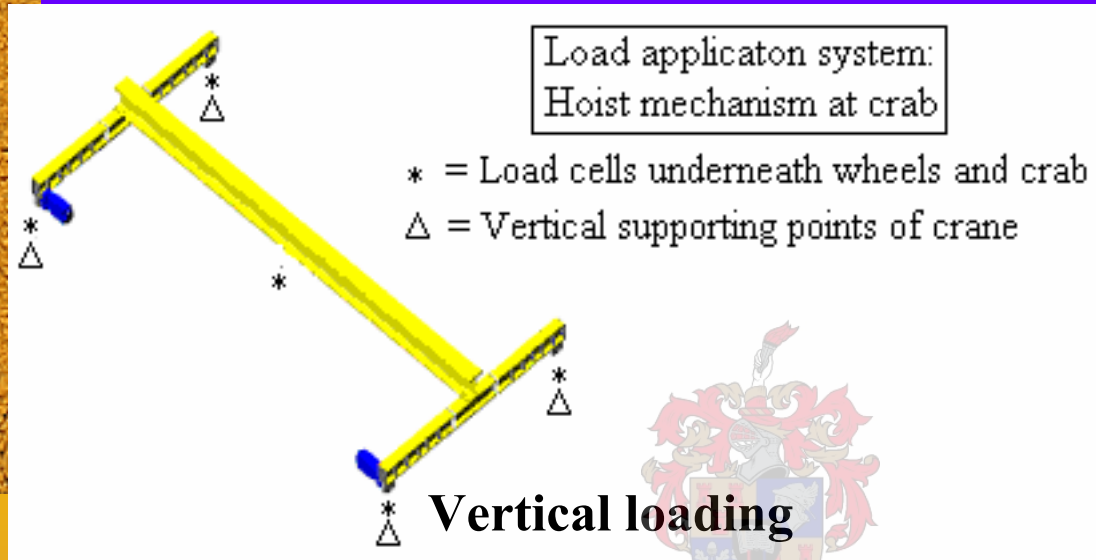


Crane bridge restrains top flange of end carriage only



Eccentricities of loads, from centroid of end carriage

Supporting points underneath crane, during controlled loading



Load application points, during controlled loading on crane



Pedraza, Cabrerof, Cullis, Tech





- **Results**

Vertical wheel loads:

Deflection of crane bridge and end carriages

Bending stress behaviour in end carriages



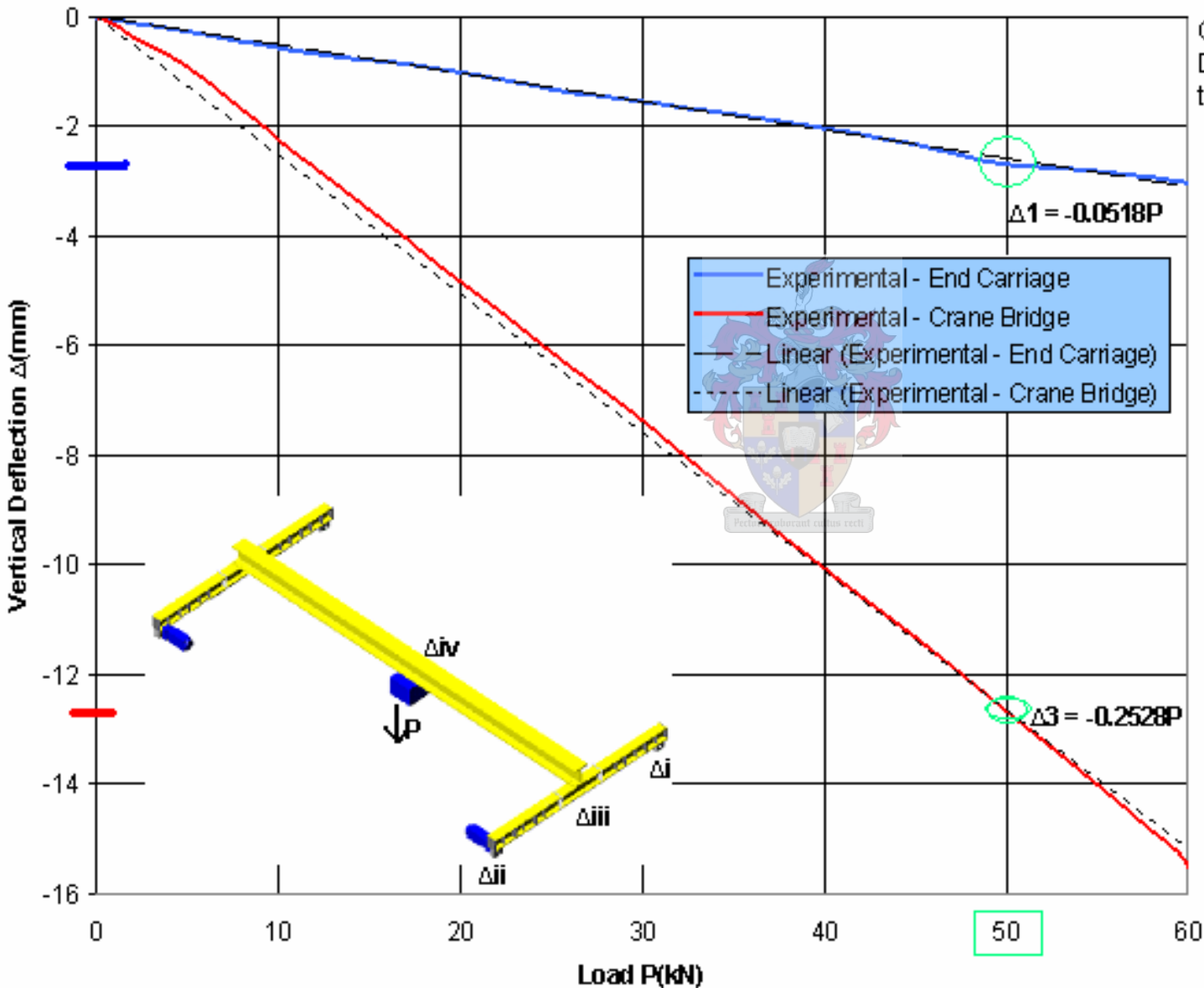
Lateral horizontal wheel loads:

Normal stress behaviour in end carriages

Stresses which cannot be measured currently

Vertical wheel loads

Load vs Deflection of Crane



Crane was measured at $\Delta_i - \Delta_{iv}$. Data was interpreted as follows, to give accurate results.

End Carriage:

$$\Delta_1 = \Delta_{iii} - (\Delta_i + \Delta_{ii})/2$$

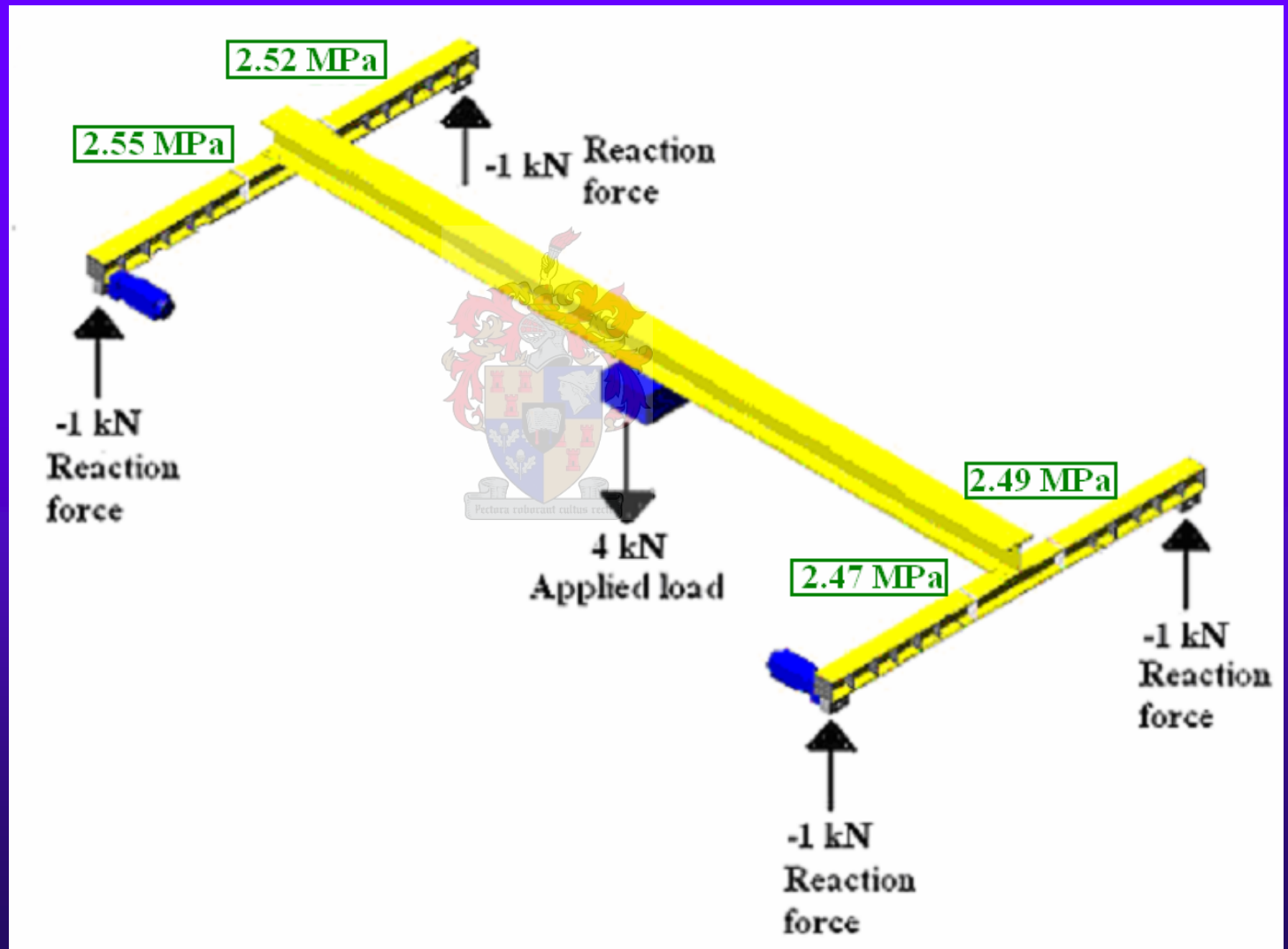
$$\Delta_1 = -0.0518P$$

Crane Bridge:

$$\Delta_3 = \Delta_{iv} - (\Delta_i + \Delta_{ii})/2$$

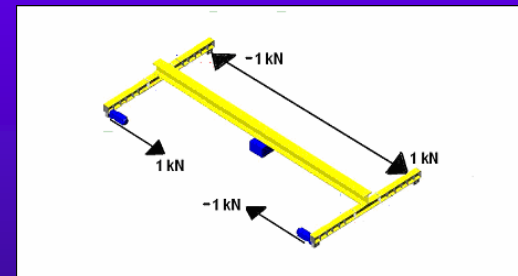
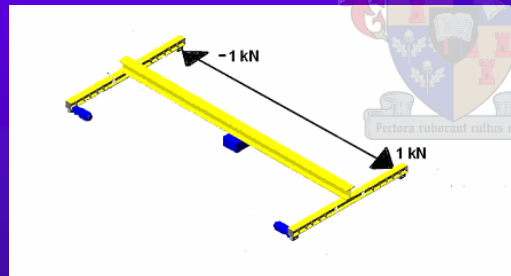
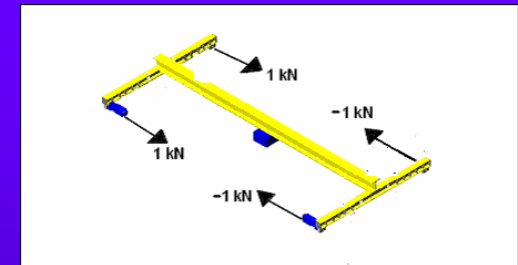
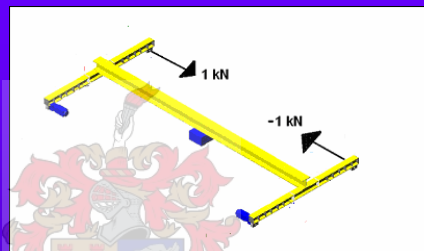
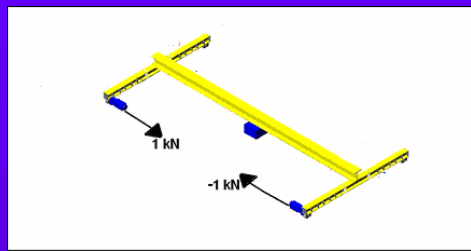
$$\Delta_3 = -0.2528P$$

Vertical wheel loads : Bending stress behaviour



Lateral horizontal wheel loads : Normal stress behaviour

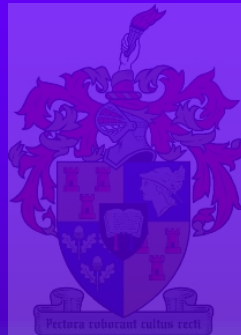
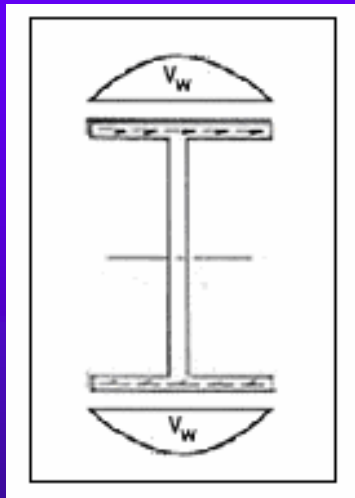
- ◆ 5 combinations of lateral horizontal wheel load scenario's were experimentally investigated.



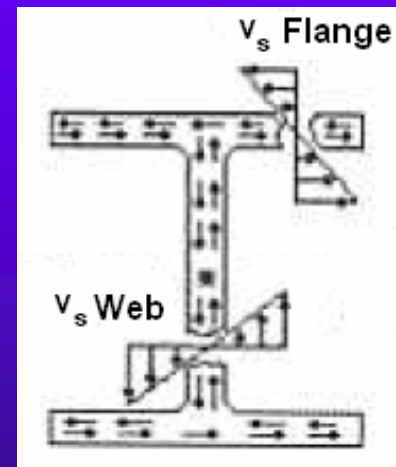
- ◆ Each scenario resulted in 16 average linear normal stress results at the strain gauges on the edges of the flanges of the end carriages.
- ◆ $5 \times 16 = 80$ different linear normal stress results
- ◆ Off these 80 stress results, the 4 main typical stress results will be compared with the results from the numerical model, later on in this presentation.

Stresses that the current end carriage load measuring system is not capable of measuring

Warping
shear stress



Saint Venant
Torsional
shear stress

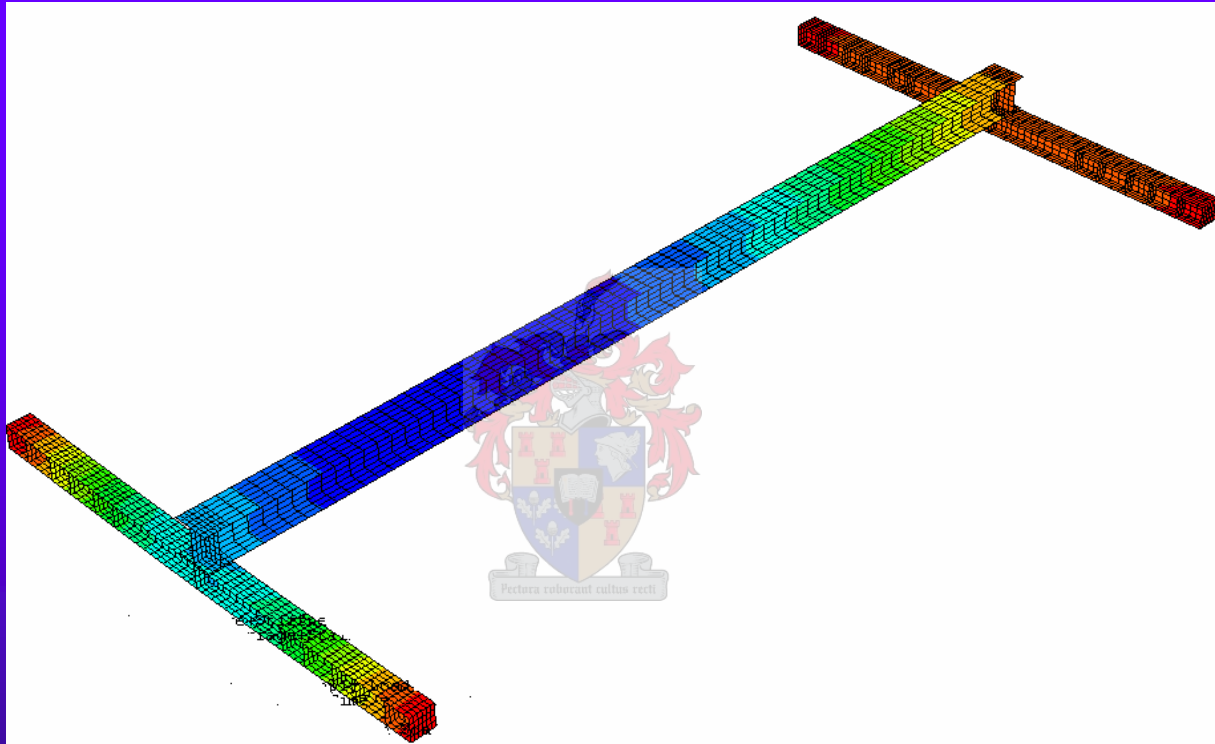


Contents

- 1) Background to research on EOTC at Univ. of Stellenbosch
- 2) Crane load models of the loading codes under investigation
- 3) Description of experimental system
- 4) Behaviour of supporting structure under controlled loading
- 5) Behaviour under controlled loading
- 6) Numerical modelling of overhead crane
- 7) Comparison of calibration results
- 8) Implementation of experimental crane
- 9) Comparison of accuracy of crane load models
- 10) Conclusions



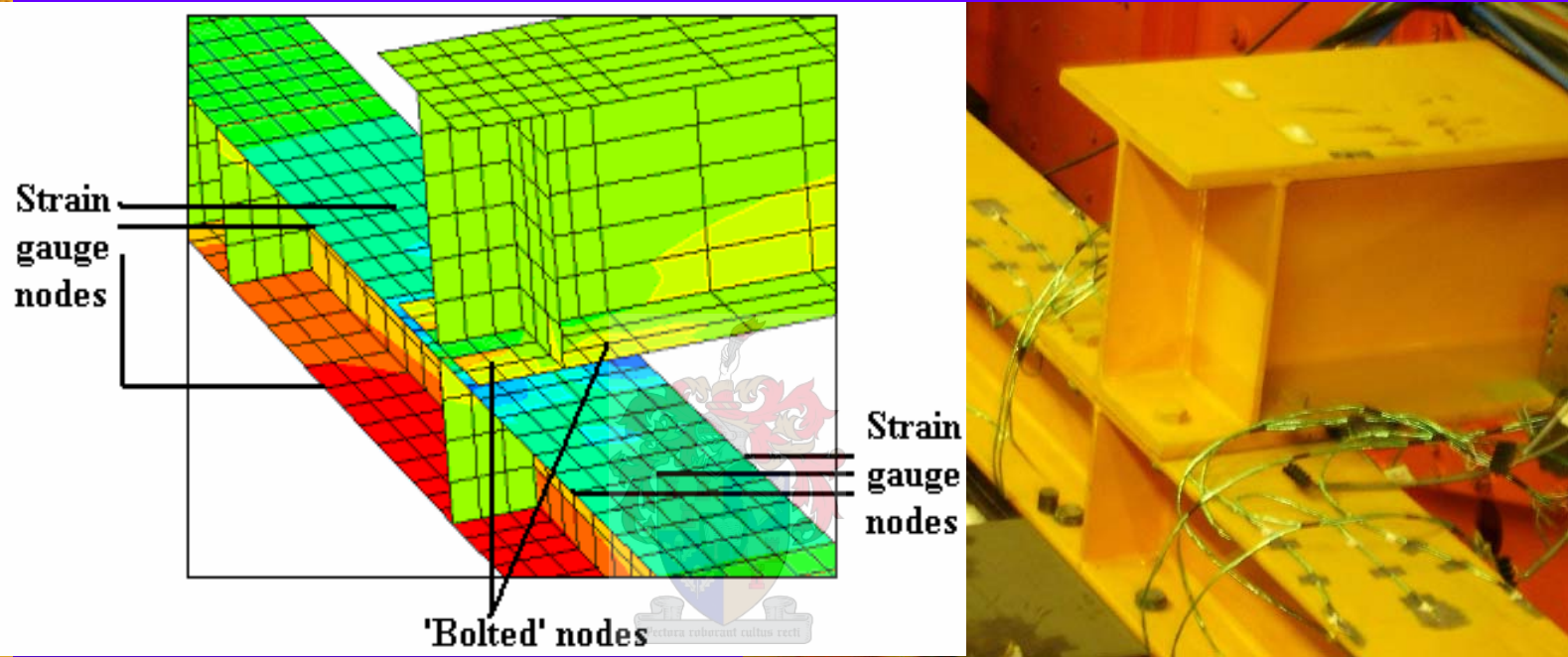
6) Numerical modelling of overhead crane



Why use numerical modelling?

An experimental investigation is limited to information from specific data capturing points, while a numerical model gives a view into the global behaviour. This helps to interpret the experimental results better. All the crane load models can be also be investigated, without months of experimental preparation work!

Points on numerical model, relating to those on actual crane



- ◆ The meshing of the numerical model was performed in such a way, that 'important points' on the experimental crane and nodal points on the numerical model correspond.
- ◆ These 'important points' are the bolts connecting the crane bridge with the end carriages, the wheel contact points, the positions of strain gauges on the end carriages and the restraints of the crane during controlled loading experiments.
- ◆ Rigid links were used in the numerical model to connect the crane bridge nodes and the end carriage nodes at the bolt positions.



Contents

- 1) Background to research on EOTC at Univ. of Stellenbosch
- 2) Crane load models of the loading codes under investigation
- 3) Description of experimental system
- 4) Behaviour of supporting structure under controlled loading
- 5) Behaviour of crane under controlled loading
- 6) Numerical modelling of overhead crane
- 7) Comparison of crane behaviour under loading
- 8) Implementation of experimental crane
- 9) Comparison of accuracy of crane load models
- 10) Conclusions

7) Comparison of crane behaviour under loading

Vertical wheel loads

	Experimental results	Numerical results	Deviation %
Bending stress at strain gauges (MPa / kN)	2.51	2.56	2
Maximum static deflection (mm)	12.6	13.2	4

Lateral horizontal wheel loads

Loading situations	Experimental results	Numerical results	Average Deviation %
Pulling the wheels together on a side: (MPa / kN)	Top flange : 7.9 Bottom flange : 6.6	Top flange : 5.4 Bottom flange: 7.3	14
Pulling the wheels together on both sides: (MPa / kN)	Bottom flange : 12.5	Bottom flange : 13.2	6
Pulling the wheels on one side and pushing the wheels on the other side: (MPa / kN)	Top flange : 14.1	Top flange : 11.0	28




Contents

- 1) Background to research on EOTC at Univ. of Stellenbosch
- 2) Crane load models of the loading codes under investigation
- 3) Description of experimental system
- 4) Behaviour of supporting structure under controlled loading
- 5) Behaviour of crane under controlled loading
- 6) Numerical modelling of overhead crane
- 7) Comparison of calibration results
- 8) Implementation of experimental crane
 - Classification of wheel loads
 - Kinematic characteristics of the crane
 - Preconceptions on the behaviour of the crane
 - Skewing behaviour of the crane
- 9) Comparison of accuracy of crane load models
- 10) Conclusions



8) Implementation of experimental crane





Classification of wheel loads, during implementation of experimental crane

Regular wheel loads

1. Normal payload hoisting
2. Normal payload lowering
3. Longitudinal crane travel with / without payload
4. Lateral crab travel with / without payload

Exceptional wheel loads

1. Eccentric payload hoisting (lateral and longitudinal)
2. Impact forces on end-stops
3. Maximum hoisting of payload
4. Induce skewing behaviour on the crane by restraining and end carriage longitudinally
5. Longitudinal crane travel with one of the driving mechanisms disabled
6. Misalignment of the supporting structure

Kinematic characteristics of the crane

	Maximum acceleration (m/s²)	Maximum continuous speed (m/s)	Maximum deceleration (m/s²)
Longitudinal crane travel	Regular : 0.2 Exceptional: 11.0	Regular : 0.45	Regular : 0.2 Exceptional : 11.0
Lateral crab travel	Regular : 0.5 Exceptional: 8.0	Regular : 0.55	Regular : 0.35 Exceptional : 14.0
Vertical payload hoisting	Regular : 0.5 Exceptional : 1.2	Regular : 0.075	Regular : 0.7 Exceptional : 1.2

Observation:

Exceptional wheel loads correspond with high acceleration and deceleration of the crane, crab or payload

Preconceptions on the behaviour of the crane, which were found to be incorrect.

- ◆ Critical dynamic wheel loads will occur, during payload hoisting, the moment the payload lifts off the ground.
- ◆ The higher the payload is lifted of the ground, during crane or crab travel, the higher the lateral horizontal wheel forces will be.
- ◆ Increasing the height of the payload carried on a hook by the crane during end-stop impacts, will increase the magnitude of the horizontal impact forces substantially.
- ◆ Skewing behaviour occurs continuous, once it is induced, until the crane comes to a halt.
- ◆ De-activating an electrical driving motor could cause the crane to de-rail easily.

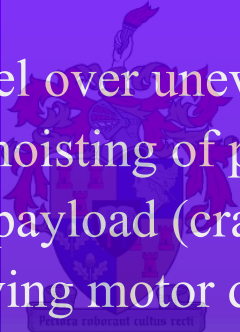




Skewing behaviour of the crane

The following are situations that the crane was exposed to, where skewing behaviour was observed:

- ◆ End buffer impact
- ◆ Longitudinal crane travel over uneven rail surface (at connections)
- ◆ Longitudinal eccentric hoisting of payload
- ◆ Longitudinal swinging payload (crane accelerates)
- ◆ Defective electrical driving motor during longitudinal crane travel



Skewing of the crane is influenced by the longitudinal equilibrium of the crane system, relative to the centre of gravity of the system. When the electrical driving motors are working correctly during normal longitudinal crane motion, there are no large lateral horizontal wheel loads if the payload is eccentric and the crane accelerates. When the crane decelerates, the swinging eccentric payload causes the highest lateral horizontal wheel loads, during normal longitudinal crane travel.

Contents

- 1) Background to research on EOTC at Univ. of Stellenbosch
- 2) Crane load models of the loading codes under investigation
- 3) Description of experimental system
- 4) Behaviour of crane under controlled loading
- 5) Numerical modelling of overhead crane
- 6) Comparison of calibration results
- 7) Behaviour of supporting structure under controlled loading
- 8) Implementation of experimental crane
- 9) Comparison of experimental and crane loading code results
 - Looking past the experimental results
- 10) Conclusions



9) Comparison of experimental and crane loading code results

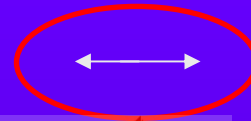
Critical dynamic forces (kN)	Experimental results	SABS 0160	SANS 10160
Vertical wheel loads			
Maximum	28.7	34	32.5
Minimum	5.7	6.8	5
Lateral horizontal wheel loads			
Due to acceleration of crab	1.3	1.3	1.3
Misalignment	2.9	2.2	2.2
Skewing due to acceleration of crane,	2.0	3.2	2.7
defective electrical motor,	2.8	~	~
wheel guide mechanism	~	~	6.5
Longitudinal horizontal force per rail			
Electrical driving motors	2.7	5.6	1.9
Force on each end stop	11	21 or 11.2	22.7



Looking past the experimental results

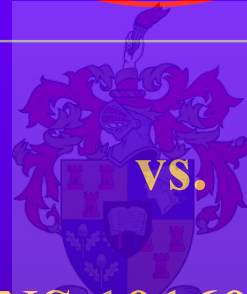
SABS 0160 - 1989

Horizontal longitudinal force (acceleration and deceleration)

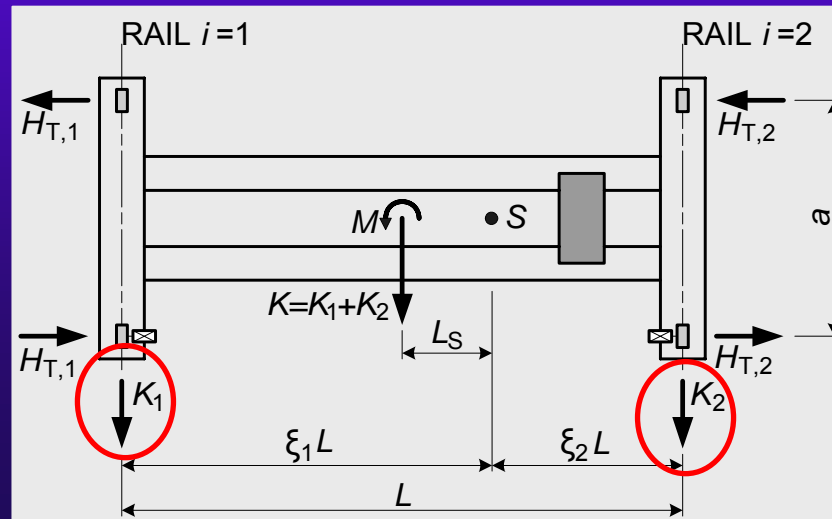


Force = $0.1 (\sum W \text{ of line per rail})$

(W = max. static wheel load)



SANS 10160 - 2005





13) Conclusions

- ◆ SABS 0160 –1989 gives empirical wheel load results based on the static weight of the crane and payload which are quite accurate, while SANS 10160-2005 gives results based on force equilibrium of the system, due to the geometric properties and external forces being exerted on the system.
- ◆ Thus implementing the new SANS 10160-2005 is a must, if we are to follow sound engineering principles.



Any easy questions?